POLITECNICO DI TORINO

Master's Degree in Communications and Computer Networks Engineering

Master's Degree Thesis

Modeling and controlling optical transponder white-boxes based on the physical layer digital twin

Supervisors

Prof. Vittorio CURRI

Ph.D. Emanuele VIRGILLITO

Dr. Renato AMBROSONE

Dr. Rocco D'INGILLO

Candidate

Andrea ROSSO

2024

Acknowledgements

I would like to thank the entire PLANET team, starting with Professor Vittorio Curri, for the opportunity he gave me and for his invaluable advice. I would like to thank the supervisors Emanuele, Renato and Rocco, who actively contributed to the success of this project with their patience, professionalism and helpfulness, as well as Stefano and Francesco from the LINKS Foundation, who always went the extra mile to provide the laboratory and their expertise.
Finally, I would like to thank my friends and family who have always been with me and have supported me along the way.

Andrea

Summary

The growing demand for high data rates and the increasing popularity and capillary of high-speed access, both wired and for mobile use, have made it clear that a robust and reliable core data network is essential.

The improvement of the network performances can be obtained in several ways; however, a crucial aspect is defining an open way of controlling all network devices, exploiting multi-vendor setups in an innovative and efficient way. This is a first step towards the realization of a digital twin, a software representation of a real network, which can be used to make simulations and to plan improvements.

This is the foundation of the initial section of this work, which examines the potential of an open approach to control a popular whitebox transponder that is compatible with commercial transceivers. These pluggable devices are at the basis of the optical networks, since they are the elements in charge of converting the signals between the electrical and the optical domain. In recent years, their implementation and performance have improved significantly, allowing them to be used in a wide range of operating conditions while increasing their flexibility to operate at different frequencies, rates, and modulation formats, resulting in the development of extremely high-speed products that can achieve data rates of up to 400 Gbps or more.

This lead to the need of defining and implementing a new and innovative open driver that requires no proprietary software and can be used to configure the device's central operating frequency, baud rate, modulation format, and output power, which are the key parameters typical of any coherent optical transceiver. Additionally, the same driver can be used to collect statistical measurements from transceiver itself, such as bit error rate or received power, which can be used to fully define its operating conditions, that can be easily integrated into a more complex network topology control software. In this way, it has been shown how the main characteristics of the optical transceivers are made available to be controlled in an open and flexible way instead of the typical proprietary software provided by the device vendor.

The second part of the work, instead, has been devoted to the modeling of the device, taking advantage of the open control driver developed in the first part. For this purpose, an experimental setup has been configured in a laboratory

environment, used to emulate a wide range of different network conditions. In addition to the transceiver under test, it was possible to add the contribution of Erbium-Doped Fiber Amplifiers (EDFA), widely used in long-haul links, attenuators used to emulate the effects of the fibers at long distances, and an Optical Spectrum Analyzer (OSA) used to study in detail the shape of the power spectral density with respect to the frequency. In practice, the use of these devices is of great importance in order to perform a large data collection of several important parameters of the device's behavior in different operating conditions. With the help of the open drivers, each device has been configured independently and has cooperated with the other to emulate the configuration of a real network, and it was also possible to implement an additional noise generation which could be used to test different network conditions. With the described setup, it was possible to perform an extensive data collection by testing a large list of configuration parameters on all the mentioned devices, which resulted in a complete database containing all possible combinations of network configurations, along with statistical measurements obtained from the transponder and the traces captured by the OSA. The comparison of the obtained numerical results with the well-known equations from the literature made it clear that it was required to consider additional contributions usually neglected, like the characteristics of the transceiver, in order to accurately predict the performances.

Furthermore, in parallel with the experimental data collection, a detailed analytical study of the internal device components has been conducted to mathematically define the source of internal noise at the transmitter and receiver, which, along with the amplifiers, represent the primary source of noise in a lightpath. For this reason, the starting point has been the definition of a typical block diagram of the main internal components, highlighting the most important sources of non-idealities. Then, a mathematical model has been defined in order to accurately describe the expected behavior of the said components, together with an analytical description of the introduced noise contributions that will ultimately affect the quality of the overall signal transmission.

At that point, the joint use of the mathematical model and the experimental results made it possible to define a complete model capable of accurately predicting the performance of the device with the help of some key parameters that can be interpolated directly from the data collection itself. In addition, a simplified experimental setup has been designed to perform an alternative low-cost data collection for other similar devices, to validate the model and to compare the results obtained with the ones typical of other devices from different manufacturers.

Lastly, the work establishes a solid foundation for additional analysis that can be used to further improve the model or tailor it to different devices and user goals. This makes it an open solution and starting point for the definition of a complete open network design, which is at the basis of the realization of a full network digital twin.

Table of Contents

List of Tables

List of Figures

Acronyms

ASE Amplified Spontaneous Emission

BER Bit Error Rate

CD Chromatic Dispersion

DSP Digital Signal Processing

EDFA Erbium-doped Fiber Amplifier

FEC Forward Error Correction

IMDD Intensity Modulation Direct Detection

NLI Non-Linear Interference

OSA Optical Spectrum Analyser

OSNR Optical Signal to Noise Ratio

PRBS Pseudo-Random Bit Sequence

SNR Signal to Noise Ratio

SSH Secure Shell

VOA Variable Optical Attenuator

WDM Wavelength Division Multiplexing

Chapter 1

Introduction

The increasing demand for high data rates and the widespread adoption of high-speed access, both wired and wireless, underscore the need for a robust and reliable core data network. In general, different network technologies can be employed to provide varying services to end users, each with distinct constraints and goals.

Among the various options, optical networks are becoming increasingly important due to their flexibility in adapting to different needs, and in recent years, they have also become widely used by end users, thanks to the growing availability of technologies such as Fiber to the Home. However, one of the most notable applications of optical networks is in the core network, which requires an infrastructure capable of carrying huge amounts of traffic over long distances. In fact, even if the connections to the end users can be realized with different techniques, the interoperability between the networks requires such a high throughput that only optical networks are able to provide [1].

1.1 History of optical communication

Since ancient times, light has been a medium for transmitting information over long distances. Early civilizations used fire beacons, mirrors, and smoke signals to transmit simple information in a fast way. However, this communication technology did not improve significantly until the last years of the 18^{th} century, with the advent of the optical telegraph [2], which then evolved in its electrical implementation [3], making it possible to connect even more distant locations without line-of-sight.

Optical communications returned to prominence in the 1960s and 1970s, when researchers achieved remarkable successes in the implementation of lasers and the realization of optical fibers, capable of carrying light over long distances while being contained within a small and flexible fiber cable [4].

In the years that followed, advances in research made it clear that optical

communications could be used effectively for both long-haul connections and for short high-speed access, becoming cheaper and more popular [5], up to the current times in which optical networks are at the basis of the *core networks* worldwide, while in parallel there is a growing demand for very high speed data access, both for the end users to the widespread of connected devices.

1.2 The open networks

Thanks to continuous improvements in optical research, it is now possible to benefit from a wide range of devices that work together to provide the best performance and quality of service. At the same time, the ability to operate in a multi-vendor scenario, where different components from different brands can be used together to minimize costs and improve the overall reliability of the system, is becoming increasingly important. However, such interoperability is often difficult to achieve because most devices have proprietary designs and software that do not integrate well with others [6].

This is why it is necessary to develop *open networks* where all network elements can be controlled using open standards that enable interoperability between different vendors and devices. This is at the basis of the Software Defined Networks, which enable the possibility of decoupling the control plane from the data plane, with the goal of providing more efficient configuration, better performance, and higher flexibility required for the new and innovative network designs [7].

In addition, open networking can be effectively used to define a network *digital twin*, which is a software representation of a real network that can be used to run simulations or test new configurations before implementing them in the real world, helping researchers and companies make thoughtful decisions about the best improvements to develop [8].

A notable aspect related to this topic is that a digital twin of a device can only be effectively realized if its behavior is accurately modeled in such a way that it is possible to predict its performance under different network conditions. This makes it clear that the two ideas of open control and device characterization are closely related, in the sense that a digital twin can only be realized with in-depth knowledge of the device characteristics, but the said characterization can only be performed effectively with the help of open interfaces. This is the basis of the work described in the following chapters, which focuses on the modeling and characterization of an optical transponder and its pluggable transceivers, knowing that it can be extended to similar devices or to completely different optical network elements. Additionally, in the next sections it will follow a brief description of the main elements used in all the main optical networks, which are required to introduce the components considered in the following chapters.

1.3 Optical Network Elements

In all optical networks, there are a set of key elements used for signal transmission and reception, whereas other elements are responsible for signal propagation and transparent routing. This section will provide a brief description of the most common devices and their basic functionality.

1.3.1 Transceiver

The transceiver is a device similar to those shown in Figure 1.1 that serves as the interface between fiber optics and electronic components. They are full-duplex, meaning that they can transmit and receive simultaneously. Nowadays, they are *plug-in* devices that can be inserted into a standardized transponder that can control and use them.

Figure 1.1: Generic set of transceivers [9].

1.3.2 Fiber

An optical fiber cable is a thin and flexible tube of glass or plastic able to carry light. It is composed of three parts, one inside the other, as visible in Figure 1.2. The outermost one is called *coating* and its purpose is to protect the inner layers, but it does not contribute to the propagation of the signal. On the contrary, the two inner layers are used to guide the light: for this reason they are transparent and their material is chosen to have a different refractive index, creating a reflection and a refraction at their interface. In fact, each material is characterized by a specific refractive index $n \geq 1$, which is a dimensionless number that indicates the ability of that medium to bend light. This behavior is described by the Snell's law reported in 1.1 that considers the relationship between the angles of incidence and refraction when the light passes through a boundary between two different isotropic media, such as the glass that compose the core and the cladding.

$$\frac{\sin(\theta_1)}{\sin(\theta_2)} = \frac{n_2}{n_1} \tag{1.1}$$

In particular, when the light beam enters the fiber's core, it reflects on the boundary between the core and the cladding. In order to have the light propagation along the fiber, it is required to reach the condition of total internal reflection, which is achieved when the light's angle of incidence is less than the critical value θ_c obtained in the equation 1.2.

$$\theta_c = \arcsin \frac{n_2}{n_1} \tag{1.2}$$

As a side note, an additional effect of the refractive index is that it determines the phase velocity v of the light as $v = c/n$, with c the speed of light in the vacuum. Since it is common to consider $n \approx 1.5$, for most fiber cables the signal propagation velocity in the medium is around $2/3$ of the speed of the light in the vacuum.

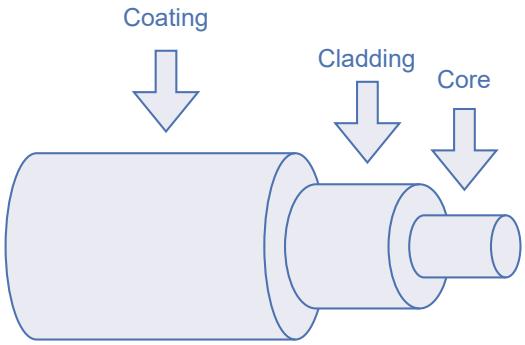

Figure 1.2: Optical fiber cable composition

The usable bands

Fiber characteristics are highly dependent on the frequency of the signal. For this reason, the spectrum has been divided into several regions, called *bands*, that are similar in their behavior. One of the most commonly used regions is known as the *Conventional Band* (or *C-Band*), which roughly lies between 1530 nm and 1565 nm. In terms of frequency, it is generally considered to be a 5 THz band centered around 193.5 THz. Although several other usable bands exist, this is the region in which most devices operate, and it was chosen because of its very low attenuation and because it was the first band in which optical amplifiers were developed.

The signal attenuation

Any medium is known to reduce the power of the signal passing through it, and in the case of optical transmission, attenuation is one of the main impairments introduced by the fiber cable. In general, in addition to the material and its characteristics, the attenuation does also depend on the frequency of the considered signal: however, in most of the typical applications related to the fiber communications, this value can be considered almost constant in the bands of interest. Additionally, it is important to note that the attenuation of fiber is much less than that of any other medium, and this is one of the main reasons why it can be used over very long distances.

For practical applications, a common attenuation value is 0.2 dB/km in the *C-Band*, which means that the power of the signal is reduced by 0.2 dB per kilometer of fiber. As anticipated, this value is orders of magnitude lower than that of any other medium, and the best cables can reduce it even further, even around 0.14 dB/km [10, 11].

Chromatic dispersion

The phenomenon whereby the phase velocity of a wave depends on its frequency is known as chromatic dispersion. The dispersive nature of the medium causes distortion of the pulse, resulting in different delays depending on the frequency. In fact, since each channel occupies a bandwidth of tens of Gigahertz, there are components at different frequencies, and depending on the characteristics of the fiber cable used, the higher frequencies may propagate faster or slower than the lower ones. This difference in speed results in a difference in the time it takes for the components to reach the receiver, causing distortion that can affect the ability to receive the symbol correctly [12].

In general, at least three contributions have to be taken into account:

- The material of the fiber may affect the amount of introduced distortion, and in some cases also the sign: in fact, there exists fibers that distort the optical signal in opposite directions.
- An increase in the symbol rate makes it more difficult to find the correct transmitted symbol, as each symbol lasts less time, and its duration becomes comparable with the introduced distortion.
- The total length of the fiber increases the total distortion, since a difference in speed corresponds to a greater difference in time over a longer distance in the network.

In the older networks, chromatic dispersion was a limiting factor in the maximum distance that could be achieved. To overcome this limitation, various techniques

were employed, one of which was to use a sequence of different fiber types with opposite distorting effects along the path so that the overall distortion was negligible.

On the contrary, with the advent of modern receivers, this compensation can instead be avoided as the Digital Signal Processing (DSP) unit inside the receiver completely compensates for it, and for this reason the physical compensation is generally not utilized [13].

The Kerr effect

In the previous equation 1.1, it has been considered the importance of the refractive index n, and it has been defined as constant with respect to the material of the fiber. However, this is not always the case: in fact, the so-called Kerr effect is a phenomenon where the refractive index of a material changes in response to the power P crossing the fiber, following the rule in equation 1.3. It is anyway important to remember that, similarly to the already described Chromatic Dispersion, the Kerr effect becomes prominent especially for longer distances or when the transmitted power becomes too large [14].

$$n = n_{\mathrm{L}} + n_2 \frac{P}{A_{\mathrm{eff}}} \tag{1.3}$$

1.3.3 Optical Amplifiers

Optical amplifiers are active devices that can counteract the effect of attenuation by increasing the power of the optical signal without the need for regeneration in the electrical domain. Although there are several types of amplifiers, one of the most commonly used is the so-called *Erbium-Doped Fiber Amplifier* (EDFA), which contains a short span of fiber whose core is doped with erbium ions, which can be efficiently pumped with a laser. It is possible to use a quantum physical mechanism where an energy transfer takes place between the energy pumped by a dedicated laser and the propagating photons, with the end result of increasing the power of the signal [15].

An important advantage of these optical amplifiers is the fact that they can operate in a very wide band (around the 5 THz of the C-band): this way, only one amplifier is needed, no matter how many frequencies are used in the fiber, providing a reliable and cost-effective way to extend the range of the transmitted signal without leaving the optical domain. Moreover, in general it is possible to dynamically configure the devices in order to select a gain G and a tilt T to be applied to the input signal [16].

ASE noise

Optical amplifiers produce a main side effect known as *Amplified Spontaneous Emission* (ASE). This is a random generation of photons on the same frequency bands as the useful signal, and is considered an additive noise term that affects the other signal components. Figure 1.3 shows a simplified representation of an amplifier, illustrating its amplification effects, including gain and tilt of the input signal, as well as the additional noise term [17].

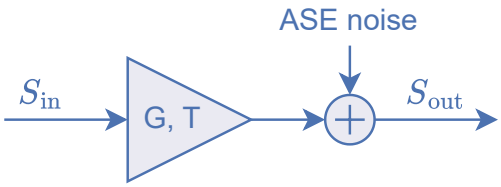

Figure 1.3: Schematic representation of an optical amplifier and the additive noise contribution

The Raman amplifiers

An interesting additional optical amplifier is based on the Raman effect, which provides a *continuous* amplification along tens of kilometers of fiber, contrary to the EDFAs which instead can be considered lumped devices. Furthermore, they can provide an amplification across a wider range of frequencies, usually with a lower noise figure, and in general can be effectively used especially for long distances [18].

1.3.4 ROADMs

An Optical Add/Drop Multiplexer (OADM) is a complex component used to perform signal switching in a network directly in the optical domain, without the need for electrical signal retransmission. One of its main applications is its ability to route input signals to different output ports based on their wavelength, allowing the signal to traverse the node in a fully transparent manner. The same switching can also be applied within the same node: in fact, its add/drop capabilities allow the possibility of inserting or removing data flows from the network, accessing them locally [19].

The traditional OADM devices are composed of a multiplexer and a demultiplexer able to split and merge signals based on their optical frequency, and a fiber patch panel or a switching component able to connect the other stages in the proper way to deploy the configuration of interest. On the contrary, the more advanced

Reconfigurable OADMs (ROADM) enable the possibility of having a remote control of the device, allowing it to change it configuration according to the needs. [20]

Furthermore, some of these devices have additional features such as the ability to equalize the output channels to provide an equal power level to all frequencies in the same fiber, which is especially important when combining channels from different sources and therefore different power levels [21].

1.3.5 Optical Line System

An Optical Line System (OLS) is a transparent link that connects the nodes in a network [22]. It consists of three main components:

- Fiber spans: used to connect the components together. There are typically two per link to provide a bidirectional connection;
- Inline Optical Amplifiers (ILA): amplify the power of the signal. As with the fibers, they are usually used in pairs;
- ROADMs: switch the signals in the optical domain between network nodes;
- Boosters and Preamplifiers: installed in the switching nodes, can adjust and optimize the input and output power.

1.4 Optical transmission

1.4.1 Optical Transmission Techniques

Two different transmission techniques are used in optical communications, and their main differences are described in this section.

Intensity-Modulation Direct-Detection

The Intensity Modulation Direct Detection is the simplest modulation technique that can be employed effectively. The IMDD transceivers utilize On-Off-Keying (OOK) modulation to map the ones and zeros of the bit stream to the presence or absence of photons. In practice, the transmitting laser can be rapidly switched on or off, while at the receiver's end, a threshold is used to determine the received information after the photodetector. Although transmission and reception are simple, detection is limited to only two states. This limitation affects achievable performance, which is why this technology is nowadays mostly used only on the edge where the required throughput is limited [23].

Coherent Modulation

Coherent receivers are complex devices that can detect not only the power of the received signals, but also the phase and polarization of the photons. This additional information can be used to map multiple bits onto the same transmitted symbol, significantly increasing the achievable data rates, at the expense of a possible increase in the device complexity and cost [24].

In the optical domain, different modulation formats can be employed, but it is common to rely on Quadrature Amplitude Modulation (QAM), which can define a constellation of $M = 2^n$ symbols, each carrying n bits, for each of the two orthogonal polarizations. In practice, any value of n can be set to adjust the size of the constellation and find a balance between higher data rate and increased complexity. The only disadvantage of this technique is that in general only integer values of n are considered, and this leads to having increasingly large steps in the constellation size M, which will also require better channel quality to be decoded correctly. For this reason, an attempt has recently been defined to improve the data rate even in conditions where it is not possible to fully increase the constellation size: this is based on probabilistic constellation shaping [25], but its additional complexity results in the fact that for most practical use cases a simpler geometric shaping is preferred, and this is the case for the devices considered in this work.

An example of a typical constellation used in most of the coherent optical transceivers is shown in the figure 1.4, which represents the so-called *16-QAM* modulation, where 16 symbols are arranged on a grid so that each point has the same distance to the next. In the same figure, there is also an example of *Gray code*, which is used to assign a sequence of bits (four in this case) to each symbol in such a way that when moving between adjacent symbols with minimal distance (vertically or horizontally on the grid), only one bit changes with each movement. This encoding standard is not mandatory, but it is the preferred encoding scheme because it minimizes the probability of bit errors. In fact, if an error occurs on a symbol, it is most likely that the wrong symbol is close to the correct one, thus limiting the errors to only one bit. In any case, this is especially useful in conjunction with an error correction algorithm.

The Bit Rate and the Symbol Rate

In most transmission systems, bit rate is an important metric: it represents the amount of information, expressed in bits, that can be transmitted in the time unit of one second. In the specific case of optical communications, due to the high achievable rates, it is common to define the rate in terms of Gigabits per second (Gbps), which corresponds to 10^9 bps.

If the constellation used is complex ($M > 2$), each transmitted symbol carries more than one bit: in this case, it is possible to define a new quantity, the symbol

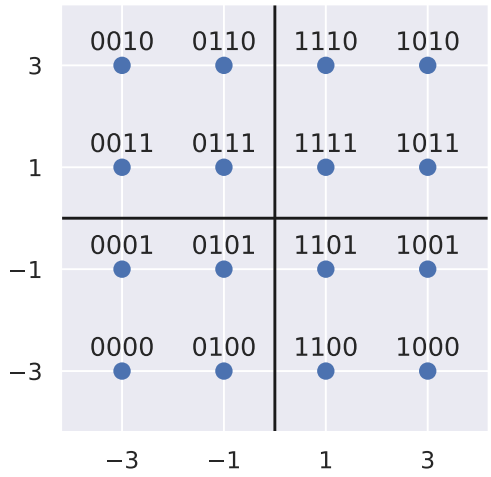

Figure 1.4: Example of 16-QAM modulation with Gray coding

rate (R_s, sometimes called *Baudrate*), which represents the number of symbols transmitted per unit of time. Since each symbol contains $n = \log_2 M$ bits, it is possible to convert from the bit rate to the symbol rate (and vice versa) using the Equation 1.4.

$$R_s = \frac{R_b}{n} = \frac{R_b}{\log_2 M} \tag{1.4}$$

The main advantage of this approach is that, for a given symbol rate, several different bit rates can be achieved depending on the size of the constellation used.

Bit Error Rate

In any digital communication system, the signal propagating from the transmitter to the receiver is affected by noise. The receiver's task is to try to detect the correct message, even if the position of the received symbols does not correspond to the theoretical one: in general, this becomes more difficult as the symbol rate increases or the chosen constellation becomes more complex. By comparing the transmitted bits with the received ones, it is possible to count the number of bit transitions, defined as the case where a zero is detected as a one, or vice versa. This value is often expressed as the ratio of the number of errors to the number of bits transmitted: this is defined as the Bit Error Rate (or BER).

Forward Error Correction

Provided that in every system there is a non-zero error probability, it is common to introduce an algorithm of error detection or correction. In optical communications, the Forward Error Correction (FEC) algorithm is used: it is a technique that improves the reliability and quality of digital transmission by adding redundant data at the transmitter, called error-correcting code, which is then used by the receiver to correct errors that occur during signal propagation. In general, the effectiveness of the FEC depends on both the algorithm used to compute the redundancy and the overhead introduced [26].

Symbol transmission and raised cosine

In all communication systems, data is transmitted around a central frequency, occupying a band B_{ch}. Although for ideal transmitters the optimal signal shape in the frequency domain is a rectangle with a base width exactly equal to the Baudrate, so that $B_{ch} = R_s$, real devices will transmit using a slightly larger bandwidth. In most of the systems, it is common to consider a shape called *raised-cosine*, which minimizes intersymbol interference (ISI) [27].

It is possible to describe its shape mathematically, which depends on several contributions, but one of the most important is called the *roll-off* factor ρ, which is a measure of the excess bandwidth of the filter. When $\rho \to 0$, the roll-off zone becomes infinitesimally narrow and the raised-cosine behaves similarly to the ideal rectangular function. For most of the practical applications, a common value is around $\rho \approx 0.2$.

1.4.2 Wavelength Division Multiplexing

Inside a fiber optic cable, data is transmitted as photons travelling from the transmitter to the receiver. Each signal transmission occupies a specific band around a central frequency, leaving all other frequencies unused. In general, the band used for signal transmission (typically a few tens of GHz) is much smaller than the total usable band, which is approximately 5 THz in the C-band. To improve the spectrum utilization, the main idea is to use a well-known technique called Frequency Division Multiplexing, also used in all the wireless transmissions. In the optical domain, for historical reasons, it is known as Wavelength Division Multiplexing (WDM). It allows the accommodation of several parallel streams, called channels, separated by their frequency (or wavelength).

This can be done by considering a generic set of N lasers, each operating at a specific central frequency, connected to a multiplexer that combines their signals in a single fiber capable of carrying all these channels simultaneously. At the receiver end, the same setup is considered, with a demultiplexer able to split the received

beam into the corresponding N components, ready to be decoded by the receivers. One example is visible in the Figure 1.5.

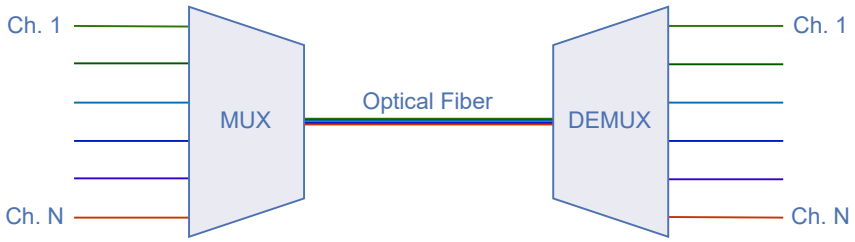

Figure 1.5: WDM example

Although it is possible to consider any central frequency and signal bandwidth, in commercial optical systems it is common to consider a fixed grid with channel spacing standardized by ITU-T in multiples of 12.5 GHz to ensure interoperability of systems.

As a consequence, the frequency band occupation of every device is in general considered to the smallest multiple of 12.5 GHz in which it can fit.

1.4.3 Signal-to-Noise ratio

The Signal-to-Noise ratio (SNR) is a measure that compares the level of the useful signal in respect to the level of background noise. This is obtained by performing the ratio of the signal power to the noise power expressed in linear units, but then it is often converted in Decibel, with a higher value representing better signal quality. This quantity is very general in the sense that it can be used to represent different characteristics of the signal and, most importantly, its relevance depends on the contributions considered in its calculation and the position in the line where it is measured.

In addition, this quantity is closely related to the BER, as a lower signal quality (and therefore lower SNR) will reduce the transceiver's ability to decode the transmitted signal, resulting in an increase in the BER. In particular, this aspect is of great importance in the computation of the device performances and will be described in greater detail in the following chapters.

For the purposes of this work, a specific convention is followed in order to avoid ambiguity on what is considered, and it is based on the following definitions:

- SNR_{ASE}: represents the contribution due to the amplified spontaneous emission of the optical amplifiers, as it has been described in section 1.3.3. This convention considers this quantity as measured in respect to the noise generated on the same band, such that the band of the noise is the same band of the

signal. However, as it will be described later, in some cases it is required to move to a reference band of 0.1 nm (or 12.5 GHz): in that case, this quantity is named OSNR to distinguish the different bandwidth considered.

- GSNR, or Generalized SNR: considers all the *additive* contributions in the optical domain. In practice, it contains the contribution of the Non-Linear Interference (NLI) and the one of the $\mathrm{SNR}_{\mathrm{ASE}}$ defined before.
- $\mathrm{SNR}_{\mathrm{TRX}}$: represents the contribution of the transceiver, and can be split in $\mathrm{SNR}_{\mathrm{TX}}$ and $\mathrm{SNR}_{\mathrm{RX}}$ to consider only the transmitting or the receiving components.
- SNR: is the Signal-to-Noise ratio computed at the receiver, which is the one that affects the ability of the transceiver to retrieve the correct information from the channel, and depends on the other contributions described before.

Chapter 2

The devices in use

2.1 The Phoenix Transponder

The Phoenix transponder is a device capable of providing optical communication links in optical transport networks. It is designed as a disaggregated system that aims to eliminate network complexity by supporting interoperability between vendors. It provides multiple interface ports and can be configured to operate in different network conditions as described in the following sections.

The Interface Ports

The Phoenix transponder can support up to 20 traffic interface ports, which are physical connections that allow data exchange. They are of two different types:

- 4 *line* ports that support 400G CFP2-DCO transceivers;
- 16 QSFP28 *client* ports at 100GbE.

QSFP Quad Small Form-factor Pluggable (QSFP) transceivers are small and hot-pluggable devices often used to provide a reliable connection for short-reach applications. In particular, the QSFP28 standard is designed to carry 100 Gigabit Ethernet.

CFP The C form-factor pluggable (CFP) aims to define a standard for the transmission of high-speed digital signals. Originally developed to support 100 Gigabit Ethernet systems, it has evolved with several variants, such as the CFP2 used in the Phoenix. These are the most common interconnections for high speed and long distance connections, and provide higher flexibility in respect to other variants, starting from a wide range of configuration parameters, as it will be described later.

ACO and DCO As described in the introduction in section 1.4.1, most modern devices use the Coherent Modulation in order to offer higher data rates and electronic dispersion compensation. In particular, coherent modules can be divided into two groups depending on the electrical interface used by the module.

In the case of the Phoenix transponder, the Digital Coherent Optics (DCO) transceivers are used.

2.1.1 The Phoenix configuration parameters

The Phoenix transponder can configure several parameters for the connected CFP2-DCO transceivers, the definition of which is given in the following paragraphs. The QSFP devices, on the other hand, offer very little configuration options and report few metrics: for this reason, they have not been used for device characterization.

The Operational Modes One of the most important configuration parameters is the *Operational Mode*. This is a four-digit number that represents the combination of line rate, modulation format and FEC algorithm.
The manual defines a total of 16 valid codes that can be set individually on each of the connected CFP2-DCO transceivers, and the corresponding configuration parameters are listed in the table 2.1.

Line Rate	Modulation Format	FEC	Operational Mode
100 Gbps	DP-QPSK	SC-FEC	1104
100 Gbps	DP-QPSK	O-FEC	1304
200 Gbps	DP-QPSK	O-FEC	2304
200 Gbps	DP-8QAM	O-FEC	2306
200 Gbps	DP-16-QAM	O-FEC	2308
200 Gbps	DP-QPSK	HG-FEC	2404
200 Gbps	DP-8QAM	HG-FEC	2406
200 Gbps	DP-16-QAM	HG-FEC	2408
300 Gbps	DP-8QAM	O-FEC	3306
300 Gbps	DP-16-QAM	HG-FEC	3408
400 Gbps	DP-16-QAM	O-FEC	4308
400 Gbps	DP-16-QAM	HG-FEC	4408

Table 2.1: Operational-mode Support Value

Values description It is interesting to observe that the four-digit Operational Mode number can be computed as follows:

- The first digit represents the bit rate and is expressed in hundreds of gigabits per second. This means that the Phoenix transponder can allow a line rate of 100, 200, 300 or 400 Gbps;
- The second digit represents the FEC coding, one among four algorithms;
- The last two digits depend on the selected modulation format. This value is expressed on two digits because there exist the definition of 12 values, but only three of them can be used with the CFP2-DCO transceivers.

FOC Transceiver Inside the Phoenix transponder, up to 4 transceivers can be plugged in at the same time, and they can be supplied by different manufacturers. The one used for characterization is the FIM38750/102, which supports only 4 of the 12 operating modes defined above.

Line Rate	Modulation Format	FEC	Operational Mode
100 Gbps	DP-QPSK	SC-FEC	1104
200 Gbps	DP-QPSK	O-FEC	2304
200 Gbps	DP-16-QAM	O-FEC	2308
400 Gbps	DP-16-QAM	O-FEC	4308

Table 2.2: Operational-modes supported by the FIM38750/102 transceiver

As it is possible to see from Table 2.2, the transceiver configuration mainly differs by the achievable bit rate, which is obtained by using different modulation formats and FEC algorithms.

In practice, this translates into the fact that the user has the possibility to choose between three different line rates, depending on the requirements, and in the case of 200 Gbps there is the additional possibility of selecting between a more robust configuration or a lower amount of spectrum used.

The Frequency and the Output Power The Phoenix transponder has the ability to configure the power and central frequency of the devices. Similarly to the operating modes, the allowable values depend on the transceivers in use. Considering the FIM38750/102 device, the following limits are enforced:

- The central frequency must be in the range between 191.3 and 196.1 THz;
- The target output power must be in the range between -5 and $+1$ dBm.

Other devices may have different limits.

Moreover, the instrument requires the use of specific units of measurement for both reading and for setting all the configuration parameters.

- The frequency must always be expressed in MHz, which means that the commonly used value in THz must be multiplied by 10^6.

- The power must be expressed in dBm, which is a logarithmic scale indicating a ratio for which the reference power is 1 mW. In this way, the value becomes dimensionless, and it is possible to calculate the corresponding *decibel* value. Thanks to this conversion, the reference power of 1 mW corresponds to 0 dBm.

2.1.2 The device connection

The Phoenix transponder has an out-of-band (OOB) Ethernet management port that can be used to remotely control the device. This enables the possibility to assign a local IP address so that it can be reached by other systems on the same network. Two different options have been analyzed.

The terminal based connection

One of the main ways to control the device is to use a Secure Shell (SSH) in order to establish a secure terminal-based connection. A wide range of commands can be executed on the device to change its configuration or to collect data. The main advantage of this approach is that the control interface is very fast and complete, making it possible to effectively control the device while collecting near real-time data. The only disadvantage of using a terminal-based control approach is that it makes it difficult to efficiently collect command responses in an automated manner. For this reason, other connection systems are preferable for unattended operation.

NETCONF

The Network Configuration Protocol (NETCONF) is a network management protocol that provides mechanisms for installing, manipulating and deleting the configuration of network devices [28]. This protocol is based on the YANG data modelling [29], whose language can be encoded in the Extensible Markup Language (XML) to be transmitted over a secure transport channel. One of the main advantages of NETCONF over other protocols is that all commands and their outputs follow a common standard, ensuring interoperability between vendors, while the XML encoding reduces the complexity of parsing the received information. In particular, in the Python code the `ncclient` library has been used to create a connection to the transponder and to exchange messages according to the NETCONF standard [30].

2.1.3 The device configuration

In order to use the instrument correctly, it must be properly configured. For the data acquisition described in the following sections, the configuration has been divided into two steps: the initial configuration and the subsequent data collection. Firstly, the terminal-based connection can be used to configure the data link and enable data transmission from the transponder. An SSH connection can be opened in order to use a remote terminal to execute the commands.

The first important command to run is the one dedicated to checking the status of the line port. In particular, in the case under test, the port name is `cpf2-1`, in which the last number 1 can be increased up to 4 to scan for the other line ports. The command to execute is the following one:

```
nos-show-platform-port --port cfp2-1
```

If the selected port is valid and the module is correctly attached and enabled, the response of the command is expected to be similar to the following;

```
1 cfp2-1
2 ------------------ ------------------------------------------------
3 oper-status        openconfig-platform-types:ACTIVE
4 admin-state        ENABLED
5 optical-port-type  openconfig-transport-types:TERMINAL_LINE
6 ------------------ ------------------------------------------------
```

In particular, the `ACTIVE` and `ENABLED` states confirm that the line card is ready for use to enable the card. Otherwise, it may be necessary to activate it, and the following command can be used:

```
nos-set-platform-port --port cfp2-1 -a admin-state -v enabled
```

In this way, it will set the `admin-state` attribute to `enabled`, and in a few minutes the card should be enabled; in fact, running the above command should confirm the correct functioning of the device.

If the card is active, it is then possible to gather its configuration and measured data. The command that can be used for this purpose is the following one:

```
nos-show-platform-port --port cfp2-opt-1-1
```

Similarly to the previous case, the port cfp2-opt-1-1 can be adapted if a different port is used: in particular, the first digit represents the port number (in this case 1), whereas the second is a *sub-number* which has always been left equal to 1 for all the ports.

An example of its output is the following:

```
config:
  frequency                        192925000M
  target-output-power              -3.2
  operational-mode                 2304
  line-als                         NONE
state:
  oper-status                      [...]:ACTIVE
  frequency                        192925000M
  target-output-power              -3.2
  operational-mode                 2304
    modulation-format              [...]:MODULATION_FORMAT_DP_QPSK
    bit-rate                       [...]:TRIB_RATE_200G
    fec-coding                     [...]:FEC_O
  line-port                        cfp2-1
  [...]
  output-power                     -3.19
  input-power                      -8.78
  chromatic-dispersion             6553.0
  polarization-dependent-loss      0.5
  osnr                             2.84e+01
  carrier-frequency-offset         -26.0M
  pre-fec-ber                      3.21e-08
  post-fec-ber                     0.00e+00
```

Note that in that output, the symbol `[...]` represents a string that has been removed to limit the length of the message.

As it is possible to see, all the parameters are directly readable from the terminal, and this can be helpful to check that the device is working correctly. However, as mentioned earlier, even if the steps performed are very effective, the text-based formatting of the output makes it difficult to collect the data in an automated way. For this reason, the terminal-based approach is recommended only for sporadic configuration and debugging, while the NETCONF approach is preferred for continuous use.

2.1.4 The Device Capabilities

The NETCONF protocol described above provides the ability to retrieve the capabilities associated with the operational modes described in the 2.1.1 section. This is done by issuing a *get* command and then applying a filter to the *operational-modes* properties. The results have been further filtered to list only the values that correspond to the operational modes given the transceiver in use. Some of the results provided have already been analyzed to study the limitations of the

equipment, but new insights have been gained, and are described in the following paragraphs.

The Baud Rate

The concept of the Baud Rate has been introduced in the section 1.4.1 related to the fundamental concepts, but in this section it is analyzed how its value affects the bit rate when other parameters are taken into account. By looking at the results provided by the capabilities request, the following values have been found:

Operational Mode	Line Rate	Modulation Format	Baud Rate [GBd]
1104	100 Gbps	DP-QPSK	27.9
2304	200 Gbps	DP-QPSK	63.1
2308	200 Gbps	DP-16-QAM	31.6
4308	400 Gbps	DP-16-QAM	63.1

Table 2.3: Baud Rate of different operational modes

As it is possible to see, the symbol rate is strictly related to both the bit rate and the modulation format as follows:

- Given a modulation format, to double the line rate, the symbol rate must also be doubled. For example, with DP-16-QAM modulation, to go from 200 Gbps to 400 Gbps, the baud rate is doubled.
- Given the baud rate, doubling the constellation size doubles the line rate. This is the case, for example, for the second and fourth modes of operation, where moving from DP-QPSK to DP-16-QAM doubles the line rate because the number of bits per symbol increases from 4 to 8.

The FEC Overhead

The importance of forward error correction has been described in the basic concepts, but thanks to the additional data collected, it is possible to calculate the overhead introduced. In fact, looking at the same table above, we can see that in all cases the baud rate appears to be higher than it should be, taking into account the other parameters. As an example, looking at the last row of the table, a rate of 400 Gbps with DP-16-QAM modulation (corresponding to 8 bits per symbol) should have a symbol rate of $400/8 = 50$ GBd. On the contrary, the symbol rate obtained is 63.1 GBd: the ratio between the two values is $63.1/50 = 1.262$, corresponding to an overhead of 26.2%. The same calculation can be carried out for all the possible combinations, obtaining the same 26.2% for all of them except the first one, where the value is reduced to 11.6%. Moreover, this difference is confirmed by the fact

that the first combination, corresponding to the 100 Gbps line rate, is the only one that uses a different error correction algorithm, as defined in the table 2.2.

The Roll-Off

The roll-off parameters defines the characteristics of the raised cosine shape, at it has been described in the section 1.4.1. In the Phoenix transponder, its value ρ is set to 0.2 for all line rates and modulation formats and cannot be changed. This results in a defined broadening of the spectrum used to transmit the channel.

The channel width

The values described above can be used to compute the total channel width. The equation of interest is:

$$B_{ch} = (1 + \rho) \cdot R_s \tag{2.1}$$

in which:

- R_s is the symbol rate;
- ρ is the roll-off factor;
- B_{ch} is the total width of the channel in use.

Taking into account the values obtained previously, the channel widths are reported in Table 2.4. However, it is important to remember that often the signal widths are approximated to the smallest multiple of 12.5 GHZ that contains the channel itself, as it has been briefly described in Section 1.4.2; in any case, the computed value is the one that is generally used to calculate the performance of the device, since it depends directly on the transponder's configuration.

Operational Mode	Line Rate	Modulation Format	Baud Rate [GBd]	Roll-Off factor	Width [GHz]
1104	100 Gbps	DP-QPSK	27.9	0.2	33.48
2304	200 Gbps	DP-QPSK	63.1	0.2	75.72
2308	200 Gbps	DP-16-QAM	31.6	0.2	37.92
4308	400 Gbps	DP-16-QAM	63.1	0.2	75.72

Table 2.4: Computed channel width

The Chromatic Dispersion

The general definition of the chromatic dispersion have been detailed in the section 1.3.2. By performing the collection of the capabilities of the transceivers, it has been discovered that the Digital Signal Processing (DSP) units can tolerate a maximum amount of chromatic dispersion that depends on the line rate and the modulation format as summarized in the table 2.5.

Operational Mode	Line Rate	Modulation Format	Maximum CD [ps/nm]
1104	100 Gbps	DP-QPSK	18000
2304	200 Gbps	DP-QPSK	24000
2308	200 Gbps	DP-16-QAM	24000
4308	400 Gbps	DP-16-QAM	12000

Table 2.5: Maximum supported Chromatic Distortion

It is important to note that for most of the experiments performed for this work, the effect of chromatic dispersion is negligible, as its effects are only visible after several kilometers of fiber, which is orders of magnitude greater than the distance over which the signals under test have propagated.

2.2 The Cassini transponder

Cassini is an open and disaggregated optical transponder with a modular optical interface design. Its high level of functionality is similar to that of the Phoenix transponder: for this reason, the following sections are focused on the main differences.

The Interface Ports

The Cassini transponder can support up to 24 traffic interface ports of two different types, similar to the ones typical of the Phoenix:

- 8 *line card* slots for QSFP28, with both DCO and ACO modules;
- 16 QSFP28 ports at 40/100GbE.

The device connections

Similarly to what is has been described in section 2.1.2, the connection with the Cassini transponder can be performed by using both the terminal based and the NETCONF approach. However, the command line syntax is different in respect to

the one described above, and for this reason the most important commands for the studies of this work are described in the next paragraphs.

2.2.1 The Cassini configuration

Even if there are several similarities in respect to the Phoenix transponder detailed above, in this case it is possible to configure independently three parameters only:

- The output power (expressed in dBm);
- The frequency (expressed in Hz in the range between 191.15 and 196.10 THz);
- The modulation format, that can be DP-QPSK or DP-16-QAM for all cards, and additionally can be DP-8-QAM for the DCO modules only.

It should be noted that due to the transponder's compatibility with both ACO and DCO modules, it is possible to compare their respective performances in the following sections. On the contrary, this was not feasible with the Phoenix transponder, as it exclusively supports DCO modules.

Similarly to the Phoenix transponder, also in this case it is possible to use the terminal-based approach to connect to the device in order to query its status. For this task it is possible to use the `OcNOS` operating system, to which it is possible to issue several commands that are detailed in this section. At first, it is useful to gather the information related to the connected transceivers, and to do so it is possible to execute:

```
show coherent-module interface-mapping
```

Since the Cassini transponder has 8 *line ports*, this command returns a list of eight elements similar to the two reported below:

```
1  ------------------------------------------------------------------------
2  Slot-no    Module Type     Port            Hostif-no       Netif-no
3  ------------------------------------------------------------------------
4  [...]
5  3          ACO             ce21            0               0
6                             ce22            1               0
7  [...]
8  5          ACO             ce25            0               0
9                             ce26            1               0
10 [...]
```

In this case, the output has been truncated to only show the used ports which, in this case, are the number 3 and 5, whereas the other six unconnected are blank. This command is especially useful to detect if the modules have been set up correctly and if they are ACO or DCO, since the second column changes accordingly.

Additional information can be obtained by running a specific command for the slot of interest, one at a time, obtaining all the collectable data from the card itself:

```
show coherent-module 3
```

The command in the given example can be used to read all the statistics from the module number 3, but in general this is not used since the length of the output makes it preferable to query the data in an automated manner, using the NETCONF approach. At the same time, however, in order to obtain a brief description of the real-time performances of the modules with one command only, it is possible to request a *summary* as follows:

```
show coherent-module summary
```

The response of the command is similar to the following, and is automatically filtered in such a way to show only the active modules, hiding the unused slots:

```
1  ------------------------------------------------
2  Slot License Information
3  ------------------------------------------------
4  Maximum Licenses      : 2
5  Available Licenses    : 0
6  Used Licenses         : 2 [Slots : 3, 5]
7
8  ------------------------------------------------------------------------------
9  Slot Module Netif       Modulation/      InputPower  preFECBER
10      Status OperStatus  OperationalMode              LaserFreq
11 ------------------------------------------------------------------------------
12 3    ready  ready       dp-qpsk          -6.75dBm    2.3427826e-10
13                                                      195800000000000Hz
14 5    ready  ready       dp-qpsk          -25.07dBm   2.514967e-10
15                                                      193468750000000Hz
```

This example can be used to check whether the device is operating correctly (using the `ready` states) and the module configuration. For the setup under test, it is possible to observe that there are two valid slots, named 3 and 5, which can be controlled independently.

the slot 3 was used, but there was a second connected card in slot 5, set to a different frequency.

The use of the command line utility was particularly useful when changing the frequency or the modulation format with the ACO cards because, as it will be described later, this operation was quite long and could lead to errors in which the Module Status changes to `Initialize` and does not come to `ready` again up to a device reboot. On the contrary, for the data collection (and in particular for reading the input power and the BER value) the NETCONF approach was preferred thanks to its easier integration in an automatic script.

2.2.2 The device capabilities

The list of the device capabilities can be retrieved by using NETCONF or via the terminal issuing the command: `show coherent-module operational-modes`.

Mode	Speed [Gbps]	Slot Width [GHz]	Modulation Format	FEC Mode
1	200	62.5	DP-8-QAM	15per-denali
2	200	37.5	DP-16-QAM	15per-denali
3	100	37.5	DP-QPSK	15per-denali
4	100	37.5	DP-QPSK	15per-everest
5	100	37.5	DP-QPSK	otu4-g709
6	100	37.5	DP-QPSK	otu4-7per-staircase

Table 2.6: Cassini capabilities

As it is possible to see from Table 2.6, differently from the Phoenix transponder, in this case it is only possible to transmit at 100 Gbps or 200 Gbps, which limits the maximum line rate. At the same time, a new modulation format is introduced, `DP-8-QAM`, which can be used to achieve the same 200 Gbps as `DP-16-QAM`, but with double the slot width, thus with a more robust modulation.

2.3 Other devices

In order to build a complete setup and perform data collection, it is necessary to use other equipment as described in this section.

2.3.1 Optical Spectrum Analyser

A spectrum analyzer measures the magnitude of an input signal with respect to its frequency: in this context, it can be used to measure the power of the spectrum of the channel under test. In the setup used in this work, it has been used toe the ANDO Optical Spectrum Analyser (OSA) from Yokogawa. It can be controlled programmatically using a GPIB interface in order to send commands and to retrieve the measurements. This device has been configured to operate considering the wavelengths (and not the frequencies); for this reason, the following parameters are expressed in nanometers:

- The resolution bandwidth is used to define how large is the bandwidth of the band-pass filter in the instrument. A reduction of the value increases the accuracy of the measurement, but increases also the time required to perform

the scanning of the whole band of interest. In all the data collections, the band of 0.01 nm has been used.

- The *span* is the bandwidth under test: if the value is increased, the device will be able to analyze a wider range of frequencies, at the expense of a larger sweeping time.

- The number of points of interest: generally set to 1000, corresponds to the amount of points to be collected in the total bandwidth defined by the span. Once again, a greater number of points will require a larger sweeping time.

Moreover, at every use it is required to specify the central wavelength, in order to keep the channel of interest centered in the spanning window. To give a practical example of its use, it is possible to set the center wavelength at 1550 nm, which corresponds to 193.5 GHz, generally considered to be the center of C-band. In this case, the band of interest will be of 10 nm (or around 1.25 THz) around 1550 nm(corresponding to $1545 - 1555$ nm range). It will then be divided into 1000 pieces of 0.01 nm each in which the OSA will measure the received power.

2.3.2 Variable Optical Attenuator

An optical attenuator is a device that reduces the power of an optical signal in a fiber, typically uniformly over a given frequency range. In particular, a Variable Optical Attenuator (VOA) allows the operator to select the specific amount of attenuation to be set in the fiber line. The devices used in the following sections are manufactured by HP and can be controlled by software to specify an attenuation (in dB) to be applied to the band of interest. Even if these devices are very accurate in varying the attenuation, it is important to note that the total *absolute* attenuation does not necessarily correspond to the one specified, since it is required to take into account also other contributions, such like the connectors and the insertion losses that are external in respect to the instrument itself. For this reason, if the attenuation is set to 4 dB and then to 6 dB, it is possible to affirm that the difference in received power will be of 2 dB, even if no information can be provided on the actual measurable power (in terms of dBm).

2.3.3 Splitter

Optical splitters are passive devices that can be used to split an incoming input signal into several outputs according to a fixed power division rule.

The device has different applications in many practical scenarios, such as in the passive optical networks (PON), where several users can be connected to the central office with only one fiber [31]. However, for the purposes of this work, the main

use is to allow both the transceiver and the OSA to receive the same transmitted signal, as it will be described later in greater detail.

A noteworthy aspect of these devices is that, being passive, they must distribute the input power among all the outputs, which means that each output receives only a fraction of the total available power. Moreover, this division can be unequal, so that some outputs receive more power than others, but it is clear that the sum of all the outputs must be less than the input, also taking into account the possible presence of internal losses.

Finally, it is interesting to note that usually these devices are bidirectional, making them suitable for merging different input signals onto the same fiber.

2.3.4 Multiplexer and Demultiplexer

In the section 1.4.2 of the introduction it has been described the concept of the Wavelength Division Multiplexing and why it is largely used in the optical communication field. In general, WDM is achieved by merging and splitting optical signals based on their wavelength, and one of the most common techniques is by employing multiplexers and demultiplexers, which are complex devices controllable remotely by using a specific protocol over the network. However, these devices can be used also in several other ways, and for the purposes of this work, their main use is to *filter* an input noise by enabling or disabling the input frequencies: in practice, it is mainly used to select the frequencies of interest, while filtering away the ones outside the band of interest. In addition, this device is also able to apply a per-channel attenuation, which is particularly useful as a simple equalizer: it can be used in such a way as to obtain a flat output, eliminating any variability of the powers with frequency, such as tilts.

As a side note, for the uses described in the next sections, the device is only used as a multiplexer, and never as a demultiplexer; for this reason, in principle it can be used twice simultaneously taking advantage of the presence of the demultiplexer, which can be used "in reverse", also acting as a multiplexer [32].

Chapter 3

The devices characterization

The characterization was carried out independently on the two transponders with the aim of collecting comparable data in order to highlight the similarities and differences between the two devices.

3.1 Phoenix analysis

The data collection for the Phoenix transponder was performed using two different setups in order to obtain different information about its behavior under different conditions. The following section provides a detailed analysis of the setup and results.

3.1.1 The setup

The first setup considered is graphically represented in figure 3.1.

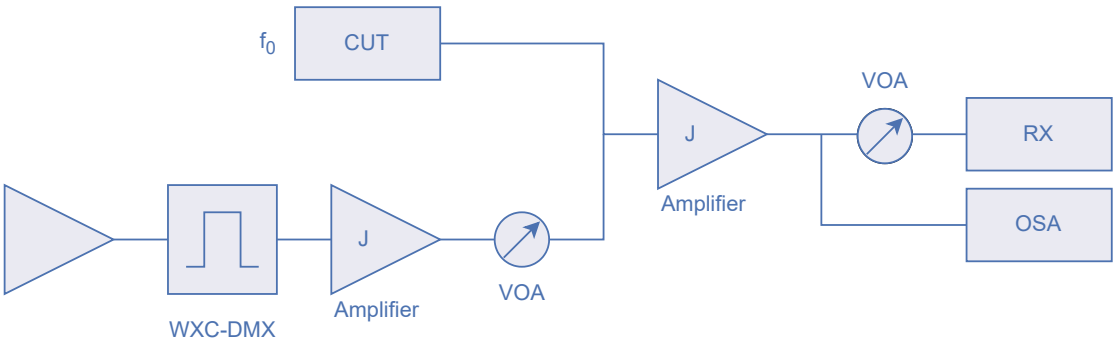

Figure 3.1: Phoenix setup

The Phoenix device is represented as the *Channel Under Test* (CUT) block on

the top-left part of the figure, and it is characterized by a central frequency f_0. The same transceiver is also used at the receiver side, named RX, which aims at detecting the transmitted signal after being affected by the different contributions of the other elements in the network under test. It is important to note that the configuration in which the same device is used at both the transmitter and receiver ends is known as *back-to-back* (sometimes *B2B*) and is a useful and cost-effective way to eliminate from the analysis the possible penalty introduced by a difference in device implementation or in the oscillator used in the two transceivers. Although this configuration is not expected to introduce any loss of generality, section 3.2.4 provides a comment on the main experimental differences observed in another scenario where two different devices (of the same type) are used together.

At the receiver end, the signal is also received by an OSA (whose functionalities have been described in section 2.3.1) in order to have the possibility of visualizing the power spectrum of the received signal, which can also be used to calculate the $\mathrm{SNR}_{\mathrm{ASE}}$. To achieve this, the signal goes through an optical splitter, which is a passive element able to split the incoming signal into two or more output ones. In particular, the device used in this setup is able to keep the 99.9% of the power in the main line towards the intended receiver, whereas the remaining 0.1% is directed to the OSA. This solution comes from the need of reserving as much power as possible to the card in order to be able to consider this split negligible from the signal's point of view. At the same time, the spectrum analyzer has a sensitivity so large that it can detect accurately also very low received power values, keeping the shape of its trace unaffected. Additional details are provided in the section related to the $\mathrm{SNR}_{\mathrm{ASE}}$ computation.

Inside the network, the signal is affected by an amplification and then by an attenuation obtained with a VOA, as it has been described in section 2.3.2. In particular, the use of the VOA is required in order to test the performances of the card when the received power is much smaller than the optimal one, whereas the amplifier (with a fixed gain) can be used to compensate for the insertion loss of the splitters and the VOA itself.

In order to study the variation of the performances in presence of noise, an additional set of instruments have been added, as it is possible to see in the bottom-left part of the same figure 3.1. In particular, the first triangle represents a noise source that can be shaped using a multiplexer to control the channels in which the noise is to be added. In this way, it is only added to a band 500 GHz wide around the channel of interest. The noise is then amplified using a fixed gain EDFA and then attenuated using an additional VOA, depending on the level of interest. In this way, the noise can be assumed to be flat on its band and its magnitude can be controlled by varying the attenuation of the VOA. This attenuator can also be switched off to measure the received signal without an additional noise source.

3.1.2 The data collection

In order to test the equipment, several configuration parameters had to be set:

- The central frequency of the channel under test. In order to fully characterize the device's behavior on the available spectrum, it has been deiced to use the frequencies in the full admissible range, always by setting the same value to several devices:
  - to the transmitter (which is also the receiver) in order to transmit at the frequency of interest;
  - to the multiplexer, in order to add the additional noise generated on the same band of the signal;
  - to the OSA to ensure that the channel is centered in the capture.
- The power of the transmitted signal, whose target value was 0 dBm in all the tests, since it corresponds to the optimal value for the device.
- The power of the received signal, controlled with its own VOA;
- The power of the additional noise, controlled with its VOA too.

At every combination of parameters, two sets of data have been collected:

- all the results provided by the Phoenix transponder;
- the full trace of the OSA.

3.1.3 The collected data analysis

As several types of data can be collected, it is possible to make some considerations about their relevance to the device characterization.

The power value

As already described in section 2.1.1, the card can be configured to provide an output power between -5 dBm and 1 dBm. This value is called *target output power* and in all the tests it has been kept constant at 0 dBm. However, since the output power depends on how the card amplifies or attenuates the signal, its real value is not guaranteed to be equal to the target one: for this reason, an additional parameter *output power* is taken into account, which is both reported as an instantaneous and an average value. In general, the obtained output power is very close to the target one: in fact, by looking at the Figure 3.2, it is possible to see that almost 84% of the cases considered had an output power equal to the

target power (to the second decimal place, which is the available resolution), and only 1.67% had an error greater than 0.02 dBm. Moreover, since no pattern in the variation is visible even by changing the frequency or the modulation format, it has been decided to consider the output power as constant during all the following tests.

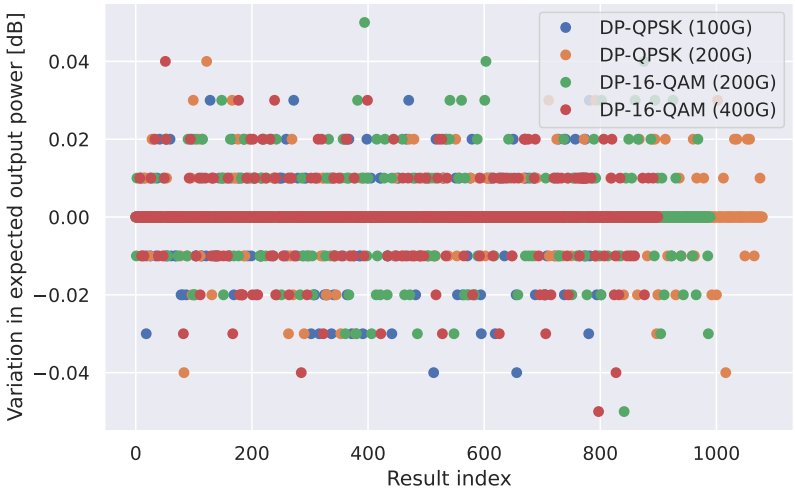

Figure 3.2: Difference in the output power in respect to the target one

With the same report from the transceiver it is possible to obtain information on the received power. It is again expressed in dBm (with two decimal places) and the "instantaneous" value is used instead of the average one, since the difference is very small, and it is not possible to easily modify the averaging time window.

The BER value

Among the several values collected by the Phoenix transponder, an interesting comment can be done in respect to the bit error rates. These values are reported by the device in two different ways:

- The *pre-FEC* BER represents the error probability typical of the signals received from the channel;
- The *post-FEC* BER represents instead the probability of having an error that cannot be corrected using the forward error correction algorithms. This quantity is provided as an "instantaneous" value, together with a minimum, maximum, and average: in order to be consistent with the *pre-FEC* quantities, only the instantaneous value is considered. [33]

Since they are probabilities, the corresponding value is a number such that, by definition, $0 \leq \text{BER} \leq 1$, even if it is very uncommon to have values greater than 0.02, since an error probability larger than 2% can not be corrected by the FEC.

In the following sections the value of interest is always the *pre-FEC* BER, since it is the only one that is related to the transceiver's ability to decode the signal from the noisy channel. Moreover, in all the applications in the optical domain, the transceiver will employ a Forward Error Correction algorithm that is expected to correct the said errors in order to provide an error-free digital output signal. These algorithms are able to work correctly only if the probability of error is limited and lower than a given maximum, which depends on the implementation characteristics. For this reason, in general, the operating conditions of the devices are always far below the *threshold* that limits the capabilities of this algorithm, making the *post-FEC* BER always zero, since all errors can be corrected.

However, it is important to know that in rare situations the error probability is higher than the threshold mentioned above, causing some errors not to be corrected, but at the same time it is lower than the amount that causes the transceiver to stop working. Under these special conditions, it is possible to briefly observe uncorrected errors, which is always an undesirable behavior from the user's point of view.

As it will be possible to see later, the range of uncorrected errors is quite narrow: in fact, if the channel conditions improve slightly, the error probability drops below the threshold that causes all errors to be corrected; otherwise, if the conditions worsen, the transceiver stops working completely.

The SNR value

The importance of the Signal to Noise Ratio has already been described in section 1.4.3, and in this context it becomes of great interest when it is compared to the device performance, in order to understand how they are affected by the quality of the received signal.

In general, the SNR can be computed in several ways, and in the setup under test there is the possibility to obtain its value by looking at the resulting values from the card's readings or by analyzing the OSA trace. Both possibilities are explored in this section.

The card OSNR

The transponder is able to provide an information related to the card SNR under two different forms:

- The OSNR, which should represent the value of the Optical SNR;
- The ESNR, which should be related to the Electrical SNR, that is moreover provided four times, with its instantaneous value, an average, and a minimum

and maximum. As a side note, "ESNR" is not compliant with the definition provided in section 1.4.3, but it does not introduce any ambiguity as it will be described later.

By comparing the 5 different values provided after each query of the instrument, it is possible to see that the values are almost always equal one with the other. The table 3.1 contains a comparison of values considering different modulation formats and line rates in the rows and different frequencies in the columns. Each cell shows the percentage of values collected at that frequency and modulation format where at least one of the 5 values is different from the others. As can be seen, these quantities are very small, often equal to 0%, and the highest values are obtained with the 100 Gbps DP-QPSK modulation, where the peak value is equal to 3.7%. As a result, it can be concluded that more than 96% of the collected data had all five values equal to one of the others. This means that the algorithms implemented in the card used to compute these quantities are most likely very similar, and for this reason it was decided to consider only the OSNR value to remove the dependence on the time average, and, as anticipated, the "ESNR" is avoided to remove any possible ambiguity.

	192 THz	193 THz	194 THz	195 THz	195.8 THz
1104	3.7%	3.7%	3.1%	2.5%	1.2%
2304	0.9%	0.0%	0.0%	0.9%	0.5%
2308	2.5%	2.0%	2.0%	2.0%	0.0%
4308	2.2%	2.2%	0.0%	1.7%	1.1%

Table 3.1: "ESNR" vs "OSNR" differences in the Phoenix's reports

Although the OSNR of the card is provided by the transponder, it is important to note that its value cannot be considered reliable because the transceiver is not able to calculate it accurately. This is due to the fact that the transceiver is not able to measure the signal power and the noise power separately, but only the total power received in the band of interest. As a result, it does not have enough data to calculate the OSNR correctly, but it tries to estimate it anyway, using a deterministic approach that always produces a predictable result.

In any case, the data collected can be used to plot a BER vs OSNR curve to show its behavior under different conditions. In order to plot them, it has been selected the whole list of points, gathered with all the frequencies, received powers and noise attenuations. The figure 3.3 shows a comparison of the curves obtained with different operational modes (i.e., changing the symbol rate and modulation format).

A notable aspect of the curves is that they differ significantly depending on the modulation format. This behavior is totally expected: in fact, the higher symbol

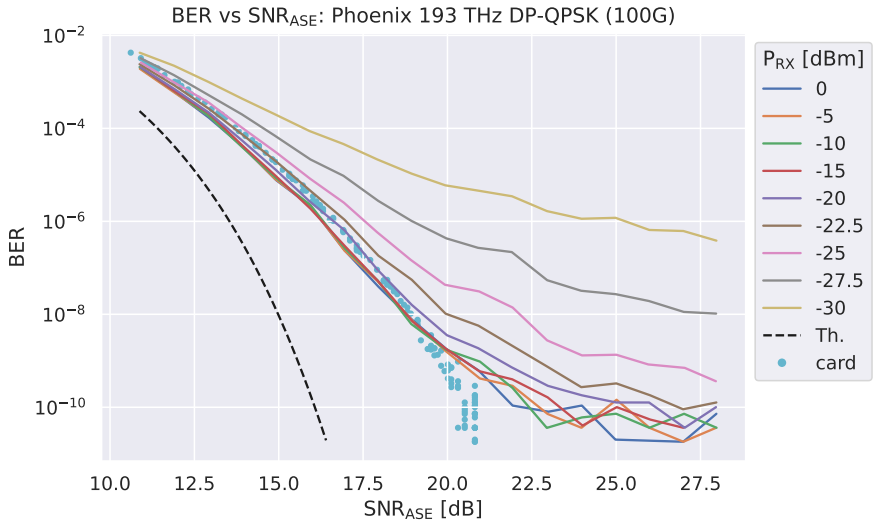

Figure 3.3: BER vs $\mathrm{SNR_{ASE}}$ plot with the Phoenix card data

rate and the more complex constellation require a higher OSNR in order to provide the same BER value. Similarly, it is possible to consider the same relation by fixing the OSNR value: in this case, it is clear that the simpler modulation formats and smaller symbol rates are able to provide a lower resulting bit error rate.

On the contrary, the unexpected behavior is that all points fall perfectly on a well-defined curve and seem to be completely unaffected by variations in frequency and received power. In practice, this result is completely unrealistic and confirms the previous comment regarding the unreliability of the OSNR values calculated by the card. For this reason, these OSNR readings can be used as an interesting comparison with other quantities, but they can never be used for practical calculations.

Moreover, an additional noteworthy comment has to be made in respect to the band of the noise. In fact, the power of the noise must always be referred to a known band, and two noise quantities can only be compared if their reference is the same.

In practice, it is common to refer the noise to the signal bandwidth R_s in order to have information about the amount of noise overlapping the signal of interest. The Phoenix transponder, on the other hand, follows a different standard where the reference band is fixed and equal to 0.01 nm, independently of the channel bandwidth. Therefore, it is required to convert the values provided by the card to the band of interest. This can be done considering the fact that the noise is defined as flat in frequency, and so it is possible to proportionally scale the values accordingly to the two definitions. In practice, it is possible to consider a band of 0.01 nm equal to 12.5 GHz around the center of the C-band, and so the power of

the noise can be multiplied by $R_s/12.5$ (with R_s in GHz). This is also especially simple in the log-scale, since this factor becomes an additive value, making this quantity easily comparable with the one provided by the OSA, as it is explained in the next section. In any case, this difference in the considered bandwidth is the reason at the basis of the fact that the OSNR of the card needs to be converted to an $\mathrm{SNR_{ASE}}$ value in order to make it compatible with the other measurements.

The OSA $\mathbf{SNR_{ASE}}$

Even if the card provides an OSNR reading, it has been shown to be unreliable. For this reason, it is possible to use the Optical Spectrum Analyser readings to accurately compute its value.

As it is possible to observe from the figure 3.1 related to the setup configuration, the OSA receives the same signal received by the card. In fact, the signal in the network is split just before the VOA, in such a way that the power received by the spectrum analyzer is not affected by the attenuation of the VOA, but it is always strongly attenuated by a constant amount that can be computed knowing the characteristics of the splitter used. In fact, it is known that the device delivers at its secondary output a power which is equal to the 0.1% of the incident power. For this reason it is possible to perform the computation provided in equation 3.1.

$$P_{out}^{dBm} = 10 \cdot \log_{10}\left(0.1\% \cdot P_{in}^{lin}\right) = P_{in}^{dBm} - 30\mathrm{dB} \tag{3.1}$$

As it is possible to see, a splitter with an output of 0.1% reduces the power values by 30 dB. In any case, it is important to note that the splitter does not affect the value of the SNR in the line: in fact, the attenuation is proportional to both the signal and the noise, keeping their ratio unchanged. For this reason, the OSA is in general not used to measure the received power level, but only in the computation of the $\mathrm{SNR_{ASE}}$ as follows.

As shown in section 2.3.1, the OSA readings consist of two equal-length arrays containing the list of scanned frequencies and the corresponding measured powers. Due to the configuration of the instrument, the central frequency of the channel is expected to be in the middle of the available frequencies, and this should also correspond to the maximum power level. The figure 3.4 shows an example of the gathered data in which it is possible to consider three main elements:

- in the center there is the channel under test, which is represented as a peak with higher power;
- around the channel there is a region around 500 GHz wide that corresponds to the additional noise;
- on the left and right side there is a region characterized by the minimum power level corresponding to the unused frequency space. In principle, no

power should be present, but due to the sensitivity limitations of the OSA, a flooring is always visible, and the corresponding power is therefore measured between −60 and −70 dBm. As a side note, the *MID* sensitivity of the device can be increased in order to provide a lower minimum, but in general it is not required to do so, since this value is so small that it doesn't introduce any useful information, and can be safely approximated to zero on the linear scale, as expected. However, it is important to note that a variation in the sensitivity causes a variation in the sweeping time of the device: as a consequence, if the sensitivity is increased, the OSA's scanning time will be larger.

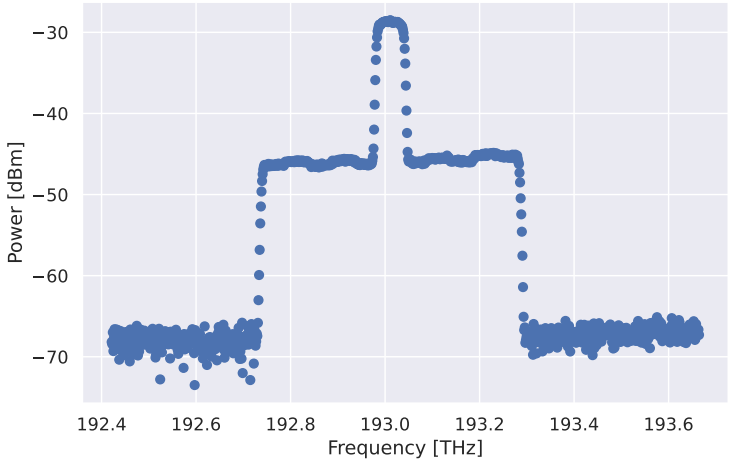

Figure 3.4: Example of an OSA capture

The $\mathrm{SNR}_{\mathrm{ASE}}$ calculation involves calculating the ratio of the power of the useful signal to the power of the additional noise: for this reason, only the first two areas described above are taken into account. The process is then split into two parts.

The power of the signal Firstly, the central frequency of the channel under test must be determined: its value is known from the configuration of the instrument, but it is checked again with the OSA to avoid any bias in the laser or detector. For this reason, the peak is found by taking into account the highest power values and the fact that the peak must be preceded and followed by a region of lower power. Once the peak has been found, the corresponding frequency is considered as the central frequency of the channel under test.

The received power must then be calculated. This is done by numerically integrating the curve representing the peak to estimate the total received power as a function of the peak width. In particular, the width of the signal is computed

analytically considering the Baud rate and the roll-off factor, as it has been described in section 2.1.4. The value obtained with this computation is considered to be the power of the signal plus the power of the noise on the bandwidth of interest; however, the power of the noise computed later can be subtracted from this value to obtain an estimate of the signal power only.

As a side note, from the same figure 3.4 it is possible to observe that the peak value has a power around $-30\,\text{dB}$, which is compatible with what has been computed with the equation 3.1, which considered a transmitted power of $0\,\text{dBm}$, while neglecting the contributions of the amplifier and the additional losses due to the splitter and its connections.

The power of the noise The definition of the SNR requires the knowledge of the power of the noise in the same band of the signal, since it is the only region in which it can affect the performances. At the same time, it is in general not possible to measure it on the same band while a signal is transmitting its own power because the two quantities will sum together, and it will not be possible to distinguish the two contributions.

However, in the setup under test, it is possible to observe that the width in frequency of the noise is much larger than the one of the signal. In fact, by looking at Figure 3.4, it is clear that the noise level can be considered as flat in frequency around the channel of interest. This property can be used in order to compute the noise power in a band close to the band of interest, but not overlapping with it. In particular, it has been decided to compute the noise power considering a central frequency shifted to the left and to the right by $120\,\text{GHz}$ in respect to the central frequency of the channel under test. In particular, this value is totally arbitrary, but in this way the new region is completely unaffected by the presence of the signal, and at the same time it is completely contained in the region in which the noise can be considered flat.

Moreover, it is important to note that it has been decided to perform the said shift both to the left and to the right in order to compensate for the possibility of having a tilt in the noise level: in this way, the two resulting values can be averaged in order to obtain a value that should represent the level of the noise under the channel of interest.

The final result of the SNR computation Knowing the powers of the signal and the noise, the SNR can be calculated by performing the ratio between the two quantities, which must be expressed in linear scale; the SNR is then converted in the more common decibel representation.

This complete process can be summarized with the figure 3.5 in which it has been highlighted the most important regions:

- the vertical red line corresponds to the central frequency of the channel;
- the region between the two green lines is the one used for the computation of the power of the signal;
- the two regions between the purple lines are the ones used for the noise computation, which will then be averaged together.

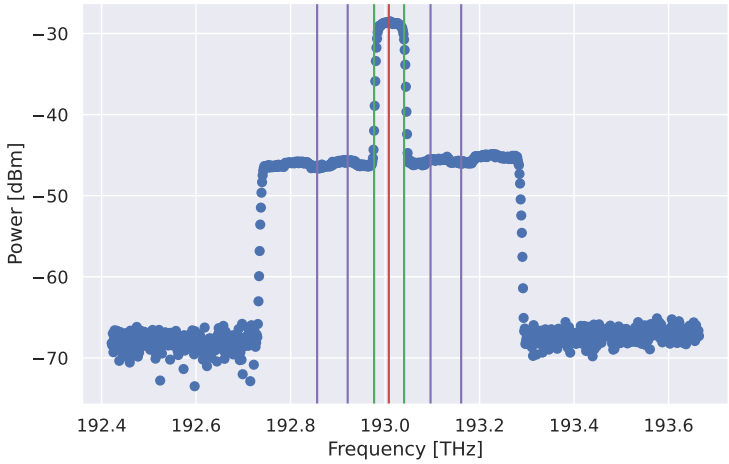

Figure 3.5: Example of an OSA capture with the bands of interest

Comparison of the card and OSA SNR values In the previous section 3.1.3 it has been described how the card computes the SNR_{ASE} value and why it cannot be considered reliable. Since the same value can also be computed accurately with the OSA, it is then possible to compare the different results.

Moreover, it is also possible to consider an additional curve that can be obtained considering the numerical relation expressed in equation 3.2 in which the BER value is computed starting from an SNR value and some constants.

$$\text{BER} = k_1 \cdot \text{erfc}\left(\sqrt{k_2 \cdot \text{SNR}}\right) \tag{3.2}$$

As it will be described in the following chapters, the SNR is expected to represent the *total* value, considering together all the possible noise contributions. Nevertheless, it is possible to consider the SNR as upper-bounded by the SNR_{ASE} introduced by the line. The mathematical reasoning will be described later in greater detail, but it is clear that if only one contribution is considered, than the

BER value will correspond to a *best case*. Even if this approximation is inaccurate, it can be used as a reference curve in the comparison of the obtained results.

On the contrary, the k_1 and k_2 values are known in the literature and depend exclusively on the selected modulation format. The values of interest for the Phoenix and the Cassini devices are only three, and are reported in Table 3.2. [34]

Modulation Format	bit/symbol	k_1	k_2
DP-QPSK	4	1/2	1/2
DP-8-QAM	6	2/3	3/14
DP-16-QAM	8	3/8	1/10

Table 3.2: k_1 and k_2 values at different modulation formats

The curve comparison can be performed in different conditions: in the setup under test, it is possible to obtain different results by varying the modulation format, the operating frequency and the received optical power. As an example, it has been decided to consider only the 193 THz central frequency and the DP-QPSK modulation format, whose theoretical limit is easily obtained using the equation 3.2 with $k_1 = k_2 = 0.5$. In figure 3.6 it is possible to see the different BER vs SNR_{ASE} curves at different received power levels, and they can be compared in several ways.

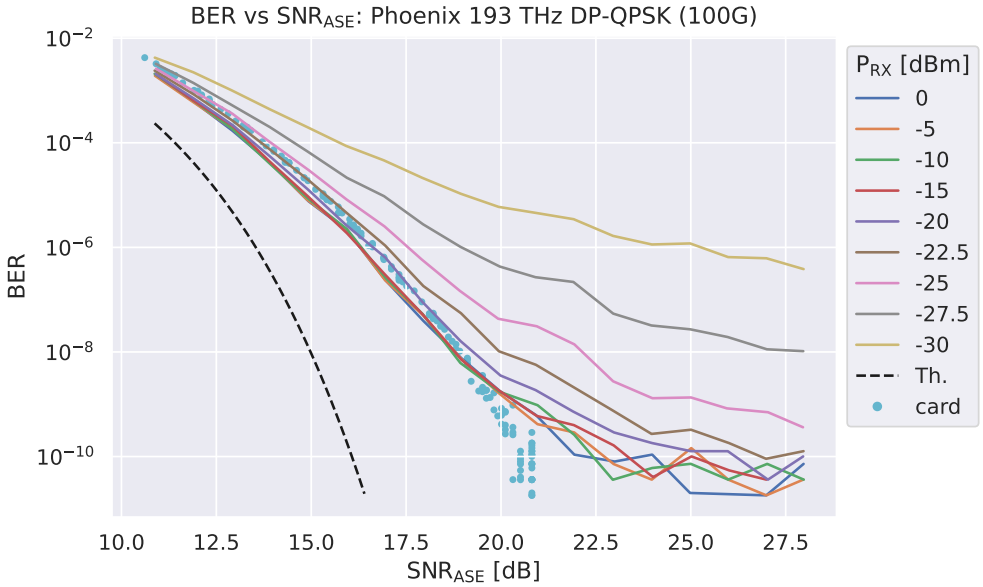

Figure 3.6: BER vs SNR_{ASE} curves (card and OSA comparison)

The theoretical curve The first important consideration regarding the shape of the curves is that the one representing the *best case* is always to the left of all the others that come from the *measured* data points. This is consistent with the fact that when considering any *measured* curve, it is necessary to use a higher SNR compared to the best case curve in order to obtain the same BER value. This is due to the fact that the *measured* curve takes into account all the additional noise contributions that are neglected in the optimal dashed curve.

The card's data A second comparison can be made with the curve representing the values obtained directly from the card. The blue points are the same as those shown in figure 3.6, and once again they are independent of the received optical power, making it clear that the values are computed by an algorithm that takes into account only the resulting BER value. Moreover, the points tend to overlap with the curves corresponding to the OSA values measured at low attenuation and low $\mathrm{SNR_{ASE}}$: this suggests that the card's calculation follows a simple characterization curve obtained close to the optimal conditions. As a consequence, it is possible to suppose that the SNR provided by the card takes into account part of the additional noise contributions due to a first approximation of the device characteristics, but completely neglects the additional penalty due to a low received power condition.

The OSA's data Finally, an interesting remark must be made regarding the curves obtained with the OSA measurements with different attenuation conditions. As it has been described before, the VOA applied before the receiver is able to reduce the power of the received signal while keeping the $\mathrm{SNR_{ASE}}$ constant: for this reason, the curves in Figure 3.6 have the same set of points on the horizontal axis, but they can vary significantly on the vertical one. In fact, the performances of the devices are not constant with the received power and for this reason a new penalty must be taken into account. In particular, it can be seen that the curves with low attenuation (which gives a higher received optical power) are almost superimposed: this means that the transceiver is able to operate close to its optimum conditions. On the contrary, when the attenuation is increased (and the received power is reduced), the curves tend to be *higher*, in the sense that for the same SNR, the corresponding BER will be much higher. In this case, in fact, the penalty due to the low received power is no longer negligible, and an additional impairment must be considered. As it will be possible to see later, this impairment is mainly due to the device characteristics that make it operate suboptimally when the received power is too low.

In any case, it is possible to observe that the measured curves follow the same trend: the BER is increased when the $\mathrm{SNR_{ASE}}$ is reduced, whereas a flat region

is met in the right part of the plot. The main reason is that the BER value is the result of several contributions, one of which is the $\mathrm{SNR_{ASE}}$ described by the values in the horizontal axis. However, several other factors are of great importance, and they may be more or less relevant in respect to the $\mathrm{SNR_{ASE}}$ itself. A greater description of the different effects is provided in the next chapters, but a qualitative comment can be made by simply looking at how the curves evolve in the plot itself. In particular, on the right-hand side, the curves reach a flat area characterized by a marginal variation with the $\mathrm{SNR_{ASE}}$: this is due to the fact that, in these conditions, the device is the limiting factor in the performances and an improvement in the channel quality can no longer improve the performances. On the contrary, in the left part, the quality of the channel becomes so low to be the most significant contribution to the performances: for this reason, not only the BER is increased, but all the different curves tend to be closer one with the others, as their difference becomes negligible with respect to the values of the $\mathrm{SNR_{ASE}}$ itself. However, this BER increase reaches a maximum value roughly around 1×10^{-2}: in fact, in the section devoted to the description of the BER value, it has been shown that this amount is the *pre-FEC* BER, or the bit error rate prior to the correction performed by the FEC algorithm. This maximum obtained value corresponds to the BER *threshold*, which is the largest BER that can be fully corrected; if it is still increased, some errors will be left uncorrected, and the *post-FEC* BER will be non-zero anymore. Since this last condition has always to be avoided, the curves in Figure 3.6 do also provide a minimum $\mathrm{SNR_{ASE}}$ that should never be reached in normal operating conditions.

The input power dependence in respect to the additional noise

Similarly to what has been described related to the card's measure of the power, it is also important to distinguish the different contributions that can affect the received power value. The most notable ones are described in the following list:

- The transmitted power has a proportional effect on the received power. However, it has already been described that in the setup under test, the transmitted power is almost always equal to 0 dBm, so this contribution does not significantly affect the received power value.

- Fiber attenuation and other equipment losses reduce the available power, but this effect is expected to be constant over all measurements.

- The signal's VOA reduces the power by an amount that can be configured according to the user's needs. In particular, it is composed of two contributions: a fixed one that depends on the characteristics of the instruments, which can be taken into account in the constant losses of the instruments, and a variable

one that can be known exactly, since it is the value that the user can configure arbitrarily.

Moreover, an additional important consideration has to be made in respect to the additive noise. In fact, it covers a large band that overlaps the signal of interest, decreasing the signal's SNR_{ASE}, as it will be discussed in greater detail in other sections. However, as a side effect, this additional (noise) power reaches the card, which in turn will measure an increase in the received optical power.

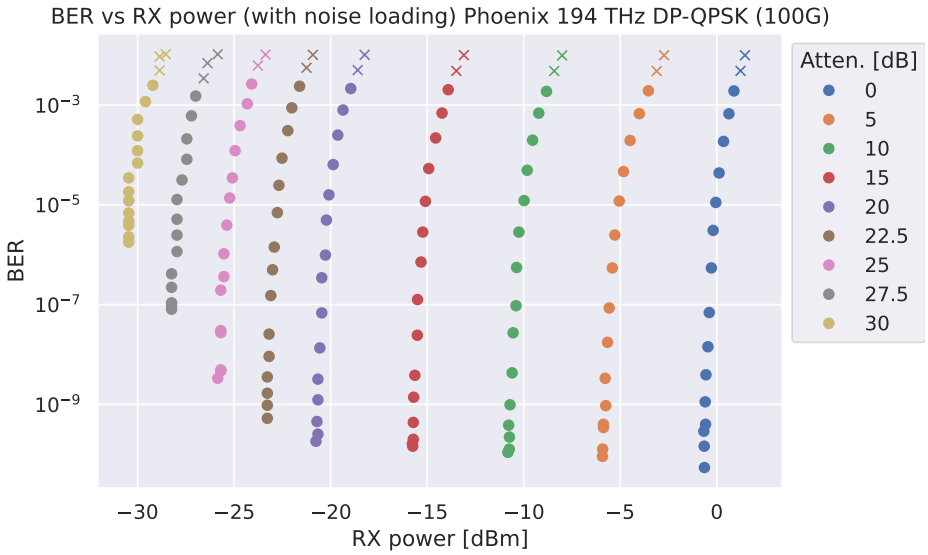

Figure 3.7: Received signal power with noise loading

This effect can be seen in Figure 3.7 in which several received powers are shown in relation to the BER value with different signal attenuations. In particular, the different colors represent signals affected by a different configuration of the VOA: as it is possible to see, when the attenuation increases (and the color changes) the points move to the left, toward a lower received power. This first consideration is totally expected since it directly reflects the change in the configuration of the VOA: in fact, the horizontal distance of the curves corresponds to the difference in the signal attenuations described in the plot's legend.

However, the interesting aspect is that given any signal attenuation (or given any color in the figure), several points can be obtained by changing the power of the additional noise. Clearly, the main effect already commented is that this causes a variation in the SNR_{ASE}, and as a consequence also the BER changes as well: an increase in the noise power increases the BER moving the points to a higher position. Moreover, at the same time the additional power due to the noise moves

the points slightly to the right, even if the same signal attenuation is enforced: the final result is that the sequence of the points is characterized by a movement towards the upper right position when the noise is increased, and the curves are not vertical but slightly bent to the right.

Additionally, it is possible to observe that the curves of different colors reach a different minimum value. In particular, the ones corresponding to a high received power (or low signal attenuation) can reach very low BERs, lower than 10^{-10}, whereas the ones with very low received power have a much higher limit, even around 10^{-6}. This is due to the fact that the low power condition introduces an additional penalty that reduces the performances of the system, even in the best conditions in terms of the $\mathrm{SNR_{ASE}}$: this behavior is the same that causes an increase in the BER vs $\mathrm{SNR_{ASE}}$ curves (for example the ones provided in Figure 3.6), and will be described in greater detail later.

Finally, the same figure can also be used to visually represent the BER threshold, as it has been described in a previous section: in fact, it has been highlighted with a filled dot the points in which the *pre-fec* errors are fully corrected, whereas a cross has been used in the cases in which some errors are left uncorrected also after the FEC. As it is possible to see, there is a clear maximum in the BER value that ensures that all the errors can be corrected, and this depends on the algorithm used and the corresponding required overhead. Moreover, it is important to note that this maximum is approximately constant with all the attenuations, and this is due to the fact that the ability of correcting the errors depends only on the FEC algorithm, and not on other transmission parameters.

The BER vs $\mathrm{SNR_{ASE}}$ curves

In previous sections it has been described how it is possible to gather the BER and to compute the OSRN values from the card and the OSA traces, respectively. With this information it is then possible to compute the BER vs $\mathrm{SNR_{ASE}}$ curves, which tries to show how the error probability changes with a variation in the received signal quality. As it has been shown in Figure 3.6, these curves are strongly affected by the receiver's input power, which tends to further increase the error probability at the same $\mathrm{SNR_{ASE}}$ value.

However, it is also important to note that a very strong dependence is due to the modulation format in use: to greatly appreciate this fact, it is possible to consider the Figure 3.8, in which the different curves have been obtained using different modulation formats, but always considering the same frequency (in this case of 193 THz) and received power (which was the highest achievable with the setup under test, around 0 dBm).

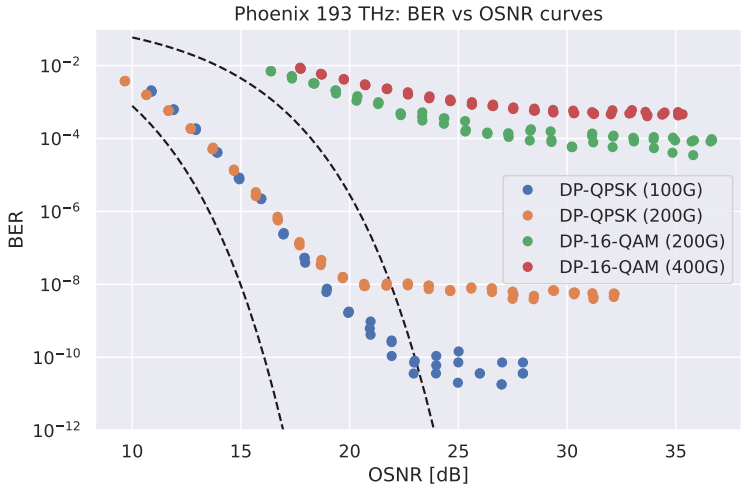

Figure 3.8: BER vs SNR_{ASE} curves with different modulation formats with high received power

As it is possible to see, all the curves have a similar shape, but there are also strong differences between them. In particular, all the curves show a strong increase in the BER when the SNR_{ASE} is reduced, whereas they find a flooring region in the right part: this result is entirely in accordance with what has been described previously, in relation to the Figure 3.6. However, the dependence on the modulation format causes two main effects on the curves that can be commented independently. At first, there is a strong difference in the minimum achievable BER values, which appears much higher when the modulation is more complex. This result is totally expected, since a more complex modulation reduces the relative distance between the transmitted symbols, increasing the probability of error at the receiver. As a consequence, the additional complexity does not allow the card to reduce the BER below a given limit even if the channel conditions are optimal.

Secondly, it is also interesting to compare the minimum SNR_{ASE} value of each curve. In principle, the SNR_{ASE} can assume any value, but the BER is directly affected by its variations, and at some point it will reach the threshold at which it is no longer possible to correct all the errors. In practice, this limit is visible in the figure since it corresponds to the maximum visible BER, after which a reliable transmission is no longer possible. The interesting aspect, however, is that the different modulation formats are characterized by a different mathematical relation between the two quantities, and for this reason, in the more complex modulation formats (like the DP-16-QAM), the given BER threshold is reached earlier in respect to the DP-QPSK case. In this particular example, the BER threshold was roughly around 1×10^{-2}, and the difference of the SNR_{ASE} values of

the two modulations in that condition is around 7 dB, which visually corresponds to the horizontal distance between the curves in the top-left part of the figure. The practical consequence of this is that in order to achieve transmission without residual errors after FEC and with the same performance, it is necessary to improve the channel quality by several dB when changing between the two modulation formats.

The other collected data

During the data collection, the card had the possibility of providing the user with additional measurements that have been collected, but that are not of great interest for the following computations. In this paragraph a brief comment is made on two of them in order to clarify the reasoning for this, whereas the *polarization dependent loss* and the *carrier frequency offset* have been neglected, the latter of which almost always returned a zero value.

The chromatic dispersion The card provides an information related to the chromatic dispersion which can be used to track its effect along the line. As it has been described in the section related to the fundamental concepts, this effect is due to the dispersive nature of the fiber and causes the distortion of the optical signal, possibly reducing the performances of the system. However, as it has been briefly anticipated before, most modern transceivers are able to fully counteract this effect in the digital domain: this means that a physical dispersion compensation is possible but is not required, and for this reason it is in general avoided.

Nevertheless, every receiver is capable of managing a maximum amount of chromatic dispersion, and for this reason it may be interesting to know the current value in order to make predictions related to safe operating margins. In any case, it is important to remember that this effect strongly depends on the fiber's length, and becomes relevant only after tens of kilometers. For this reason, in the setups under test it is safe to assume that the chromatic dispersion can be completely neglected without the introduction of any penalty. In particular, the obtained values in all the considered conditions are in a range around ± 20 ps/nm, which is orders of magnitude lower than the limits described in the table 2.5.

The Q-Factor The card provides an additional measurement of a quantity named *Q-value*, that is expected to give another representation of the quality of the received signal. In the studies related to the optical transmissions, this is sometimes used instead of the BER value, since both of them are related to the final effects that the signal's quality causes to the receiver's ability to correctly decode the symbols.

It is important to note that the relationship between the BER and the Q-Factor is mathematically described by Equation 3.3, and this implies that the knowledge

of one of the two is sufficient to compute the other, if it is required to do so [35].

$$\mathrm{BER} = \frac{1}{2}\mathrm{erfc}\left(\frac{Q}{\sqrt{2}}\right) \tag{3.3}$$

For this reason, in the next sections only the BER value is used, since it provides a clear measure of the amount of errors that are introduced in the transmission due to the quality of the received signal. However, it may be interesting to note that due to how the two quantities are defined, one increases while the other decreases. In fact, since the BER measures the amount of errors, an increase in the BER indicates a deterioration in performance, which is measured by a decrease in the Q-factor value. For completeness, a visual representation of the relation described in the Equation 3.3 is reported in Figure 3.9, in which it is possible to observe that the range of the BERs values of interest in the optical transmissions are roughly described by Q-Factors in the range between 2 and 7.

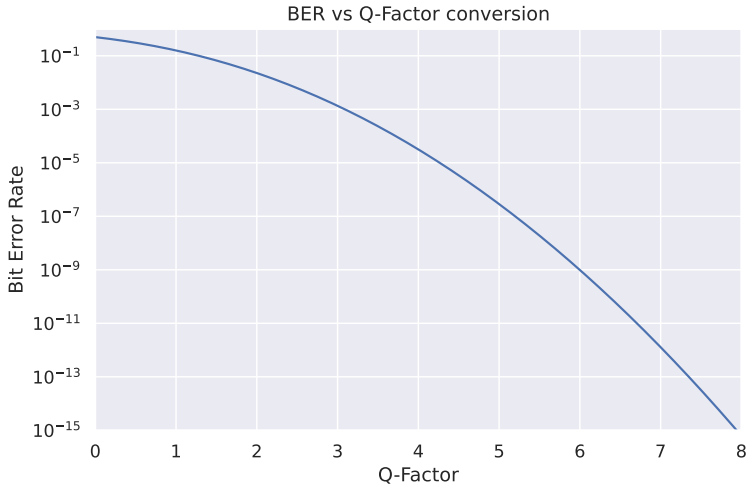

Figure 3.9: Relation between BER and Q-Factor values

3.1.4 The sensitivity setup

The data collected and analyzed in the previous sections was characterized by the superimposition of an useful signal and an additional noise source. As it has been shown, it enables the possibility of studying the variation of the performances in respect to the $\mathrm{SNR}_{\mathrm{ASE}}$. At the same time, it is interesting to study the variation in the performances when the received power changes, independently on the noise source. For this reason, a second setup described in the Figure 3.10 has been used.

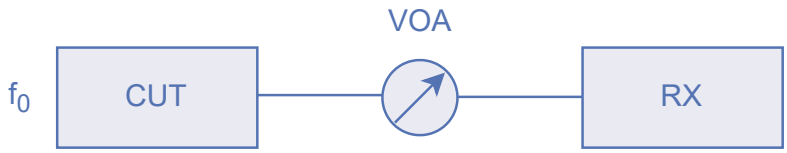

Figure 3.10: Phoenix setup without additional noise

As it is clearly possible to see, this setup is much simpler than the one used before, in Figure 3.1. The reason for this is that any additional element introduces penalties that must be taken into account: on the contrary, a very simple system is the closest to the ideal condition. In particular, by eliminating the additional noise source, several instruments can be removed from the line, leaving only the transmitter (which is also the receiver) and a VOA. It is important to note that the use of the attenuator is still necessary as the transmitter is capable of delivering an output power in the range between -5 dBm and $+1$ dBm: since it is very limited, additional attenuation is required to study the behavior of the device when the received power is much lower. Moreover, the OSA is not required anymore since with this setup it is not possible to define a noise level that can be used for the computation of the $\mathrm{SNR}_{\mathrm{ASE}}$ value. On the contrary, the configurations and the metrics collected by the transceiver remain the same, and for this reason the main steps required to perform the data collection are the same already described in section 3.1.2.

3.1.5 The sensitivity data analysis

The data collection was similar to the previous one. The main difference is that since there was no additional noise source, the corresponding noise VOA was also removed, and by avoiding the iteration over the noise attenuations, it was possible to increase the granularity of the signal noise and increase the number of points collected per configuration, resulting in a much smoother curve, without increasing the overall execution time required.

Similarly to the previous collection, the card has the possibility of reading the level of the received power. In particular, since the setup is very simple, it is possible to detail all the components involved in the power variations:

- The first important contribution is due to the transmitter, which has been configured in order to provide an output power equal to 0 dBm. For the same reasons as described in the section 3.1.3, it is possible to assume that this value is constant along all the measurements.
- The effects of the fiber can be neglected due to its length, which does not

introduce any noticeable attenuation;

- The VOA introduces an attenuation that depends on its configuration parameters. In addition, that, it is also required to consider a small additional reduction in the power due to the connectors and insertion losses.

The signal attenuation As described in the previous sections, the Variable Optical Attenuator can be used to apply an attenuation to the power of the signal.

Differently to the case considered in the previous setup, in this case there is no additional noise loading on top of the signal of interest: for this reason, the received signal power depends only on fixed quantities (that do not change during the data collection) and the configuration of the only VOA present in the setup.

In particular, the VOA can be precisely controlled, but the obtained attenuation can only be considered accurate if it is compared to another value provided by the VOA itself. For example, setting the VOA to attenuate 0 dB and then to attenuate 10 dB will change the output power by 10 dB, but will not give any information about the absolute value of the output power. In fact, even if the input power is known to be 0 dBm according to the card settings, it is necessary to take into account the additional loss due to the device: this is in principle unknown, but it can be assumed to be constant over all the valid power ranges. An example of this difference is provided in Figure 3.11.

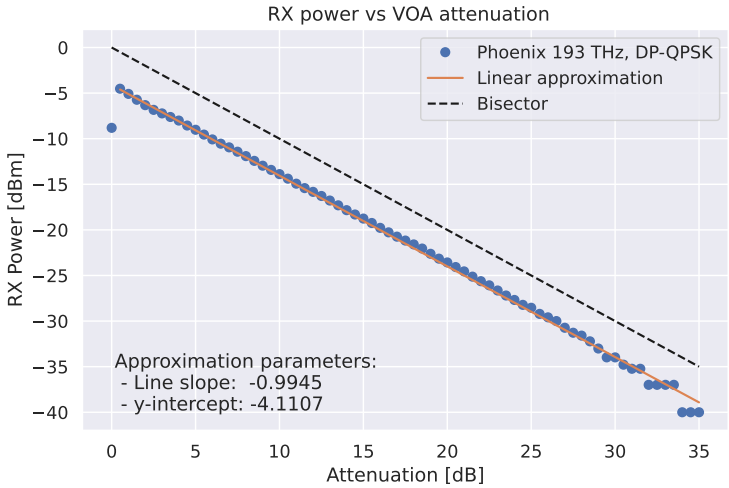

Figure 3.11: Measurable attenuation in respect to the VOA's settings

As it is possible to see, by neglecting few outliers, the relation between the required attenuation and the measured one is almost linear. This result confirms

that it is possible to accurately measure a difference in the received power by considering the same difference in the configuration of the VOA.

Moreover, it is possible to compute the linear regression that best approximates the points. In this specific case, the result is a line with almost unitary slope, and an intercept equal to $-4.11\,\text{dB}$. In particular, this final result shows that all the other contributions in the setup introduce a total additional attenuation of around $4.11\,\text{dB}$ on top of the attenuation set with the VOA configuration.

It is important to note that the same considerations can be repeated also for the first considered setup, but in that case the increased complexity due to the presence of additional elements such like the noise power, the splitters, and the amplifier would make the analysis less straightforward.

The minimum power values By considering the setup under test, it is possible to highlight specific boundaries on the possible values of the received power. In particular, since the target output power is fixed to $0\,\text{dBm}$ and all the possible contributions are attenuations, than it is clear that the received power is upper-bounded by the same value of $0\,\text{dBm}$. As it is possible to see from the vertical axes in Figure 3.11, this is further reduced by the additional elements, bringing the maximum allowed value to around $-4.11\,\text{dBm}$.

On the contrary, in principle there is no lower limit to the received power, since it is always possible to attenuate more; in particular, the used VOA can go as low as $-60\,\text{dBm}$. However, the transponder under test is strictly limited to a minimum power of $-40\,\text{dBm}$: this means that any value lower than this is always displayed as $-40\,\text{dBm}$, making it impossible to know its real value. In addition, the same number is used to represent the state in which the transceiver is not working, creating an ambiguity between the two conditions.
Although this representation is somewhat less obvious than other possible values, it is important to note that under normal operating conditions, such a low power level is never reached, and the transceiver is expected to stop operating well before this condition.

The BER values The absence of the OSA in the setup makes it useless any analysis of the BER in respect to the SNR_{ASE}, especially considering that the value provided by the card is unreliable for the same reasons as described in section 3.1.3.

On the contrary, it is interesting to compare the BER values in relation to the received power. The resulting curves are shown in Figure 3.12, which compares the different modulation formats at the same frequency of $193\,\text{THz}$.

This result shows different important characteristics of the transceiver under test. The first aspect that stands out is that the curves have a peculiar shape that clearly defines two regions:

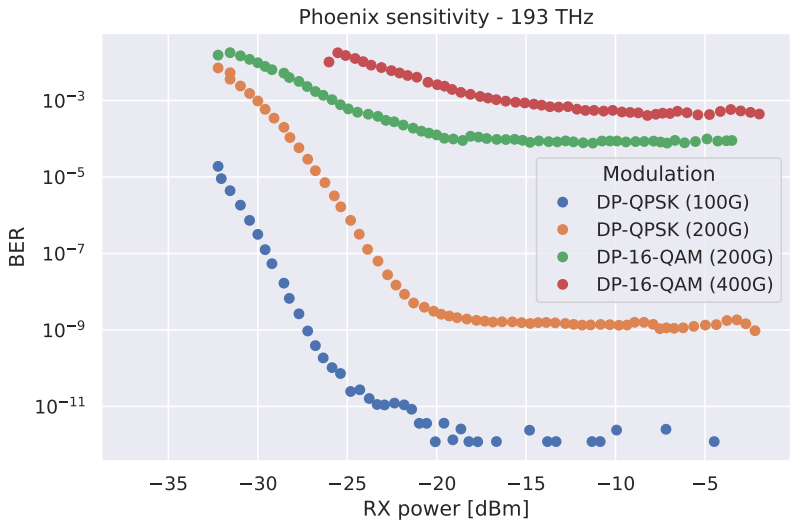

Figure 3.12: BER vs RX Powers in sensitivity configuration

- a first *high-power* region, in the right part of the chart which is characterized by almost flat curves, which tend to keep a constant BER value for large variations of received power;
- a second *low-power* region in the left part, in which the bit error rate increases rapidly when the received power decreases.

An interesting aspect is that this shape is quite similar to the one already described before in respect to the relation between BER and $\mathrm{SNR}_{\mathrm{ASE}}$ in Figure 3.6 and 3.8. However, the two characteristics are completely independent of each other and their similarity is only due to the fact that both the reduction in $\mathrm{SNR}_{\mathrm{ASE}}$ and the reduction in received power are *penalties* that affect the overall quality of the received signal.

Even if these regions are visible for all the modulation formats, it is very well-defined for the DP-QPSK modulation thanks to the fact that it spans a large range of BER values, reaching its floor after an almost straight decrease when the power increases. On the other hand, more complex modulations show the same behavior but on a much smaller range of values, making it less evident. In any case, these two regions are very different, and their properties are described in the two following paragraphs.

The minimum BER values By looking at the figure it is possible to observe that even though the overall shape is the same, they widely differ on an important aspect: the BER floor, which corresponds to the minimum level reached with their

flat part. In fact, this corresponds to the minimum bit error rate that cannot be further reduced independently on the received power level.

In particular, the DP-QPSK modulation is the only one that can obtain zero errors when the received power is high enough: this is also the reason why few points are displayed, since a zero-BER cannot be represented on a logarithmic scale. However, it is important to remember that the BER measure becomes unreliable when its numerical value is too small for the same reasons already described in respect to the Figure 3.8. In any case, such a small value can be practically considered equal to zero, since it is very far from the regions usually considered for a normal transceiver operation.

On the contrary, all the other modulations presented a minimum BER well greater than zero, which represents the fact that the received power level was not the only cause of errors in the transmitted information. In fact, the two more complex configurations, characterized by a DP-16-QAM modulation format, are the ones that hardly reduce their bit error rate with the power, following a similar curve, reaching a minimum up to six orders of magnitude higher in respect to the DP-QPSK ones. This result is expected due to the fact that a more robust modulation will always provide better performances in respect to more complex ones.

The comparison between the minimum BER values is reported in the table 3.3.

Operational Mode	Modulation Format	Line rate	Min. BER	Max. BER
1104	DP-QPSK	100 Gbps	0	1.1×10^{-5}
2304	DP-QPSK	200 Gbps	1.5×10^{-10}	6.1×10^{-3}
2308	DP-16-QAM	200 Gbps	4.6×10^{-5}	1.7×10^{-2}
4308	DP-16-QAM	400 Gbps	3.1×10^{-4}	1.7×10^{-2}

Table 3.3: Minimum and maximum BER comparison

The maximum BER values A similar consideration can be made by looking at the region of the curves on the left, characterized by a low received power. In particular, the highest bit error rate corresponds to the leftmost point in each curve, that is the one with the lowest received power. If the power is further reduced, the card will not be able to decode the signal properly, so it also corresponds to the lowest amount of power that can be received while keeping the transceiver in correct service.

As it is possible to see, all but the simplest configuration reached a similar value, whereas the DP-QPSK at 100 Gbps was the only one to support a maximum BER almost three orders of magnitude lower than the others. This result has to

be expected because this modulation is the only one that uses a weaker forward error correcting algorithm, thus all the others are able to correct a considerably higher amount of errors at the cost of having a larger FEC overhead, as it has been described in section 2.1.4.

The BER in low power conditions In addition to what has already been described related to the BER values, it is important to note that the device under test does not provide any indication to distinguish the working condition from the one in which the device can't operate correctly. In fact, as it has been anticipated in Section 3.1.5, the device keeps providing metrics even when the operating conditions do not allow correct operations. For what concerns the BER value, when the transceiver stops working because of low power, both the *pre-FEC* BER and the *post-FEC* BER report value zero. This result makes sense only considering that the absence of transmitted information implies the absence of errors, but may be confused with the state in which there are zero errors because the device is operating in optimal conditions. Clearly, this representation provided by the Phoenix transponder is ambiguous; however, by looking at the chart that relates the BER with the received power, it is clear which region corresponds to the faulty state by considering the shape of the curves. For this reason, a workaround for detecting the situation in which the device stops working is to consider the condition in which the BER becomes exactly zero after being non-null: in fact, for the reasons described above, this jump to zero always follows the peak in the BER value, so the maximum BER tends to correspond to the last working condition of the device.

The received power values Having considered the boundaries of the minimum and maximum BER values, it is interesting to compare the limits reachable by the measured received power. In particular, considering the comment on the BER values outside the working condition in section 3.1.5, the minimum measured power is considered to be the last power at which the BER was still measurable, i.e., the power at which a reliable transmission was still possible thanks to the FEC algorithms.
The Table 3.4 collects the resulting values for all the modulation formats analyzed at the central frequency of 193 THz. Moreover, in the device capabilities there is a list of minimum input powers, which are considered as a reference point in the same table.

As it is possible to see, the minimum measured values are much lower than those provided by the transceiver. This result is to be expected, as the manufacturer provides good margins to ensure correct functioning in the recommended operating range. Moreover, it is also possible to observe that the highest value between the

Operational Mode	Modulation Format	Line rate	Min Power [manual]	Min Power [measured]
1104	DP-QPSK	100 Gbps	−22 dBm	−33.0 dBm
2304	DP-QPSK	200 Gbps	−20 dBm	−33.0 dBm
2308	DP-16-QAM	200 Gbps	−20 dBm	−32.8 dBm
4308	DP-16-QAM	400 Gbps	−20 dBm	−26.4 dBm

Table 3.4: Minimum received power comparison in working conditions

minimum powers is the one corresponding to the DP-16-QAM modulation: this is to be expected as it is the most complex, thus will operate only in *better* conditions.

3.2 Cassini analysis

The previous chapter described a detailed analysis of the main parameters that can be collected using a Phoenix transponder and an OSA. However, it is important to note that most of these concepts are general and can be applied in a similar way to different devices. For this reason, the following sections are devoted to an analysis of a different transponder that can use two different cards, as will be described later. As most of the considerations are similar to what has already been commented on above, the focus in this case will be on the main differences from the previous setup.

3.2.1 The cards

An introduction on the Cassini transponder has been commented in section 2.2. A notable difference in respect to the Phoenix one is that in this case it is possible to use both ACO and DCO cards. Their differences are transparent from the user's point of view, but their implementation is quite different. In particular, the most notable aspect is the fact that with the ACO devices, part of the logic is not implemented inside the device itself, thus requiring the use of additional hardware and software components in the transponder in which they are plugged in.

An important aspect is that the Cassini transponder can be controlled in exactly the same way regardless of which type of card is used: this means that the command line parameters and NETCONF commands can be reused in both setups. However, the ACO is much more sensitive to variations in frequency and modulation formats: as a result, it was often difficult to change these parameters without waiting a long time or restarting the transponder to apply them correctly and return the device to its normal operating state.

3.2.2 The setup

The setup considered for the Cassini characterization is similar to the one that has been described for the Phoenix, but some variations have been put in place in order avoid chaining the device interconnections between the measurements with and without the additional noise. This has been done in order to limit the amount of required hardware configurations, to have a fully automated system, and also to ensure that the connector losses are always the same for all the collections. A schematic representation of the devices used in the setup is shown in Figure 3.13.

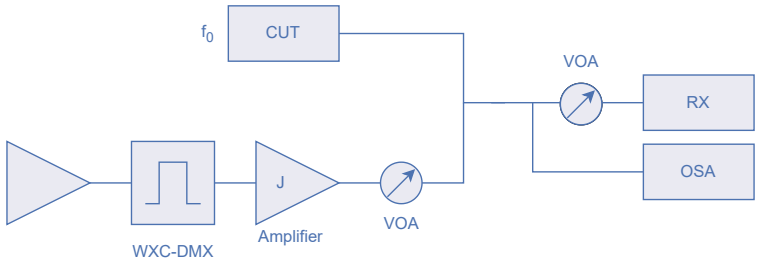

Figure 3.13: Cassini device setup

As it is possible to see, most of the devices are connected similarly to how they were with the Phoenix setup, but some notable changes must be taken into account. At first, since the same setup is used with and without the additional noise, the VOA that controls the noise has been turned off for the sensitivity curves, emulating the physical disconnection of that part of the setup.

Moreover, the Juniper amplifier in the middle of the system has been removed. This difference was necessary in order to avoid having the effects of the noise from the amplifier during the sensitivity curves, and at the same time it is not strictly required, since the results obtained in the previous data collections showed that the maximum received power (even without the additional amplification) was more than sufficient to see the BER flooring, making it unnecessary.

Apart from the said variations, the described setup can be seen as a union of the two independent solutions described for the Phoenix characterization:

- When it is required to consider the additional noise, the system behaves similarly to the previous one in Figure 3.1, with the only difference that the received power will be a few decibels lower due to the absence of the amplifier;

- When the noise is not needed, the VOA on the left is disabled and the OSA on the right is not used, obtaining a setup equal to the one in Figure 3.10.

3.2.3 The data analysis and comparison

As it has been described in Section 3.2.1, the Cassini transponder has the peculiarity of allowing the use of both ACO and DCO transceivers. For this reason, the data collection has been performed twice, and in this way it is possible to compare their reciprocal differences and also in respect to the DCO device of the Phoenix device.

The BER vs. SNR_{ASE} comparison

A first interesting comparison can be made considering the BER vs. SNR_{ASE} curves obtained with the three different transponders. In particular, the Figure 3.14 contains two plots obtained with the two common modulation formats, DP-QPSK on the left and DP-16-QAM on the right. Moreover, it has been decided to consider the same frequency of 193 THZ and a high received power (or, equivalently, an almost negligible attenuation provided by the VOA).

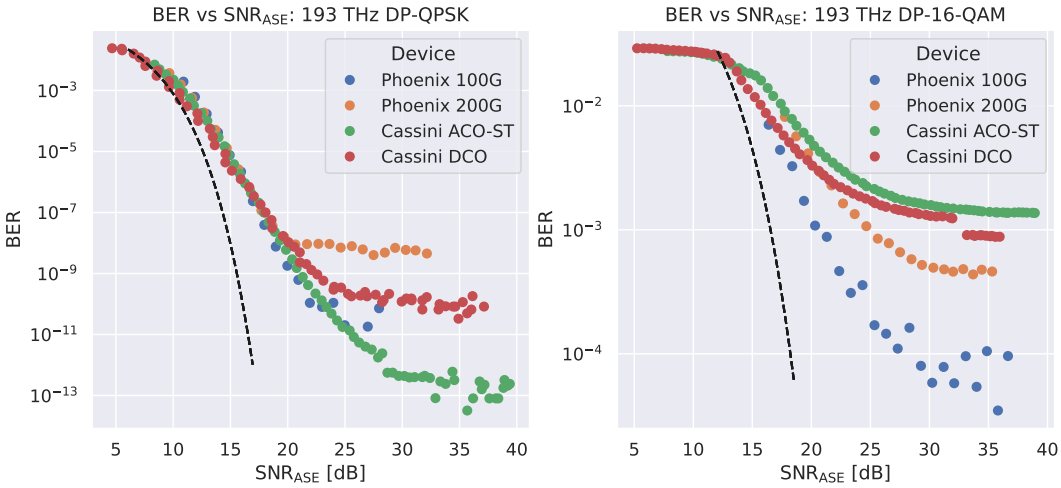

Figure 3.14: BER vs SNR comparison between Phoenix and Cassini transponder

As it is possible to see, the obtained curves have a very similar behavior in the upper-left part of the plots, where the SNR_{ASE} is lower and the BER is higher. This is due to the fact that all the devices tend to operate close to the lower limit, represented by the dashed curve, since the main contribution of the performances is the SNR_{ASE}, which is independent of the considered devices. The right part, on the other hand, is mainly due to the actual device characteristics, which is why the differences are greater. However, it is also important to remember that the lowest BER values, around 10^{-13} or 10^{-10}, cannot be considered reliable due to the high difficulty of computing them accurately, especially in a relatively short integration period. In any case, for all the devices there is a clear definition of a BER floor, or

minimum value, which is independent of the SNR_{ASE} value itself, and is instead mainly due to the SNR of the transceiver.

An additional clarification has to be made regarding the lower-bound curve. In fact, as already described for the Phoenix transponder case, the dashed curve represents the BER computation obtained using the SNR_{ASE} as the only SNR contribution: since it is only an approximation and other elements have to be considered, this is considered the *best case*, and for this reason in always represented on the left in respect to the measured values. An only exception is visible in the DP-16-QAM plot for very high BER values, and is due to the fact that the Cassini transponder is not able to provide a clear distinction on the operating condition in which there are some uncorrected errors. This translates into the fact that the lower SNR_{ASE} values cause a non-zero *post-fec* BER, whereas the *pre-fec* do not increase as expected. In any case, this area is in general of no practical interest since the normal operating conditions require keeping a safe margin in respect to the BER threshold provided by the FEC algorithm in order to avoid any unexpected behavior. For this reason, it is possible to assume that the curves provided in the Figure 3.14 can be considered only up to a minimum SNR_{ASE} value that is in any case on the right in respect to the dashed curve.

The BER vs. received power comparison

Another interesting comparison can be done by considering the Figure 3.15 that represents the relationship between the BER and the received power, obtained with the sensitivity setup.

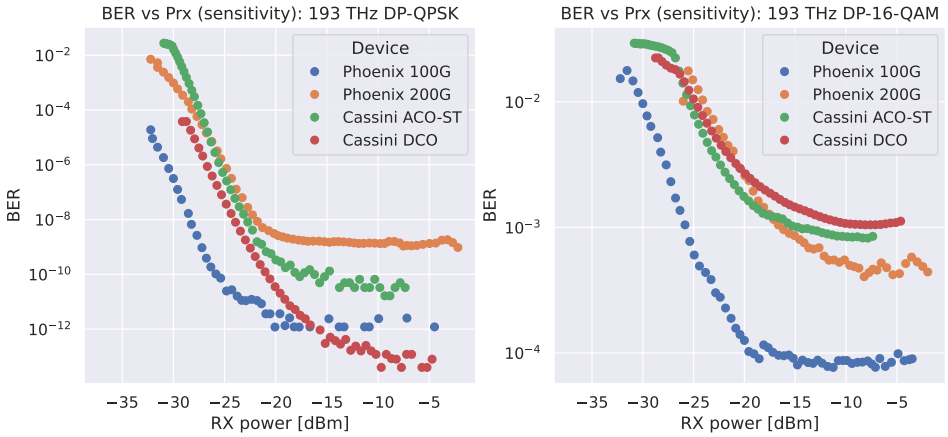

Figure 3.15: BER vs received power comparison between Phoenix and Cassini transponders line

As it is possible to see, all the devices are affected in a similar way and, as expected, the BER value tends to increase when the received power is decreased. They have also a similar minimum value of the received power, which is around −30 dBm, after which the *post-fec* BER value is not zero anymore, and have thus been removed from the plot.

The only notable difference is that the Phoenix has the possibility to use the two modulation formats in two different ways, depending on the achievable data rate, which also causes a variation in the used spectrum width. In particular, the blue curve represents the simplest configuration in the two scenarios, and it tends to perform better than the others since it is a *better* case in respect to the other valid configuration of the same device with both the modulation formats: this translates into an improvement in the performances, visible as a lower BER for any of the considered points.

The additional modulation format

Finally, as already described, the Cassini DCO is the only transponder tested that can also operate with the DP-8-QAM modulation format, and the figure 3.16 can be used to compare the three available modulations. The figure contains two graphs showing the relationship between BER and $\mathrm{SNR}_{\mathrm{ASE}}$ or received power, and the results are very similar to those expected. In particular, it can be seen that the additional DP-8-QAM modulation performs slightly better than DP-16-QAM, but clearly at the cost of doubling the signal spectrum used, while keeping the same data rate of 200 Gbps, as described in the table 2.6. These two high rate configurations have a similar shape, but are also characterized by a few dB difference in the minimum power or $\mathrm{SNR}_{\mathrm{ASE}}$ corresponding to reaching the BER threshold.

3.2.4 The use of different transceivers

In the previous sections it has been shown how to perform the data collection using an optical transceiver in a *back-to-back* configuration, which is characterized by having the same device at both the transmitter and the receiver. As it has been described before, this introduces several advantages in terms of the complexity of the system, since only one device is needed to perform the whole collection. However, this implementation cannot be considered "realistic", in the sense that for most of practical applications, the communication takes place between a transmitter and a receiver which are far away, implying the need of using two different devices.

This translates into the fact that any unidirectional communication uses only the transmitting components of one device and only the receiving components in the other. As a consequence, a complete characterization of that kind would require to use the two devices simultaneously, and then to repeat the whole process

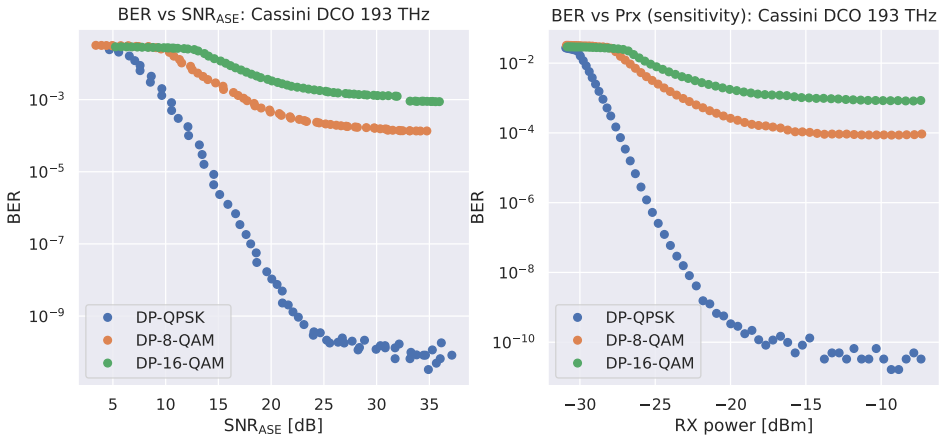

Figure 3.16: BER vs. SNR_{ASE} and BER vs. received power with different modulations on the Cassini device

considering the opposite direction on the same link.

For the purposes of this work, however, this additional complexity was not required because the additional steps have been tested on a small set of operating conditions related to the Cassini ACO transponder, and have shown that no significant difference could be observed. A possible interpretation of the result is that devices of the same brand and model are built in the same way and therefore tend to perform with similar specifications. In fact, their full interoperability makes the only difference in terms of *back-to-back* configuration the inaccuracies in the manufacturing processes and in possible dissimilar environmental conditions of the two installations, which were however removed by the fact that both the devices were tested in the same laboratory.

In summary, the possible additional penalties were very small, which explains why it was not possible to assess them using only the numerical data collected. This implies that, in general, the *back-to-back* analysis in enough provides a precise dataset that can be studied to derive the overall behavior of the devices.

Chapter 4

The transceiver SNR computation

The previous chapters analyzed the main characteristics that can be obtained from laboratory experiments and data collections.

An interesting aspect is that the results obtained can be used to extrapolate noteworthy characteristics of the devices used, in order to estimate how the device operates in conditions that are not directly tested. However, to fully understand the main effects of the various elements that constitute a transceiver, it is necessary to analyze its internal configuration in detail.

4.1 The SNR definition

4.1.1 Device performance

Within a network, each device between the transmitter and the receiver introduces a penalty that affects the quality of the signal. Different devices may introduce several contributions, but in most practical applications only a few of them are considered, while the others are neglected because they do not significantly affect the overall performance.

As described earlier, the main quantity relevant to the quality of the transmission is the BER, which must always be less than a certain threshold to allow the error correction algorithm to correct all errors and provide an error-free output data stream. This quantity is directly measurable by the devices and is useful to find a synthetic measure of the overall performance of the system.

4.1.2 How the receivers decodes the signals

The receiver receives the signal after it has been influenced by all the elements it has passed through in the network. As described in section 1 related to the fundamental concepts, the signal is composed by a sequence of symbols taken from the selected constellation, depending on the modulation format used.

An example of a common modulation format has been represented in Figure 1.4 related to the description of the coherent modulation technique: however, due to the influence of the network, the received symbols do not overlap perfectly with the ideal ones. In particular, most of the effects can be accurately modeled as AWGN noise: consequently, it can be visualized as a displacement vector that moves the point around its ideal position, creating a cloud of points around each modulated symbol.

It is important to remember that this effect is not directly visible or measurable with the setups under test, but is helpful to visualize the reasoning behind the generation of the errors, and a pictorial representation is given in Figure 4.1.

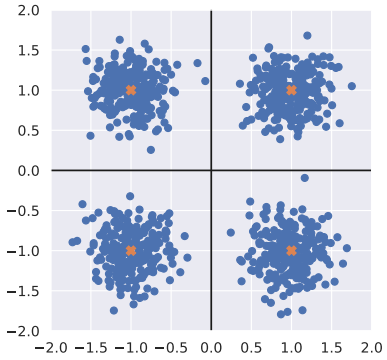

Figure 4.1: Pictorial representation of a cloud of points around their ideal location

In this case, a hypothetical constellation of four symbols is shown: clearly, the qualitative simulation provided is a simplification with respect to the modulations used in real implementations, but the aim is to visualize a possible shape of the cloud of points. As it is possible to see, the four available symbols are highlighted in red, and they are surrounded by the received ones, in blue, that form a circular area around the respective centers, whose diameter depends on the variance of the errors.

At this point, the receiver has to estimate which is the transmitted point: the simplest approach is to consider the maximum likelihood corresponding to the ideal point closest to the received one.

Even if highly sophisticated algorithms can be employed, at the basis of the

decoding it is possible to theoretically visualize the definition of a set of regions, one for every symbol in the constellation: in this way, any point that falls inside one of the regions is then decoded as equal to the corresponding symbol.

It is now possible to understand the origin of the errors: in particular, if a received point is too far from its theoretical position, it may fall into another nearby region and be decoded as a different value, causing the error. For this reason, the variance of the noise is strictly related to the BER value, and it is possible to relate it mathematically to the SNR, which numerically represents the quality of the signal.

4.1.3 The role of the SNR

The SNR (or Signal to Noise Ratio) is a quantity that describes the quality of the received symbols just before the decoder in the transceiver device.

In the section 1.4.3 it has been provided a convention that can be used to name the SNR in the proper way depending on where it is analyzed in the system. However, it is important to note that the only quantity that is directly related to the performances of the system is the one close to the receiver, which is the only device that has to convert the received optical signal to a sequence of bits.

This concept is strongly related to the definition of the cloud of points provided before, in relation to Figure 4.1: in fact, a lower SNR corresponds to larger clouds, and thus to a higher resulting BER. All the other SNR contributions in the network, which will be analyzed in greater detail later, are in fact already contained in this last device, which is at the end of the considered chain of elements.

Given this definition, it is possible to consider the relation 4.1 as *exact*, in such a way that the BER depends exclusively on the SNR value, apart from the definition of the k_1 and k_2 constants. This equation has already been used before, but in this case the role of the SNR is considered to be the superimposition of all the other effects. Additionally, as anticipated before with the Table 3.2, the values of k_1 and k_2 depend solely on the selected modulation format.

$$\mathrm{BER} = k_1 \mathrm{erfc}\left(\sqrt{k_2\ \mathrm{SNR}}\right) \tag{4.1}$$

4.1.4 The SNR contributions

In the last section it has been described the role of the SNR and why it can be used to correctly estimate the characteristics of the signal. In particular, it is considered as the *summation* of several contributions, and for this reason it can be useful to split the several components in such a way to study them separately.

The summation of the contributions

A fundamental consideration has to be made relatively to how the contributions are added together. In fact, they are *additive* also in the sense that can be summed one with the others However, it is necessary to remember that the SNR is by definition a measure of the **quality** of the signal, whereas the contributions are always **penalties**, which affect the transmission by *reducing* the overall quality. For this reason, the correct way to sum them is to consider only the summation of the inverses, always expressed in liner scale. This translates into the general equation number 4.2, which considers a generic $\mathrm{SNR}_{\mathrm{TOT}}$ obtained by the summation of several contributions SNR_i.

$$\mathrm{SNR}_{\mathrm{TOT}}^{-1} = \sum_i (\mathrm{SNR}_i)^{-1} \tag{4.2}$$

This means that the resulting SNR is generally obtained as the inverse of the sum of the inverse of the individual contributions.

The corresponding numerical effect is that an additional contribution always corresponds to a reduction of the SNR value. Although this result is not intuitive, it is clear that an additional penalty can only reduce the overall quality. Moreover, this definition also implies that the total SNR is mainly affected by the smallest numerical values, since they represent the quantities that introduce a stronger penalty: this is especially useful when considering a large number of contributions, since the largest one may have a negligible impact on the numerical results.

The contributions to be considered

As described in the previous sections, several contributions must be considered. In principle, it should be necessary to model *every* contribution in order to have an accurate definition of the characteristics of the devices, but in any setup there are generally only a few contributions that are needed to provide results with very limited approximation.

Moreover, for the setups described in the previous chapters, it is possible to consider only additive quantities: this does not worsen the result, but strongly simplifies the computations. For this reason, in this specific condition it is possible to consider every contribution due to the line as additive and contained in the GSNR, and then add separately the contribution of the transceiver.

To provide a general description of the system, it should be noted that some devices in more complex scenarios may require a non-AWGN contribution, which is ignored in this case. A possible example is the filtering penalty that may be introduced by some optical components. This causes a shrinkage of the signal shape that can only be modeled with more complex functions and not just with an

additional SNR contribution. In any case, it should be noted that the devices used in the two setups described above have a working band much larger than that of the signal of interest: for this reason, this effect is completely negligible.

The contribution due to the additional noise

The first contribution that can be studied is the one due to the additional noise source. In fact, as it has been described by using the Figure 3.13, there is a specific input branch in the bottom-left part of the setup which is dedicated to the generation of an optical AWGN noise that is added on top of the useful signal. This contribution is in general denoted as $\mathrm{SNR}_{\mathrm{ASE}}$, and it can be measured in the optical domain with the use of an OSA, as it has been described in section 3.1.3. Moreover, since it is measured in the same band of the useful signal, it is directly comparable with all the other contributions.

The use of the setup in this configuration aims at simulating the effect of the noise generated by the optical amplifiers along the line: in fact, as briefly commented in the fundamental concepts in section 1.3.3, the amplifiers are used to increase the power of the signal, but at the same time their Amplified Spontaneous Emission effect generates unwanted photons in the same band. This causes an additional noise contribution, which is in general modelled as $\mathrm{SNR}_{\mathrm{ASE}} = P_{ch}/P_{\mathrm{ASE}}$, where P_{ch} represents the power of the useful signal and P_{ASE} the power of the additive noise, caused by the spontaneous emission.

As a side note, it can be helpful to remember that this $\mathrm{SNR}_{\mathrm{ASE}}$ value can be indirectly changed arbitrarily by modifying the configuration of the VOA of the noise, as described in detail in section 3.1.2.

The contribution due to the transmitter

A second important contribution is the one due to the transmitter. In fact, it is positioned at the beginning of the line and its effect are then propagated through all the following elements. It is composed by several internal components, but it is possible to suppose that the one that mostly affects the quality of the transmission is its amplifier, whose role is to set a configurable output power of all the transmitted symbols.

Moreover, it is also possible to suppose that its contribution is independent on the data transmitted. However, it may depend on the configured output power. In fact, the power may be obtained in several different ways that are not distinguishable from the user's point of view. As an example, a first technique could be to have a tunable amplifier that is able to increase or decrease its gain as needed: in this case, the penalty imposed by the device may be related to its configuration, and in principle it may be possible to characterize this dependence. At the same time, however, the device can be configured to always have a strong amplification effect, and then an additional variable optical attenuator can be used to precisely

control the output power: in this case, the overall penalty can be assumed to be independent of the settings, since the VOA attenuates the signal and the noise in the same way, without affecting their ratio.

Unfortunately, it is not possible to know the internal implementation of any device. In any case, it is important to remember that in the setups considered before it has always been set the same target output power of 0 dBm. This translates into the fact that the two conditions described above can be considered totally similar: even if a variation in the performances is present when the power is changed, in all the measurements the power has been kept constant, and no effect is expected to be affecting the results. Moreover, in most of the cases there is no need to change this setting: in fact, a reduction of the transmitted power can only reduce the performances, whereas an increase may introduce distortions and should be for this reason avoided.

To summarize, the contribution of the transmitter may be relevant in the overall performances of the system, but in the cases considered in these setups it has to be considered as a constant value for every one of the tested devices.

The contribution due to the receiver

Another important contribution of the SNR is due to the receiving component in the transceiver. Similarly to what it has been commented regarding the transmitter, in general it is not possible to have a full knowledge of the receiver's implementation, and for this reason it is required to make some assumptions on which may be the most relevant components that can affect the overall performances. Nevertheless, the elements that are surely of great importance are the photodetectors, which are devoted to converting the incident optical power in an output current that can be used by the electrical components.

In practice, the ideal device should implement a well-defined function that relates the input and the output powers, but the real implementations need to take into account the generation of an additional noise on top of the useful signal that causes small variations in the currents, which has to be taken into account when considering the performances of the system. In particular, there exist three main contributions, namely the thermal noise, shot noise, and dark current noise that contribute together to form this additional penalty.

Although the various contributions will be described in more detail later, it is important to note at this stage that an important characteristic common to all receivers is that the performance is strongly influenced by the power received. This behavior was already visible in Figure 3.6 by the fact that the same BER vs. $\mathrm{SNR}_{\mathrm{ASE}}$ curves tend to move to the right (or to higher bit error rates) when the received power is reduced.

This effect is of great interest for transceiver characterization because, unlike the transmitter component where the transmit power can be set arbitrarily, the

penalty at the receiver side depends strongly on the received power, which in turn depends on the line characteristics, which are rarely fully controllable.

4.1.5 The SNR of the transceiver

As it has been described in the previous sections, there exist several contributions that may affect the overall quality of the signal. In this section, the main goal is to provide a qualitative description of this contribution mainly by considering the experimental data collected as it has been described in the previous chapters.

At first, it is possible to define two quantities that correspond to the effects due to the transmitter and the receiver, respectively. In some cases, it is possible to study them independently, as it will be described later; however, at first they can also be joined together in order to form a quantity $\mathrm{SNR}_{\mathrm{TRX}}$ that represents the total contributions of the transceiver, as shown in equation 4.3, obtained considering the usual summation rule for the SNR as in the previous equation 4.2.

$$\mathrm{SNR}_{\mathrm{TRX}}^{-1} = \mathrm{SNR}_{\mathrm{TX}}^{-1} + \mathrm{SNR}_{\mathrm{RX}}^{-1} \tag{4.3}$$

Clearly, this quantity follows the rules described in the previous section related to both the transmitter and the receiver, and for this reason it is affected by the received power. This implies that its numerical value has to be defined at a specific P_{RX}, and that every device is characterized by different $\mathrm{SNR}_{\mathrm{TRX}}$ at different received powers. However, it is important to note that for practical uses this value is expected to change only marginally when the received power is high enough, and for this reason knowing the device characteristic at a high P_{RX} can usually give a good approximation of its behavior in most operating conditions.

In the next sections there is a comment related to a practical procedure that can be used to find this value.

The role of the penalty k

Before performing the fitting in order to find the $\mathrm{SNR}_{\mathrm{TRX}}$ value, it can be interesting to define a new parameter k that can sometimes be used to explain some results obtained with some transceivers. In fact, the previously described equation 4.1 relates the BER and the SNR quantities by means of only two constants, namely k_1 and k_2, that depend uniquely on the selected modulation format.

However, it is possible to define an additional parameter $k \leq 1$ within the error function, which can be used to represent a penalty due to a filtering effect in the receiver. At this stage, it is not easy to understand the reasons for the possible

presence of this factor, but it is possible to study the effects it has on the results. In any case, the complete function that can be used to compute the BER is provided in Equation 4.4, in which the SNR contribution is defined in Equation 4.5, as it has been described before.

$$\mathrm{BER} = k_1 \cdot \mathrm{erfc}\left(k \cdot \sqrt{k_2 \cdot \mathrm{SNR}}\right) \tag{4.4}$$

$$\mathrm{SNR}^{-1} = {\mathrm{SNR}_{\mathrm{ASE}}}^{-1} + \mathrm{SNR}_{\mathrm{TRX}}^{-1} \tag{4.5}$$

At this point, it is then possible to observe that there two parameters that have to be found: the penalty k and the $\mathrm{SNR}_{\mathrm{TRX}}$ contribution. In particular, the former can at this point be analyzed in greater detail.

In fact, since k is a multiplicative factor to a generic SNR, it behaves similarly to a shift on the same axis, if the logarithmic scale is used. A visual representation of this effect can be seen in Figure 4.2, in which several values of k are compared in respect in a condition in which the $\mathrm{SNR}_{\mathrm{TRX}}$ is neglected. Clearly, this corresponds to a rough approximation of a best-case scenario, similarly to what has been done in the previously described Figure 3.6.

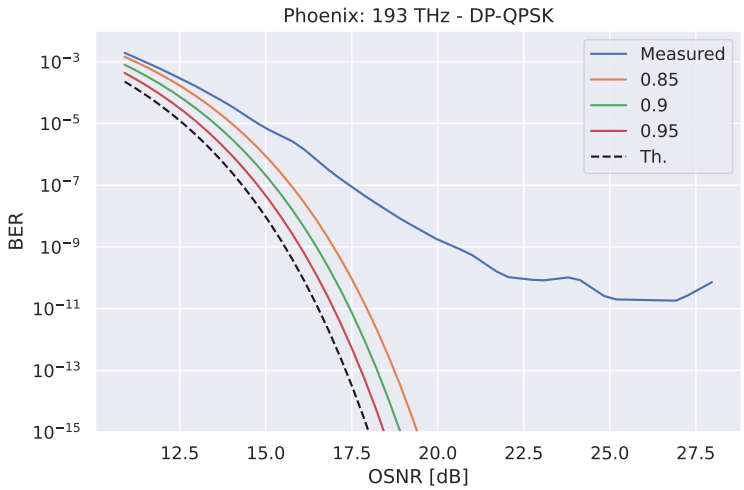

Figure 4.2: The role of the parameter k in the BER curves

The ideal case is represented with a dashed curve, in which $k = 1$, which corresponds to the condition in which the equation 4.4 does not contain the k factor completely. In the other cases, the curve is instead shifted to the right by an amount that increases when the k is reduced.

Clearly, the same figure can be used to visually understand why $k \leq 1$: this is consequence of the fact that k represents a penalty, and this condition ensures

that the BER is increased in respect to the value it would have had at the same SNR_{ASE} value (or, equivalently, it is required an higher SNR_{ASE} to measure the same BER).

An interesting additional note can be discussed related to the equation 4.4: in fact, it has been decided to place the k value inside the error function and outside the square root, but it is not the only option. Apart from the trivial alternative of placing the k inside the square root, there is also the additional possibility of making it multiply only the SNR_{ASE} value, and not the SNR_{TRX} contribution, effectively moving the k in front of the first addend in equation 4.5. This can be useful if it is required to consider k as a penalty in the line which is independent on the behavior of the transceiver, which is in fact estimated independently. In any case, it is important to remember that the SNR_{TRX} is a free parameter that has to be fitted independently, and if k is defined as multiplying only the SNR_{ASE}, it corresponds to finding the fit of SNR_{TRX}/k, which, in practice, does not change the final result. The two possible definitions are, for this reason, numerically interchangeable by simply multiplying or dividing the contribution due to the transceiver by k itself.

The SNR_{TRX} computation

Once the k coefficient has been defined, it is possible to interpolate the curve relating the BER to the SNR_{ASE}, trying to fit the two parameters k and SNR_{TRX}. As described in previous chapters, these curves are strongly dependent on the received power, but may also depend on the operating frequency. In this case, it has been decided to consider a reference curve obtained as the average of the measured values at all the frequencies, in order to obtain a greater number of points that can best approximate the real conditions. In addition, only the high power curves, where the received power is close to 0 dBm, have been used: this helps to reduce the effect of the receiver penalty, which will be studied independently later.

An example of the obtainable result is provided in Figure 4.3, in which the Cassini transponder has been tested in the DP-QPSK modulation. At first, it is possible to observe that the blue curve, corresponding to the collected data, is in accordance to the expected results, since its characteristic shape tends to increase when the SNR_{ASE} is reduced towards the left, while it finds a flooring on the right, when the SNR_{ASE} is large enough.

The interesting aspect is related to the orange curve and how it differs from the dashed one. In practice, the theoretical curve is the one largely described before, which contains only the SNR_{ASE} contribution; this has been defined as a *best case* scenario, since all the other elements have been neglected. On the contrary, the orange curve is defined following the description provided in equation 4.4, in which it is also considered the effect of both the parameter k and the SNR_{TRX}.

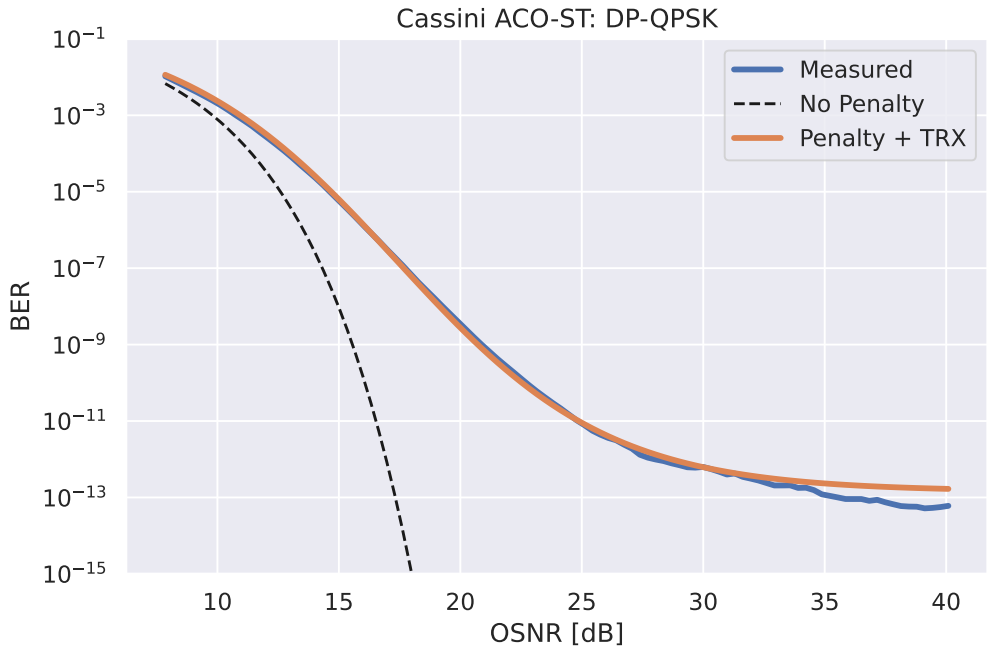

Figure 4.3: $\mathrm{SNR}_{\mathrm{TRX}}$ and k fitting on the Cassini transponder

In order to make the orange curve fit the blue one, an interpolation has been performed in order to fit the two values trying to minimize the difference between the measured and the computed curves. As it is possible to see, the result is a very good approximation of the collected data, and this translates into the fact that these two parameters can be used to precisely predict the behavior of the curve.

The important result of this fitting is that it shows the basic steps that have to be followed in order to characterize the device, and that the two described parameters are in general enough to obtain a good modelling of the setup.

Finally, it is important to remark that for this computation it has been decided to always consider the curves obtained in high received power condition. Similarly to what has been defined related to the Figure 3.7, the received power is not exactly constant during the test because when the $\mathrm{SNR}_{\mathrm{ASE}}$ is lower, the noise power is higher, and the received power will be higher as well. In any case, this variation is quite small, in general only few dB, and for this reason it has been decided to consider it constant and equal to the case in which the minimum amount of additional noise is present. For example, the case described above in Figure 4.3 corresponds to a received power of 0 dBm.

However, due to how the quantities have been defined in Section 4.1.5, it is expected that the value k is independent in respect to the power, and for this

reason a similar value should be obtained also in different operating conditions. On the contrary, the $\mathrm{SNR}_{\mathrm{TRX}}$ changes with a different signal attenuation because its $\mathrm{SNR}_{\mathrm{RX}}$ contribution is largely affected by the input power. Moreover, these quantities are expected to remain unaltered when the frequency changes: for this reason, in principle it is possible to use any available frequency. In this case it has been decided to use several frequencies in the central part of the C-band, and then average the obtained curves: this should help remove small variations that may occur during different repetitions of the data collection. The effects of this are shown in Figure 4.4.

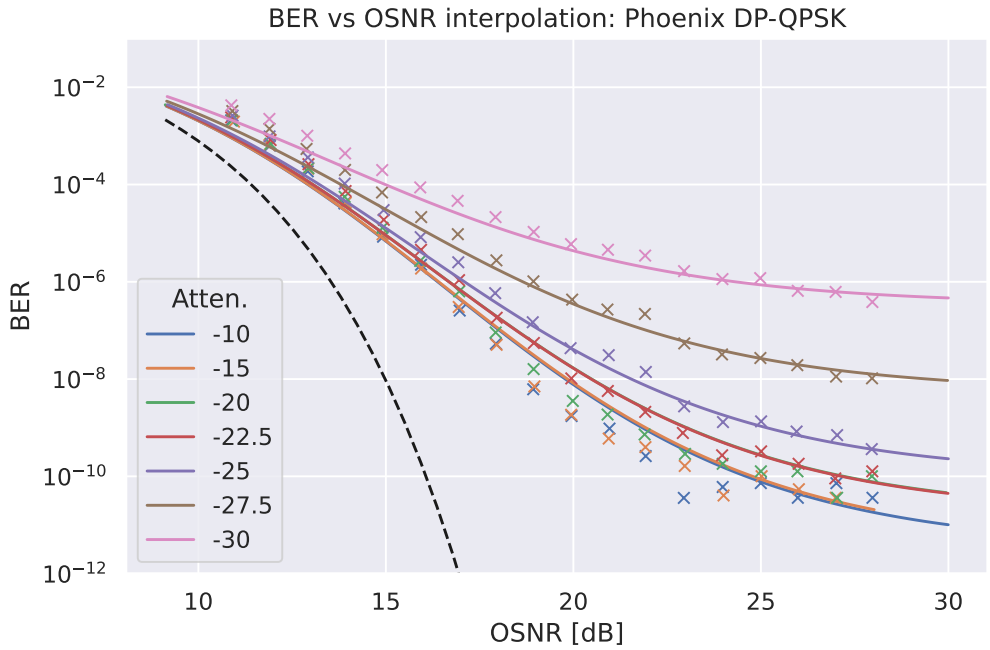

Figure 4.4: BER curve interpolation at different received powers for the Phoenix transponder

In this case, it has been decided to study the behavior of the curves at different receiving powers, averaging the measurements between 192 and 194 THz: in the following sections it will be clarified that neglecting the effects of the frequency does not worsen the result, at least in the central part of the operating band.

As an additional interpolation, it has been decided to merge the curves with the received power 0, −5 and −10 dBm: in fact, as previously shown in Figure 3.6, they almost overlap but have small variations that can be smoothed in this way. This is due to the fact that the received power is still high enough to make the receiver's penalty negligible in respect to the power itself. Moreover, since these are

also the curves in which the BER is lower, it is also known with higher uncertainty due to how it is measured: also in this case, an additional averaging can improve the final result.

Finally, the figure also shows the additional representation of the collected data points. To reduce the number of visual elements, only those at 193 THz are shown, but for the same reasons as above, there should be minimal differences with respect to the other frequencies.

As it is possible to see, the obtained curves are a very good approximation of the collected data points, especially when the BER is not too low: this result clearly confirms that the described fitting which considers the $\mathrm{SNR}_{\mathrm{ASE}}$, the $\mathrm{SNR}_{\mathrm{TRX}}$ and the k factor can provide an accurate description of the measured quantities. Moreover, it also shows that keeping k constant does not worsen the quality of the result when the power is reduced, since the only affected contribution is the $\mathrm{SNR}_{\mathrm{TRX}}$ itself. In particular, in the provided example, this last quantity changed by almost 3 dB between the different curves, and this is the reason why the curves are largely different, especially in the right part of the chart.

An interesting aspect is that the difference between the curves is not constant with the $\mathrm{SNR}_{\mathrm{ASE}}$ variations: in fact, by looking at the Figure 4.4 it is clear that the curves are further apart on the right and closer together on the left.

The reasoning is a direct consequence of the way in which the generic SNR contributions are summed together: in fact, as described by the equation 4.5, the inverse of the result is given by the sum of the inverse of the contributions. Since $\mathrm{SNR}_{\mathrm{TRX}}$ is constant in each curve, the only variable is the $\mathrm{SNR}_{\mathrm{ASE}}$: in the right part, the latter is large and therefore negligible with respect to the former, which, being constant, allows the BER to find its floor. On the other hand, in the left part, the $\mathrm{SNR}_{\mathrm{ASE}}$ becomes very small and thus becomes the dominant contribution, so that all the curves almost overlap one another.

A similar comment can be made in respect to the dashed curve in the same figure, which depends only on the $\mathrm{SNR}_{\mathrm{ASE}}$ contribution, totally neglecting the SNR of the transceiver. Also in this case it is possible to observe that this is in general not a good approximation, and for the reasons described before it can only be used to compute a *lower bound* of the BER. However, the curve tends to be closer to the measured points as the $\mathrm{SNR}_{\mathrm{ASE}}$ decreases: this is due to the fact that in this left-hand region the $\mathrm{SNR}_{\mathrm{ASE}}$ is the dominant term and so the neglected contributions have only a marginal effect on the final result.

To conclude, the described technique can be used to perform the characterization of a transceiver in order to estimate its $\mathrm{SNR}_{\mathrm{TRX}}$ in the power ranges of interest. This can then be used jointly with an estimation of the $\mathrm{SNR}_{\mathrm{ASE}}$ of the line in order

to have the GSNR which can then be used to accurately estimate the performances of the system and to compute the expected BER value in the different operating conditions.

At the same time, the main disadvantage of this technique is that it is required to perform the data collection similarly to what has been described in section 3.2.2 for every one of the powers of interest. In general, this can take some time as the collection has to be repeated for several attenuations of the signal and several attenuations of the noise, effectively having a quadratic dependence on the number of curves and points per curve. For this reason, in the next section it is presented an additional approach that can be used to extrapolate a new quantity that can be used to approximate the result also in the conditions that have not directly been tested with the experimental setup.

4.1.6 The contributions of the transmitter and the receiver

In the previous section it has been described how it is possible to estimate the value of the $\mathrm{SNR}_{\mathrm{TRX}}$, whereas in this case the goal is to further study this quantity in order to split it into two parts, highlighting the difference in the effects of the transmitter by the ones of the receiver, as it has been defined in equation 4.3.

In most of the cases it is difficult to define which contributions are due to the two devices, since the observable quantities can only be obtained by the OSA (which is located before the receiver) or the receiver itself (which is affected by both the transmitter and the first part of the elements in the receiver). However, it is interesting to study the behavior of the SNR in respect to the received power, and this is analyzed in the next section. Subsequently, it will be commented a possible approach that can be used to distinguish the contributions between the different elements in the network and, in particular, between the transmitter and the receiver.

The SNR in respect to the $P_{\mathbf{RX}}$

In the previous sections it has been described the reasons why the $\mathrm{SNR}_{\mathrm{TRX}}$ changes with the received power, and as a consequence it is interesting to understand the numerical dependence between the two quantities.

In order to simplify the study, it is possible to consider the sensitivity setup: this is characterized by the removal of the additional noise, as it has already been described in respect to the figure 3.10. The main advantage of this solution is that it is completely removed the dependency with the $\mathrm{SNR}_{\mathrm{ASE}}$, making the $\mathrm{SNR}_{\mathrm{TRX}}$ the only relevant contribution of the SNR. However, this is not necessary required

and, similarly to the previous descriptions, also in this case all the quantities are additive, and for this reason the $\mathrm{SNR}_{\mathrm{ASE}}$ can be added later, similarly to what has been described by the equation 4.5.

The sensitivity setup can be used to obtain the curves that relate the BER and the received power, both measured by the card. Similarly to what has been described in section 3.1.4, for any device there is only one curve for every frequency and modulation format. Moreover, the well-known general equation 4.1 can be used to define a relation between the BER and the SNR, computed theoretically for any possible value. These two kind of curves can be used together to build an SNR curve in respect to the received power, and this will be detailed in the next sections.

The computation of the SNR vs P_{RX} curve

As briefly anticipated before, in order to compute the relation between the SNR and the received power without any additional noise loading, it is required to consider two curves:

- The measured curve that contains the BER and the received power values collected by the receiver;
- The theoretical relation between the BER and the SNR, which only depends on the k_1 and k_2 coefficients typical of every modulation format.

Since the BER is the only common quantity in the two curves, it can be used in order to move from one to the other: in fact, every BER corresponds to a specific received power taken from the first curve and a specific SNR from the second.

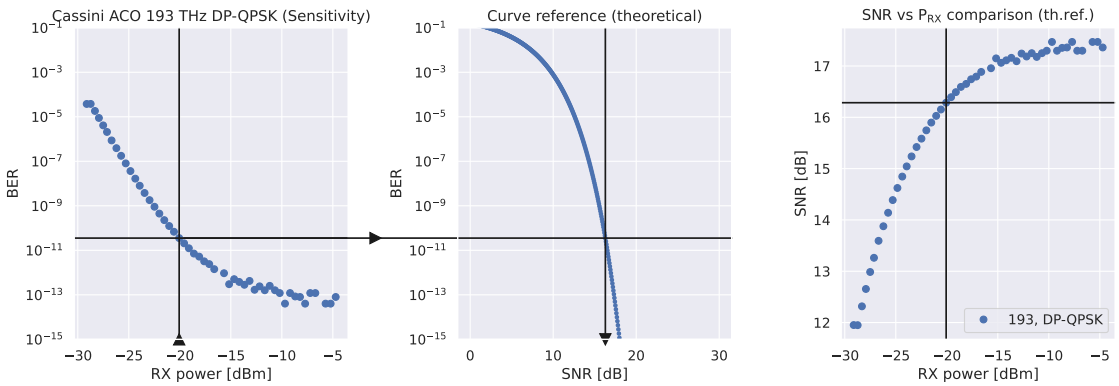

Figure 4.5: The step-by-step generation of the SNR curve

A practical example of the steps required is depicted in Figure 4.5, obtained

considering the Cassini transponder at 193 THz with the DP-QPSK modulation, and is now commented in detail.

The figure contains three plots in which the first two contain the input quantities, whereas the last one is the output. Then, the following steps are followed in this order:

- An input power value is selected in the range of the collected data points available in the first chart; in the example provided it has been decided to consider the value equal to -20 dBm;
- The first curve is then used to find the corresponding BER value, for example 3.54×10^{-11}, which has been measured using the sensitivity setup;
- The same BER value is then searched in the second curve in order to obtain the corresponding SNR, in this case 16.28 dB.

With this approach, the obtained result is that in the conditions under test a received power of -20 dBm corresponds to a computed SNR of 16.28 dB, and this point can be added in the third chart of the figure above.

Clearly, the described approach can be repeated multiple times for a large list of P_{RX} values: in the provided example, it has been repeated for every collected data point, but alternatively it is also possible to consider an interpolated curve, in order to smooth the original dataset. The final result is in the third plot in the same Figure 4.5, which contains one point for every received power value, paired with the corresponding SNR value just computed.

As an aside, a brief comment can be made about the reference curve. In this case, the theoretical one has been used to find the SNR by considering simultaneously all the contributions responsible for the measured BER value; however, various other possibilities could be used to find additional relationships between the quantities. The only requirement is that the considered quantity must be monotone (in order to avoid any ambiguity on the output values) and must be defined on a range of BERs at least as large as the ones provided during the sensitivity (otherwise the resulting curve will appear cropped since not enough data points are available).

The SNR vs P_{RX} curve characteristics

In the previous sections it has been provided a procedure that can be employed to obtain the relationship between the SNR and the received power in a sensitivity scenario. The newly obtained curve is of great interest since it shows how the transceiver's characteristics evolve with the variations of the received power.

In particular, the first important result is that the curve appears as a monotonous crescent with the power, confirming the fact that the P_{RX} is an important parameter that can greatly influence the quality of the transmission.

Moreover, even if the increase of the received power always causes an increase in the SNR, in the top-right region it is reached a flat condition, in which the power variations tend to affect only marginally the final result. This is due to the fact that when the P_{RX} is high enough, it does not represent a limiting factor anymore, and the performances are instead limited to other contributions which become predominant. This result is in accordance to what has been described in the previous chapters, and in fact a similar conclusion has been described also in respect to the Figure 3.6, in which different curves obtained considering an additional noise source were largely affected also by the received power. Moreover, also in that condition, it was possible to affirm that the first curves, obtained with a high received power level, were almost overlapped: this is a direct consequence of the fact that in that power condition, the flat region makes the SNR almost constant in the different curves, making its relative effect negligible in respect to the other contributions.

Finally, it is also important to make a brief comment related to the accuracy of the provided results. In fact, the transformation used to move from the received power to the SNR by using the common BER values largely described in the previous section can be performed without the introduction of additional errors only if all the BER values used are common in the two datasets. In a more general scenario, this may not be the case, and a specific BER value may not be available at least in one of the two curves: in that case, if it is numerically contained in the range of observed ones, it is possible to perform an interpolation of the curves in order to find a usable value. Due to the nature of the curves, if the amount of collected data points is large enough, it is possible to consider a simple but effective linear interpolation between the two closest measures, in order to obtain a very good approximation of the correct value. However, it is also helpful to remember that in the provided example, the reference curve in the chart in the middle is known mathematically: for this reason, it can be inverted without the introduction of any additional approximation.

In any case, since the final result is affected by the two input curves, it can be at most as good as the measured BER values in the first chart, and this can in some cases be a limiting factor. In fact, similarly to what has been described related to the sensitivity setup in section 3.1.4, the measure of the BER can be performed with good accuracy only when its numerical value is high enough. On the contrary, when the BER is too low, its reading becomes unreliable since the noisy measure has a variance too large to be averaged in the short time window of the data collection. The consequence of this are visible in the bottom right part of the first *input* curve of Figure 4.5, and consequently they will be present also in the flooring region of the top-right part of the resulting curve. Even if in principle the use of a larger integration time could lead to better results, it is also important to remember that it would further increase the total measuring time, and the final

improvements would be relatively marginal.

The SNR vs $P_{\mathbf{RX}}$ differences at different frequencies and modulation formats

In the previous sections it has been described which are the main characteristics of the SNR curve in respect to the received power in a sensitivity scenario. However, it is interesting to observe that in the previous comments it has been considered the use of only one frequency and modulation format, but in principle it is possible to expect some variations when these parameters change. For this reason, the two contributions are analyzed independently.

The role of the frequency

The steps described in the previous sections can be repeated for the data collected at different frequencies, obtaining different BER measurements at the received power levels of interest. However, the reference curve used to relate the BER values with the SNR remains exactly the same: in fact, its definition provided in Equation 4.1 does not contain any reference to the frequency itself. As a consequence, any difference in the measured curve corresponds directly to a variation in the output one.

A practical example is provided in the Figure 4.6 in which the same device has been tested several times in a large set of frequencies trying to cover the whole C-Band. As it is possible to see, different curves have different colors, and their points are not fully overlapped, but the overall behavior is almost exactly the same. This translates into the fact that the device under test has a negligible difference in its performances at different frequencies: clearly, this is closer to the ideal design, but there is no guarantee that any device would perform in the same way. In other cases, instead, it may be helpful to consider an additional margin that can be characterized independently to compensate for the worst performance, for example near the bounds of the operating bands.

The role of the modulation format

In the steps commented in a previous section related to the computation of the curve that relates the SNR with the received power it has been used a theoretical reference curve in order to consider simultaneously all the contributions that can affect the BER value. In particular, in the plot in the middle of Figure 4.5 the used function was the well-known equation 4.1, which is defined with the use of two coefficients k_1 and k_2. When the modulation format is changed, these two values have to be updated accordingly in order to have a meaningful result, selecting the proper ones from Table 3.2. As a consequence, when the modulation format

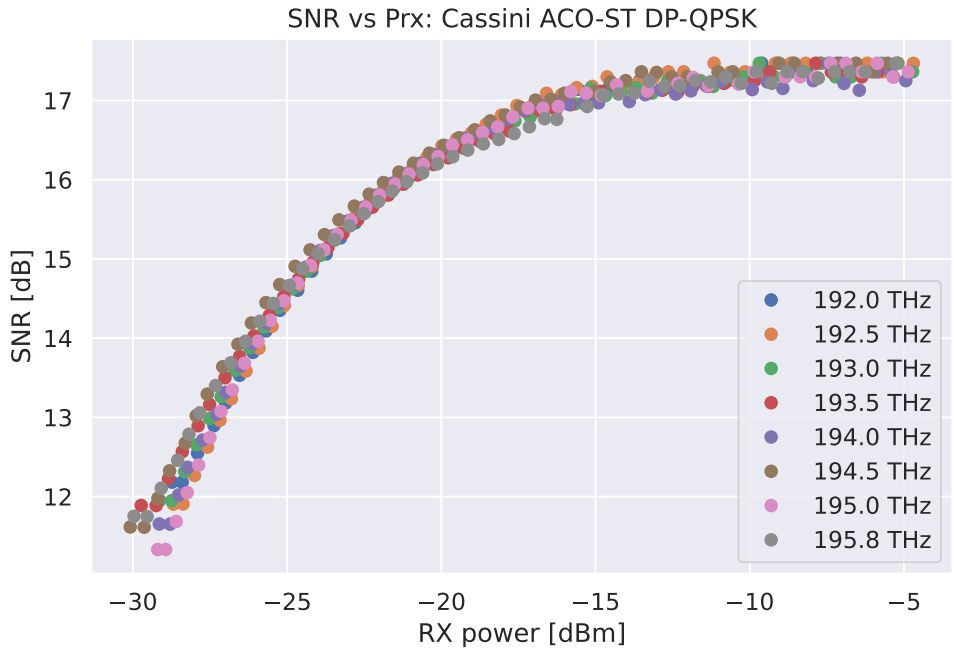

Figure 4.6: SNR evolution in respect to the received power for the Cassini transponder at different operating frequencies

changes, the reference curve changes as well.

Moreover, during the description of the data collection it has been commented that different modulation formats are characterized by having a very different shape of the BER values in respect to the received power: the main reason was that the smaller constellations are more robust than the more complex ones. The interesting aspect is that the measured effect is concordant with the difference in the k_1 and k_2 coefficients; in other words, the two input curves change in a coherent way. This implies that even if the differences are quite remarkable, the final result is only partially affected by these variations. A practical example is provided in Figure 4.7, in which it has been decided to show the Cassini device with a DCO transponder, in order to have the comparison between three modulation formats.

The first chart is the expected relation between the BER and the received power, whose characteristics have been largely described in section 3.1.4 related to the sensitivity setup, whereas in the middle there is the typical theoretical curves obtained with the equation 4.1 with the proper k_1 and k_2.

As briefly mentioned above, these two graphs present the curves in a well-defined *vertical order*: in other words, for any value of received power (or SNR), the lowest

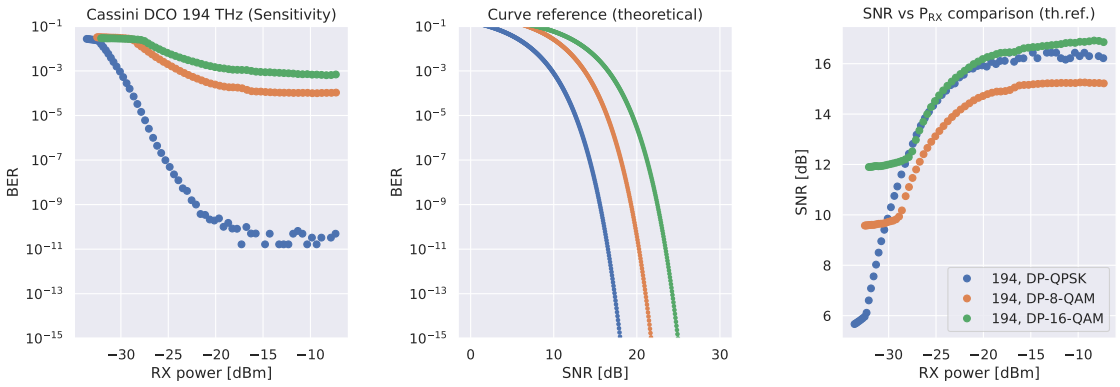

Figure 4.7: Step-by-step SNR computation for different modulation formats available for the Cassini-DCO transponder

BER is always that of the simplest modulation, and then the others follow up to the most complex. This means that the two effects partially compensate each other when calculating the final SNR curve with respect to the received power, following the procedure described before. In fact, even if the BER differences are quite remarkable, the final curves are very similar one with the other, and the final result is that the various modulation formats cause only a small difference in the transceiver performances. Nevertheless, all the other comments related on the curve shape in respect to the power still apply, and the flat region in the top-right part of the chart is still reached, as described before. As a side note, it is interesting to note that the simplest modulation format (in this case, the DP-QPSK) is also the one with is characterized by the curve measured with the lowest precision: however, this is a direct consequence of the way in which the BER is measured by the card. In fact, as it has been shown during the description of the computation procedure, the use of the theoretical curve does not introduce any uncertainty, and for this reason the quality of the numerical values of the SNR only depend on how the BERs are measured. For this reason, following the previous comments, any value lower than 1×10^{-10} is unreliable since it is too small to be measured precisely in a short integration time window. Nevertheless, the results shown in Figure 4.7 can be smoothed by both increasing the integration interval or by performing an interpolation on the points.

4.2 The internal components of a transceiver

In the previous sections it has been presented a practical way that can be employed to obtain an experimental curve that relates the $\mathrm{SNR}_{\mathrm{TRX}}$ with the received power. Even if this quantity is of great importance, it can also be of interest to define

an analytical function that describes the transceiver's characteristics. In addition to the general goal of gaining additional insight into its behavior, this function can also be used to perform curve fitting, allowing users to smooth the measured quantities and predict the results under untested conditions.

However, as it has been anticipated before, it is generally not possible to know the exact internal implementation of the optical transceivers because they are proprietary, but there are some common elements that must be introduced into every coherent device. In particular, since every device is bidirectional, it is possible to study the two parts independently and then merge the results in order to obtain the complete model.

4.2.1 The transmitter implementation

In previous chapters it has been shown that for coherent modulation it is very common to use the DP-QPSK or the DP-16-QAM modulation formats, which have the common characteristic of being defined on the two in-line and quadrature axis of two orthogonal polarizations, obtaining in total four different *PAM* modulations.

For this reason, it is possible to define a block diagram similar to the one shown in Figure 4.8.

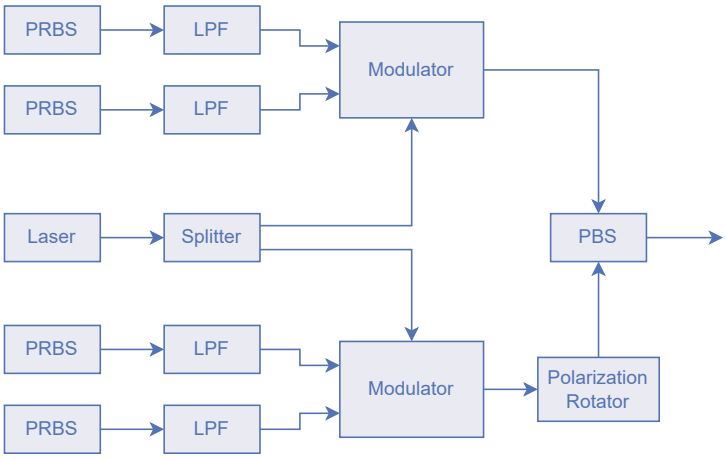

Figure 4.8: Block diagram of the main elements inside a coherent transmitter

At first, as it is possible to see, every transmitter has four input channels, named PRBS in the figure, which represent the data stream that has to be converted from the electrical to the optical domain.

As a side note, it is interesting to observe that these can be any kind of input

bit sequence, usually containing an appropriate representation of the data to be transmitted. However, the name PRBS is particularly appropriate to the aims of this work, since it represents a Pseudo-Random Bit Sequence that can be easily generated by both the transmitter and the receiver. In this way, the former has an "infinite" amount of data to transmit all the symbols in the chosen modulation format, while the latter can use the same sequence to effectively count the number of errors in the received sequence.

In any case, the four input sequences are filtered by a low pass filter (LPF) and are used in pairs by the modulators to construct the symbols to be transmitted. Additionally, as it is possible to see, the two optical sequences are generated with the use of only one laser, both for economical reasons and to ensure that they are subject to the same characteristics of the input light. In fact, an important aspect is that the laser provides a light beam with a linear polarization, and this configuration ensures that the two photon streams are polarized in the same way. Subsequently, one of the two streams is rotated by 90° using a polarization rotator, in order to produce the orthogonal polarization. At that point, the two streams are combined in the same output fiber, and the result is a pair of orthogonal polarizations, each containing a quadrature amplitude modulation.

From the previously described figure 4.8 it is clear that inside an optical coherent transmitter there are several different components that work together in order to provide its output signal; however, in most of the cases, this device can be represented in a simplified version which considers only two contributions: the useful signal and a noise component that joins the effect of all the different elements together. This result is represented in the Figure 4.9, which highlights the quantities S_{in}, representing the power of the useful signal, and N_{TX}, the power of the noise introduced by the transmitter.

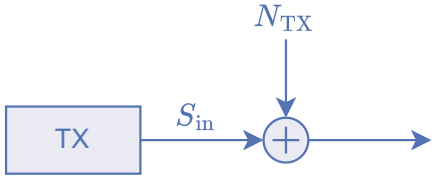

Figure 4.9: Schematic representation of an optical transmitter

4.2.2 The receiver implementation

The implementation of the receiver is complementary to the one of the transmitter described in the previous section, since its main goal is to decode the original data streams that have been combined inside the same optical symbols. A schematic representation of the core components is shown in the block diagram in figure 4.10.

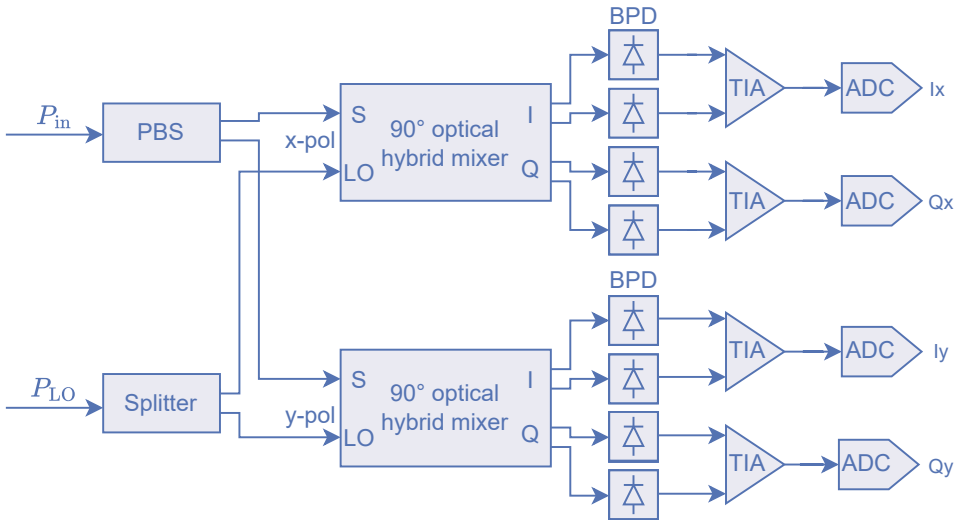

Figure 4.10: Block diagram of the main elements inside a coherent receiver

As it is possible to see, this device presents one input only, represented in the top-left part as the power P_{in}, and it has four output signals corresponding to the received data on the two complex axis of the two orthogonal polarizations. However, in order to fully understand the characteristics of a coherent transceiver, it is important to observe that there exist an additional input signal, named P_{LO}, representing the power coming from a Local Oscillator (LO). This is a signal generated directly by the receiver at the same frequency of the signal intended to be received, and has a central role in the 90° Optical Hybrid Mixer, as it will be commented later.

Furthermore, as a side note, it is interesting to note that in most of the commercial devices, this Local Oscillator signal is taken directly from the laser used for signal transmission. The main advantage of this technique is that only one device is needed for both directions, which reduces the cost and size of the transceiver. However, the main disadvantage is that the transceiver can only operate on one frequency in both directions, so it can only transmit on the frequency it is receiving.

The 90° Optical Hybrid Mixer

The 90° Optical Hybrid Mixer is a passive optical device with two inputs and four outputs able to *mix* the input signals into four output ones. Its internal implementation is outside the scope of this work, but the important aspect of its characteristics is the mathematical relation between the inputs and the outputs, as described in Figure 4.11. Moreover, the device is supposed *ideal* in the sense that there is no power loss: for this reason, the summation of the input powers is considered equal to the summation of the output ones.

In this specific case it has been decided to consider the *fields* E, in which E_{x} and E_{LO} are related to the input signal and the local oscillator, properly split between the two mixers as it will be detailed later. In addition, whenever a field is split equally in two directions, it is divided by $\sqrt{2}$, and since in this case it is split twice (to obtain four outputs from one input), the input field is divided by 2. In addition, it is important to note that in a complete receiver it is required to have two 90° Optical Hybrid Mixers in order to operate simultaneously on the two polarizations [36].

This procedure is repeated in the same way for both the inputs, but in the case of the Local Oscillator, it is introduced an additional complex phase rotation of 90° between each output.

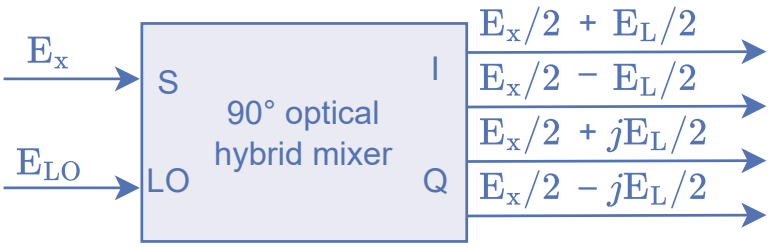

Figure 4.11: Generic representation of the 90° Optical Hybrid Mixer

As a side note, is it important to remember that the two inputs, the signal of interest and the signal coming from the local oscillator, are in general at the frequencies ω_c and ω_{LO} respectively. The nonlinear mixing operation downconverts the signal to the intermediate frequency $\omega_{IF} = \omega_c - \omega_{LO}$. However, for the purposes of this work, the *homodyne* coherent detection considers $\omega_{IF} = 0$ and no other downconversion is required [37].

Balanced Photodetectors

A photodetector (PD) is a device capable of converting an incident optical signal into an electrical current following the relation described in equation 4.6.

$$i \propto E(t)E(t)^* \tag{4.6}$$

This is at the basis of the detection of an optical signal, and is applied in all the receivers. However, the generated current is proportional to the modulo-square of the input power, and this causes the fact that any information related to the polarization or the phase of the incident photons is lost.

Clearly, this prevents the possibility of using only one photodetector for decoding a coherent signal, but this problem can be solved with the use of two *balanced* photodetectors, as in Figure 4.12, in which the two inputs are directly connected to two outputs of the 90° Optical Hybrid Mixer described before.

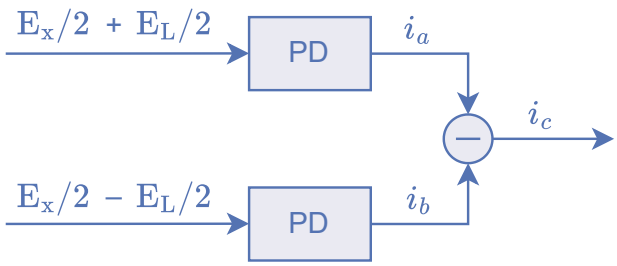

Figure 4.12: Block diagram of a balanced photodetector

By applying the rule just described in equation 4.6, it is possible to find the currents i_a and i_b provided as the output of the two photodetectors. An example is in equation 4.7, in which the symbol $\pm$ is used to denote that the sign of the component b is inverted in respect to the one of the current a.

$$\begin{aligned} i_{a,b} &= R\left|\frac{E_\mathrm{x}}{2} \pm \frac{E_\mathrm{L}}{2}\right|^2 \\ &= R\left|\frac{E_\mathrm{x}}{2}\right|^2 + R\left|\frac{E_\mathrm{L}}{2}\right|^2 \pm \frac{R}{2} \cdot \Re\left(E_\mathrm{x}E_\mathrm{L}^*\right) \end{aligned} \tag{4.7}$$

In this case, it has been used the relation provided in Equation 4.8, in which $\Re$ denotes the real part of a complex quantity.

$$|a+b|^2 = |a|^2 + |b|^2 + 2\Re\left(ab^*\right) \tag{4.8}$$

As a side note, the proportionality in equation 4.6 has been substituted with an equality in which it is considered the additional factor R, called *responsivity* and expressed in A/W. This value is related to the *quantum efficiency* η by the equation 4.9, which in turn depends on the frequency ν, the electron charge q and the Plank

constant h; usually, a simplified numerical approximation is considered, in which it is used the wavelength λ expressed in micrometers [38]. The consequence of this is that the responsivity R depends slightly on the frequency of the incident signal, since at lower frequency more photons are present at the same optical power; however, for the use in the C-band, this variation can be considered negligible.

$$R = \frac{\eta q}{h\nu} \approx \frac{\eta \lambda}{1.24} \tag{4.9}$$

As it is possible to see, the two defined currents i_a and i_b are defined in a very similar way, with only a difference in the sign of the last one. For this reason, it is now interesting to compute the current i_c as their difference [39], removing the contributions corresponding to the powers of the received signal and the local oscillator, as in Equation 4.10.

$$i_c = i_a - i_b = R \cdot \Re\left(E_{\mathrm{x}} E_{\mathrm{L}}^{*}\right) \tag{4.10}$$

In this way, it is now clear that the final current provided as the output of the photodetector is directly proportional to the incident fields coming from the useful signal and the local oscillator, together with the responsivity.

4.2.3 The complete transceiver model

In the previous sections it has been shown the list of the main components in the optical transmitters and receivers, and now it is possible to merge them in order to have a complete view of the system. A schematic representation of the complete transceiver model is provided in Figure 4.13, which considers all the contributions that affect the received signal [40, 41].
As it is possible to see, the first block on the top-left part is the one representing the transmitter, which is the same already defined in section 4.2.1. Its signal is then affected by the noise N_{ASE} introduced in the line, so that the overall received power P_{in} can be defined as in equation 4.11, in which N_{in} represents the summation of the noises, like N_{TX} and N_{ASE}. Similarly to what has been described in section 3.1.4, in the case of the *sensitivity setup*, characterized by the absence of additioanl noise loading, it is possible to consider $N_{\mathrm{ASE}} \approx 0$.

$$P_{\mathrm{in}} = S_{\mathrm{in}} + N_{\mathrm{TX}} + N_{\mathrm{ASE}} = S_{\mathrm{in}} + N_{\mathrm{in}} \tag{4.11}$$

Similarly, the equation 4.12 represents the power received from the local oscillator, with its additional noise component.

$$P_{\mathrm{LO}} = S_{\mathrm{LO}} + N_{\mathrm{LO}} \tag{4.12}$$

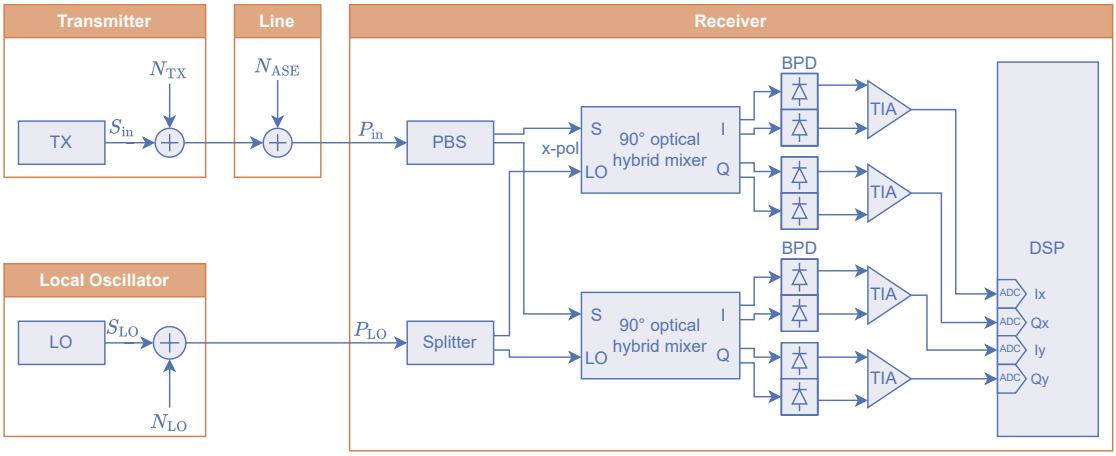

Figure 4.13: Block diagram of the main elements inside a coherent receiver and their interconnections with the line

Then, the same Figure 4.13 shows the presence of the two splitters, which divide the power equally in their two arms (or divides the field by $\sqrt{2}$, as described before), connecting the signals to the inputs of the two 90° Optical Hybrid Mixers, whose behavior has been described with the figure 4.11.

At this point it is possible to merge all the equations described before, considering all the inputs inside the equation of the current i_c described before, obtaining the relation in equation 4.13 related to the current *in phase* (I). Moreover, the signal from the local oscillator is considered as a pure real tone with field s_{LO} and noise n_{LO}; on the contrary, the incident signal is split into its phase and quadrature components:

$$\begin{aligned} i_c^I &= i_a^I - i_b^I \\ &= 4R \cdot \Re\left(\frac{E_{\mathrm{in}}}{2\sqrt{2}}\frac{E_{\mathrm{LO}}^*}{2\sqrt{2}}\right) \\ &= \frac{R}{2} \cdot \Re\left(E_{\mathrm{in}} E_{\mathrm{LO}}^*\right) \\ &= \frac{\mathrm{R}}{2}\left[(s_{\mathrm{in},I} + j s_{\mathrm{in},Q} + n_{\mathrm{in},I} + n_{\mathrm{in},Q})(s_{\mathrm{LO}} + n_{\mathrm{LO}})\right] \\ &= \frac{\mathrm{R}}{2}\left[s_{\mathrm{in},I} s_{\mathrm{LO}} + s_{\mathrm{in},I} n_{\mathrm{LO}} + n_{\mathrm{in},I} s_{\mathrm{LO}} + n_{\mathrm{in},I} n_{\mathrm{LO}}\right] \end{aligned} \tag{4.13}$$

With the same procedure it is then possible to obtain the expression of the output current i_c^Q related to the *quadrature* (Q) component:

$$i_c^Q = \frac{\mathrm{R}}{2}\left[s_{\mathrm{in},Q}s_{\mathrm{LO}} + s_{\mathrm{in},Q}n_{\mathrm{LO}} + n_{\mathrm{in},Q}s_{\mathrm{LO}} + n_{\mathrm{in},Q}n_{\mathrm{LO}}\right] \tag{4.14}$$

As it is possible to see, the result shows that the output current i_c is proportional to the incident field s_{in} multiplied by the field of the local oscillator s_{LO}.

This result is of great interest because it shows that the incident power S_{in} is increased proportionally to the power of the Local Oscillator. At the same time, it is also clear that the same oscillator introduces two additional noise components, which affect the quality of the final received signal.

However, during this computation it has been neglected the effect of two additional noise components that have to be further analyzed in the next sections.

The square of the current

The previous equations 4.13 and 4.14 show the contributions of the current in phase and in quadrature; however for the following computations it will be required to know the modulo-square of the complete description of the current. It can be calculated with the steps detailed in equation 4.15. In particular, in the last steps, the power of the signals in phase and in quadrature have been considered equal so that $S_{\mathrm{in},I} = S_{\mathrm{in},Q} = S_{\mathrm{in}}/2$.

$$\begin{aligned}
\mathrm{E}\left[|i|^2\right] &= \mathrm{E}\left[|i_I|^2\right] + \mathrm{E}\left[|i_Q|^2\right] + 2\cdot\mathrm{E}\left[\Re\left(i_i i_Q^*\right)\right] \\
&= \mathrm{E}\left\{\left[\frac{R}{2}\left(s_{\mathrm{in},I}s_{\mathrm{LO}} + s_{\mathrm{in},I}n_{\mathrm{LO}} + n_{\mathrm{in},I}s_{\mathrm{LO}} + n_{\mathrm{in},I}n_{\mathrm{LO}}\right)\right]^2\right\} + \\
&\quad + \mathrm{E}\left\{\left[\frac{R}{2}\left(s_{\mathrm{in},Q}s_{\mathrm{LO}} + s_{\mathrm{in},Q}n_{\mathrm{LO}} + n_{\mathrm{in},Q}s_{\mathrm{LO}} + n_{\mathrm{in},Q}n_{\mathrm{LO}}\right)\right]^2\right\} \\
&= \frac{R^2}{4}\{S_{\mathrm{in},I}S_{\mathrm{LO}} + S_{\mathrm{in},I}N_{\mathrm{LO}} + N_{\mathrm{in},I}S_{\mathrm{LO}} + N_{\mathrm{in},I}N_{\mathrm{LO}} + \\
&\quad + S_{\mathrm{in},Q}S_{\mathrm{LO}} + S_{\mathrm{in},Q}N_{\mathrm{LO}} + N_{\mathrm{in},Q}S_{\mathrm{LO}} + N_{\mathrm{in},Q}N_{\mathrm{LO}}\} \\
&= \frac{R^2}{4}\{S_{\mathrm{in}}S_{\mathrm{LO}} + P_{\mathrm{in}}N_{\mathrm{LO}} + N_{\mathrm{in}}S_{\mathrm{LO}}\}
\end{aligned} \tag{4.15}$$

The additional noise contributions

In the previous paragraphs it has been shown how the noise on the input N_{in} and the one on the local oscillator N_{LO} are relevant quantities in the computation of the device performances. However, it is important to consider two additional contributions added by the receiver itself, that are common on both the IMDD and the coherent devices.

The first contribution is called *shot* (or *quantum*) noise: it consists of a stream of electrons that are generated at random times and depends directly on the total

power managed by the device. A general description of this quantity is provided by equation 4.16, in which I_p represents the photogenerated current and q is the electron charge. Moreover, the parameter B represents the effective noise bandwidth of the receiver and depends on its implementation. Finally, I_d represents the dark current contribution, which corresponds to an output current that is generated also in absence of incident photons [42].

$$P_{\text{sh}} = 2q(I_p + I_d)B \tag{4.16}$$

Lastly, there exist the additional term named *thermal noise* (also known as *Johnson noise*), which has an additional dependence on the absolute temperature T and an internal equivalent resistor R_L, as shown in equation 4.17. It is due to the fact that at finite temperature electrons tend to move randomly in any electric resistance, and this produces a noise current in the load resistance, which results into an additional current noise of the photodetector [43].

$$P_{\text{th}} = 4k_B TB/R_L \tag{4.17}$$

The additional noise currents

All the noise contributions have the effects of changing the overall current outputted by the device. For this reason it is helpful to consider the overall current (in phase) I_I provided to the input of the DSP as in equation 4.18, in which $i_{a,I}$ and $i_{b,I}$ are the same currents described above, $n^a_{s,I}$ and $n^b_{s,I}$ are the shot noises introduced by the two photodetectors and n_T is the thermal noise generated by the transimpedance amplifier. The names i_s and i_T are defined for the last two quantities in order to study them independently.

$$i_I = \underbrace{[i_{a,I} - i_{b,I}]}_{i_c} + \underbrace{\left[n^a_{s,I} - n^b_{s,I}\right]}_{i_s} + \underbrace{[n_T]}_{i_t} \tag{4.18}$$

The shot noise contribution

In equation 4.16 it has been shown that the shot noise depends on the photogenerated current $I_p = R\,P_{inc}$ with P_{inc} the incident optical power. This quantity can be computed considering for example the upper arm of Figure 4.12, knowing that its value will be the same for all the other cases thanks to the symmetry of the system.

$$\begin{aligned} I_p &= \mathrm{E}\left[\left|\frac{E_{\mathrm{in}}}{2\sqrt{2}} + \frac{E_{\mathrm{LO}}}{2\sqrt{2}}\right|^2\right] \\ &= \frac{R}{8}\mathrm{E}\left[|E_{\mathrm{in}}|^2\right] + \frac{R}{8}\mathrm{E}\left[|E_{\mathrm{LO}}|^2\right] + \frac{R}{4}\mathrm{E}\left[\Re\left(E_{\mathrm{in}}E_{\mathrm{LO}}^*\right)\right] \\ &= \frac{R}{8}P_{\mathrm{in}} + \frac{R}{8}P_{\mathrm{LO}} \\ &= \frac{R}{8}\left(P_{\mathrm{in}} + P_{\mathrm{LO}}\right) \end{aligned} \tag{4.19}$$

This quantity can be used to fully compute the shot noise for every photodetector:

$$\begin{aligned} \sigma_{SH}^2 &= 2q(I_p + I_d)B \\ &= \frac{1}{4}q\left[R\left(P_{\mathrm{in}} + P_{\mathrm{LO}}\right) + 8I_d\right]B \end{aligned} \tag{4.20}$$

Merging all the terms

The total current coming into the DSP is obtained as the summation between the photogenerated signal, the shot noise and the thermal noise, as in equation 4.21. A similar result holds also for the in-quadrature case.

$$\mathrm{E}\left[|i_I|^2\right] = \mathrm{E}\left[|i_c|^2\right] + \mathrm{E}\left[|i_s|^2\right] + \mathrm{E}\left[|i_T|^2\right] \tag{4.21}$$

The total power is in this way defined as in equation 4.22, in which the two expected values of the in-phase and quadrature components are considered equal.

$$\begin{aligned} P_{out} &= \mathrm{E}\left[|i|^2\right] = \mathrm{E}\left[|i_I|^2\right] + \mathrm{E}\left[|i_Q|^2\right] \\ &= \frac{R^2}{2}(S_{\mathrm{in}}S_{\mathrm{LO}} + P_{\mathrm{in}}N_{\mathrm{LO}} + N_{\mathrm{in}}S_{\mathrm{LO}}) + q\left[R(P_{\mathrm{in}} + P_{\mathrm{LO}}) + 8I_d\right]B + 8k_BTB/R_L \end{aligned} \tag{4.22}$$

The computation of the final SNR can be performed in steps in order to highlight the different contributions, knowing that $R^2S_{\mathrm{in}}S_{\mathrm{LO}}/2$ is the contribution of the useful signal. In particular, the components are reported in equation 4.23:

$$\begin{aligned}
\mathrm{SNR}_{\mathrm{LO}} &= \frac{P_{\mathrm{s}}}{P_{\mathrm{NLO}}} = \frac{R^2 S_{\mathrm{in}} S_{\mathrm{LO}}/2}{R^2 P_{\mathrm{in}} N_{\mathrm{LO}}/2} = \frac{S_{\mathrm{in}} S_{\mathrm{LO}}}{P_{\mathrm{in}} N_{\mathrm{LO}}} \\
\mathrm{SNR}_{\mathrm{in}} &= \frac{P_{\mathrm{s}}}{P_{\mathrm{Nin}}} = \frac{R^2 S_{\mathrm{in}} S_{\mathrm{LO}}/2}{R^2 N_{\mathrm{in}} S_{\mathrm{LO}}/2} = \frac{S_{\mathrm{in}}}{N_{\mathrm{in}}} \\
\mathrm{SNR}_{\mathrm{th}} &= \frac{P_{\mathrm{s}}}{P_{\mathrm{th}}} = \frac{R^2 S_{\mathrm{in}} S_{\mathrm{LO}}/2}{8 k_B T B / R_L} \\
\mathrm{SNR}_{\mathrm{sh}} &= \frac{P_{\mathrm{s}}}{P_{\mathrm{sh}}} = \frac{R^2 S_{\mathrm{in}} S_{\mathrm{LO}}/2}{q\left[R(P_{\mathrm{in}} + P_{\mathrm{LO}}) + 8 I_d\right] B}
\end{aligned} \tag{4.23}$$

Finally, the overall SNR equation is obtained by considering their joint effects: for this reason, it is possible to *sum* them knowing the general summation rule for the SNR quantities presented in equation 4.2, for which the inverse of the result is equal to the summation of the inverse of the components:

$$\mathrm{SNR}^{-1} = \mathrm{SNR}_{\mathrm{LO}}^{-1} + \mathrm{SNR}_{\mathrm{in}}^{-1} + \mathrm{SNR}_{\mathrm{th}}^{-1} + \mathrm{SNR}_{\mathrm{sh}}^{-1} \tag{4.24}$$

By substituting the quantities defined above and making the necessary adjustments to the factors, the complete model of the SNR of the transceiver is presented in the equation 4.25:

$$\mathrm{SNR} = \frac{R^2 S_{\mathrm{in}} S_{\mathrm{LO}}/2}{q(R\left(P_{\mathrm{in}} + P_{\mathrm{LO}}\right) + 8 I_d) B + 8 k_B T B / R_L + R^2 \left(N_{\mathrm{in}} S_{\mathrm{LO}} + P_{\mathrm{in}} N_{\mathrm{LO}}\right)/2} \tag{4.25}$$

The shape of the $\mathrm{SNR}_{\mathrm{TRX}}$ function

In previous sections it has been described how it is possible to obtain an analytical equation similar to 4.25 able to relate the SNR of the transceiver with some parameters typical of the device under test and the incident power value. As it is possible to see, this function is quite complex since it contains several parameters which are, in principle, unknown.

To do so, a first step has been the assignment of possible values to all the parameters, and the corresponding curve is visible in Figure 4.14. In particular, the only parameter that does not need to be estimated (or assigned) is the power of the received signal S_{in}, since it can be measured by the transceiver; moreover, it is in general of great interest to study the variation in the SNR in respect to the power, and so it can be used as the horizontal axes in the following plots.

In this case, as anticipated before, the parameters typical of the equation 4.25 have been set in such a way to provide a meaningful result, but it is important to

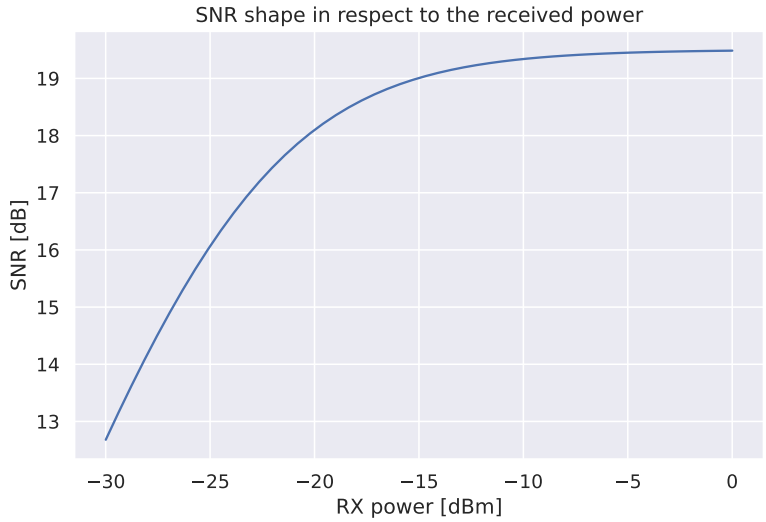

Figure 4.14: Qualitative SNR curve in respect to the received input power

remember that they have been set arbitrarily: the consequence is that the values on the vertical axis cannot be considered accurate.

As it is possible to see, when the axes are set in the log-scale, so that the power is expressed in dBm and the SNR in dB, the obtained shape is very similar to the experimental results already described related to the Figure 4.6. In particular, the fundamental aspect is that the SNR tends to increase rapidly with the power S_{in}, but then it reaches a maximum after which it stays basically constant, independently on other variations. This is completely coherent with the results largely commented during the device characterization, for example in Figure 3.6, in which the performances of the transceiver appear almost constant when the received power is large enough. This is mainly due to the fact that at some point the received power value does not represent a penalty anymore, and so its effect becomes negligible in respect to other contributions.

These results confirm that the previously defined equation 4.25 can be used to accurately estimate the performances of the device in respect to the variation of the received power S_{in}. However, how it has been anticipated in the previous sections, that equation requires the knowledge of several parameters, and for this reason it is interesting to observe how the curve changes according to their variations.

A qualitative example is provided in Figure 4.15, in which different curves are characterized by a different bandwidth B or absolute temperature T.

As it has been anticipated before, the effective noise bandwidth is a relevant contribution for the computation of the noise since an increase in B enlarges both the thermal and the shot noises. This is mainly due to the fact that a larger band

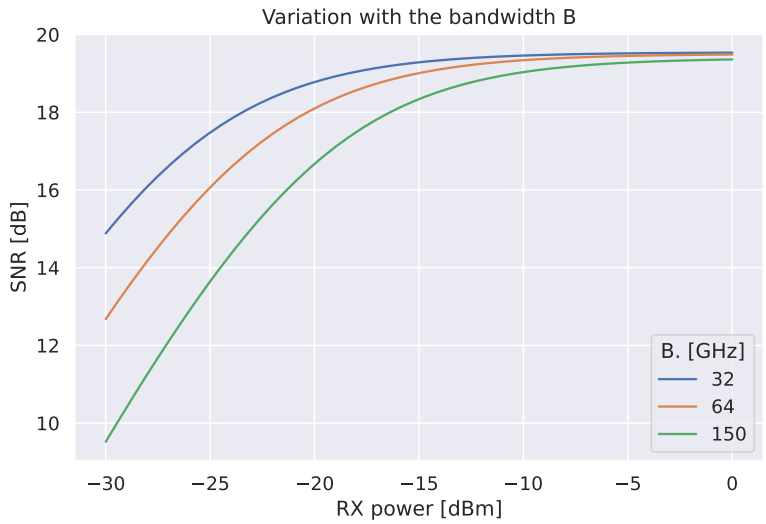

Figure 4.15: Qualitative SNR curve in respect to the received input power with different values of the effective noise bandwidth B

causes a larger power of the nose to cross the internal filter, and thus this will reduce the overall SNR.

A visually different result is instead obtained when it is performed a variation in the responsivity R of the photodetectors or in the power of the local oscillator S_{LO}. Unlike the previous example, in this case an increase in both the quantities is able to improve the final SNR. In particular, the responsivity enables the photodetector to produce a stronger current with the same incident signal, and this effect will be more relevant in respect to the corresponding increase in the noise. Similarly, a stronger power S_{LO} coming from the local oscillator can "pump up" the power of the useful signal, largely improving the performance. A qualitative visualization is provided in Figure 4.16, but similarly to the previous cases it is important to remember that the numerical values can only be used as a "reference" when comparing curves inside the same plot, since all the other quantities have a fixed value that may not correspond to the physical characteristics of any real device.

4.3 The SNR fitting

At this point, it is possible to merge the results obtained in all the previous chapters, performing a fitting on the collected data in order to obtain an understanding of the internal characteristics of the devices under test.

In order to simplify the design, it is possible to consider only the *sensitivity*

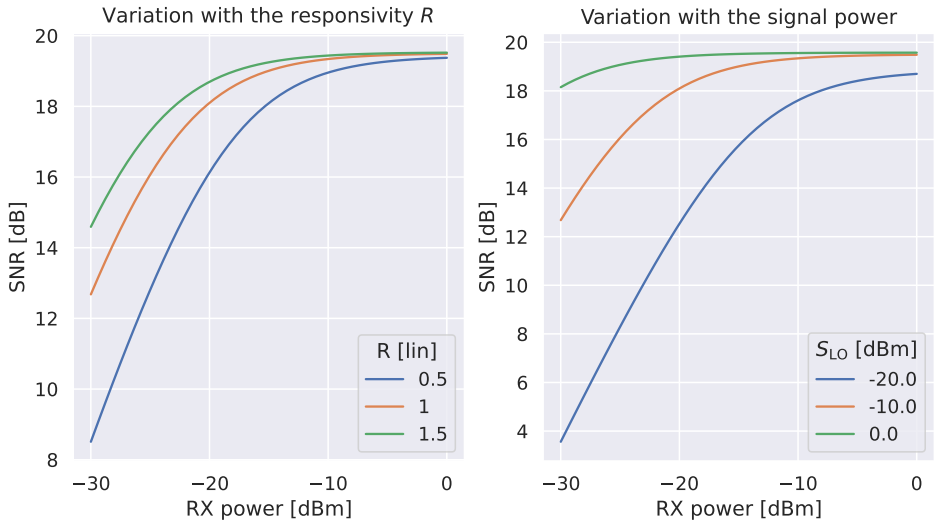

Figure 4.16: Qualitative SNR curve in respect to the received input power with different values of the responsivity R and the power of the local oscillator S_{LO}

setup, as it has been described in section 3.1.4. The corresponding removal of some contributions from the network simplifies the model because it removes the dependency on the additional noise introduced in the line, but it should keep the dependency on the power unaltered. As a consequence, in this specific context it is possible to suppose $N_{\text{ASE}} = 0$, which implies having $N_{\text{in}} \approx N_{\text{TX}}$ in respect to the equation 4.11.

Moreover, the dependency on the SNR_{ASE} introduced by the line has been largely commented in the previous chapters, and for this reason it is possible to suppose that be added independently on the system later, after having obtained the characterization of the transceiver in a *noiseless* environment.

As a result, the overall description of the transceiver should be limited to the knowledge of the following parameters:

- The power of the input signal S_{in}, that changes with its operating conditions, and the power of the local oscillator S_{LO};
- The noise on both the input N_{in} and the local oscillator N_{LO};
- The characteristics of the device internal implementation, like the responsivity R, the dark current I_d, the equivalent load resistor R_L, the temperature T and the effective bandwidth B.

However, as anticipated, apart from the input power, the level of which can be accurately measured, the other parameters are unknown. In general, similarly to

what has been done in the previous sections, it is possible to assign them "reasonable" values, but to get a more precise prediction of the device performance it is instead preferable to perform a mathematical interpolation. A brief and qualitative comment related to the curve interpolation is provided in the Appendix A.1, and it is based on an iterative approach in finding the most accurate values of the parameters able to make the analytical curve similar to the one in Figure 4.14, approximate the measured values. This is based on a *least squares* approach that minimizes the difference between the computed values and the expected one; at each iteration, the parameters are then modified to test new conditions, trying to reach a minimum.

As a side note, it is important to note that this problem is in principle quite complex: in fact, there are a total of 8 unknowns, which are a lot in respect to the shape of equation 4.25, and this translates into the fact that it is not always possible to expect exact results. However, by setting proper *bounds* in the allowed values, it is at least possible to obtain reasonable values that can be used to draw the corresponding output line. One example is provided in Figure 4.17, which contains the same data as in the previously described Figure 4.6, with the additional representation of the fitted curve as a black dashed line.

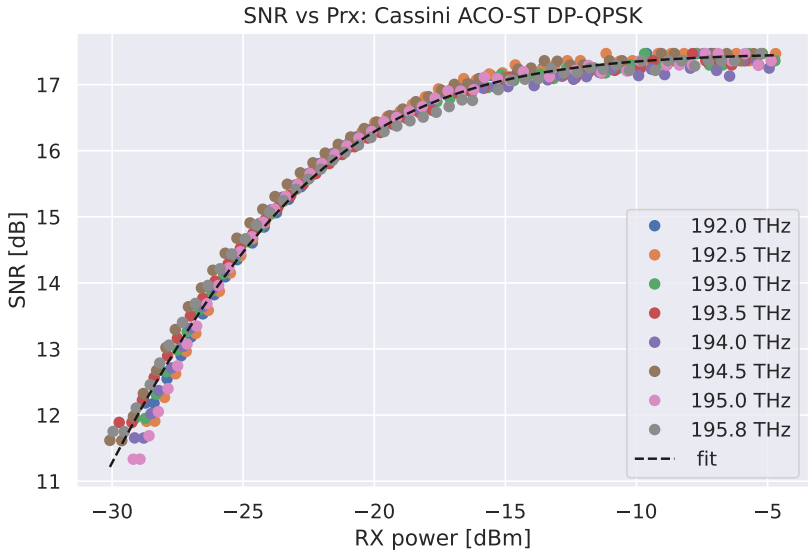

Figure 4.17: SNR evolution in respect to the received power for the Cassini transponder at different operating frequencies, fitted with the new transceiver model of equation 4.25

As it is possible to see, the fitted curve overlaps exactly with the measured curve. This is a visual representation of the quality of the results, which are fully

compatible with the analytical description discussed earlier and are not incompatible with the difficulty of estimating a large set of parameters. At the same time, it is also clear that, for the equipment under test, there is no significant penalty introduced by the different frequencies: in fact, they all follow the same trend and are correctly approximated by the fit provided.

The same technique can be repeated for other devices to obtain a complete description of their behavior in different operating conditions. Finally, this curve can be used to quickly obtain information on the quality of the transceiver for each input power, and this can be used to know what is the additional penalty introduced by the device.

4.3.1 The additional ASE noise

As it has been described in the previous sections, in order to compute the performances of the transceiver it has been decided to use the Sensitivity setup, described in section 3.1.4. The main benefit of this approach is the fact that the performances of the system are only due to the characteristics of the transceiver, and thus the $\mathrm{SNR}_{\mathrm{TRX}}$ becomes the predominant contribution, and can be studied effectively in respect to the input power S_{in}.

In general, it can be considered as a simplified case in the sense that in most real applications there is always an additional noise source $\mathrm{SNR}_{\mathrm{ASE}}$ that further reduces the performances of the system. However, the purpose of this additional section is to show that, thanks to the fact that all considered SNR contributions are additive, the removal of the additional noise cannot be considered as a loss of generality, since it can be added back by considering the general equation 4.5.

An example of a result is provided in Figure 4.18, in which it is shown the typical relation between the BER and the $\mathrm{SNR}_{\mathrm{ASE}}$ in different operating conditions with a Phoenix transponder using the DP-QPSK modulation format. As a side note, it is only shown the curves with stronger signal attenuation since they are the most relevant in terms of the penalty introduced by the receiver.
As it is possible to see, the plot shows three types of data, which have been obtained in different ways, and for this reason it is relevant to clarify their differences:

- The $\times$ represents the data points collected with the "complete" setup, which considers the additional noise loading described in section 3.1. This has the same characteristics of the curves in Figure 3.3;

- The dashed lines represents the estimation of the points considering the *optimal* fitting defined in respect to the Figure 4.4, in which the $\mathrm{SNR}_{\mathrm{TRX}}$ is fitted independently for every line;

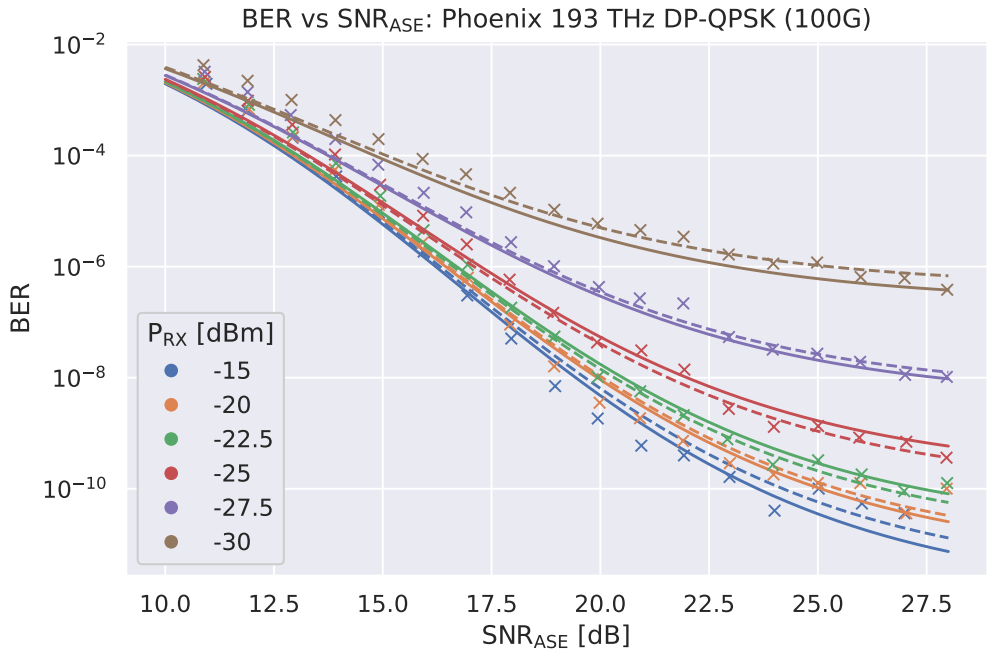

Figure 4.18: BER curve interpolation with two fitting techniques

- The solid lines represent the results obtained considering the analytical SNR filtering presented in Section 4.3, in which the SNR_{ASE} is measured and the SNR_{TRX} is computed analytically with the parameters fitted using the sensitivity setup.

The three conditions are very different because, although they represent the same quantities, they are obtained in completely different scenarios. The most interesting comparison is between the two fittings, since they describe the results of two procedures that can be performed on any device under test.

In particular, the figure clearly shows that both the techniques are able to provide very good results that approximate precisely the measured data points. Moreover, since the curves corresponding to the two techniques almost overlap, it is clear that the transceiver model can accurately predict the device performance, similar to what a full characterization with noise loading can provide after the result interpolation, even if this requires a more complex setup and greater data collection times.

Chapter 5

Conclusions

The work focused on two main topics, which are however closely related, and were developed in parallel by exploiting the features of the former to make the latter possible.

The device control

The first objective of this work was the development of open software capable of controlling an optical white box transponder using only open interfaces. This has been achieved by implementing a driver capable of sending commands and retrieving measurements from a Phoenix transponder, a commercially available device that uses off-the-shelf transceivers capable of deploying light paths at state-of-the-art data rates up to 400 Gbps.

The device characterization

The second goal has been the transponder characterization, which has been performed in successive stages, starting from an exhaustive data collection, which allowed the realization of a complete database with the most relevant measures in very diverse network conditions. Then, a comprehensive data analysis has been carried out to gain an insight into its operating characteristics, with the goal of finding common trends between different network configurations or optical devices. Subsequently, it was possible to develop a complete modelling of the main contributions of the device internal implementation, in order to find an analytical description of its behavior in order to accurately predict its performances. Lastly, it was possible to compare the experimental results obtained also with the helpful open model put together in the first part to validate the accuracy of the mathematical results, fully confirming the predictions.

The two results obtained in the two parts are strictly related one with the other since they enable the possibility of defining accurate and analytical models that can be used as an important building block towards the goal of the realization of a complete open and disaggregated optical network, which allows the interoperability between devices in a multi-vendor scenario, one of the paradigms of the most modern and future networks.

This is in fact one of the most important long-term results, since the development of such an open network is of great interest in order to be able to fully take advantage of the diverse network elements and build a complete and efficient network implementation.

Simultaneously, it is also possible to continue the developing of a network digital twin, or a digital representation of a real network, which is a very important goal in the view of being able to fully predict the real network performances in the very diverse operating conditions. In order to reach this goal, it is clearly required to have a full control of the device characteristics, and such a complete data collection and device modelling can be of great interest in order to further improve the accuracy of the results.

Possible future improvements of this work can be based on the increase of the dataset in order to explore even more different network conditions, considering additional more complex elements in the network, trying to further adapt the models toward the accurate description of a real wide optical network. Additionally, the said results can be integrated into open network digital twin software in order to test their effectiveness when cooperating with other modules in providing an accurate prediction of the performance of the devices under test.

Appendix A

Appendix

A.1 Curve interpolation and fitting

During this study it was necessary to perform both the interpolation and the fitting of various curves, but a rigorous mathematical description of the two techniques is beyond the scope of this work; for this reason, this section provides only a high-level description of their basic concepts, limited to the purpose of understanding the calculations performed.

In both cases, the starting point is always a set of measured data relating two different quantities, such as BER and SNR, but this can in principle be extended to any pair of measured quantities. The two techniques can then be used to obtain different results, as shown in the following paragraphs.

The curve interpolation

The measured quantities are, by definition, discrete: this translates into the fact that the amount of available points is finite, and there is no measured data between two adjacent points. In practice, this enables the possibility of knowing the precise mapping between the two different domains only in the exact conditions that have been tested. However, sometimes it is necessary to consider different points that have never been directly evaluated, and in this case it is possible to use an interpolation of the available data to estimate a possible value in the missing spots. This can be done in several different ways, but a simple and effective algorithm is based on a linear interpolation between the two closest available points. To provide a practical example, it is possible to consider an experimental curve which is numerically defined as a set of (x_i, y_i) points, but then it is required to know the value y_T corresponding to an x_T which is not in the set of measured points. To solve this problem, it is possible to find the two points x_a and x_b which are the closest to the x_T of interest, and then perform a linear interpolation as in equation

A.1, obtaining an estimation of y_T in the desired point x_T.

$$y_T = y_a + (y_b - y_a)\frac{x_T - x_a}{x_b - x_a} \tag{A.1}$$

This interpolation is called *linear* because the first order polynomial used corresponds to a linear function that can be evaluated at any point of interest and that crosses exactly the two selected measured points.

Clearly, this solution is not necessarily optimal in all of the conditions since it relies only on the two closest points, neglecting the overall shape of the curve. For this reason, it is in principle possible to consider a higher order polynomial that crosses other points on the same curve, but this increase in complexity does not necessarily translate into a significant improvement in the final solution, which is in fact quite accurate for most practical applications. It is also important to consider that if the size of the collected data set is large enough, the values x_a and x_b will be close together, further reducing the error introduced by the calculation.

The curve fitting

For the purposes of this work, the fitting consists in finding a curve able to accurately approximate (or *fit*) the measured data points. In general, this curve has to be mathematically defined by using a set of parameters, which can then be estimated in such a way to improve the quality of the result.

In practice, the first step is to define such parametric curve, which largely depends on the phenomena that it tries to represent. In some cases, polynomial functions can be used as a starting point, but in the specific cases described in this work, good results can be reached only by using more complex functions that come from the physical description at the basis of the study.

Then, when a parametric function is selected, a regression must be performed to find the correct values of the parameters. Although several techniques can be used, in this case it was decided to follow a simple algorithm based on the minimization of the residuals between the measured quantities and the estimated ones. In practice, the iterative algorithm starts by setting a list of parameters in the neighborhood of a possible valid solutions, and then computes the estimated quantities $\bar{y}_e$ in the measured conditions $\bar{x}$, and then subtracts them from the measured quantities $\bar{y}$. From his difference $\bar{y}_e - \bar{y}$, it is often computed the modulo-square and then the values are added together: the final result is a value that describes the quality of the fitting, since when it is smaller the fit is better. At this point, the algorithm can be executed again several times with a variation in the definition of the parameters, trying to minimize this final cost function, and the output will be the set of parameters that gives the smallest result after a given number of iterations. It is important to note that the final result is not necessary *optimal*, but in most of the

cases it is able to provide a very good description of the *trend* of the values in the different operating conditions.

The main advantage of this techniques is that the knowledge of a mathematical equation can be used to understand the main characteristics of the experimental setup. Moreover, this approach can be considered as an alternative to the interpolation described before, since it enables the possibility to compute any value $y_T = f(x_T)$ even if x_T has not directly been tested empirically. However, it is important to remember that the additional complexity can be justified only under some special conditions, and the need to know a mathematical curve to fit is a strict and very complex requirement that can be met only in some peculiar cases. Nevertheless, it is interesting to highlight an additional characteristic of this fitting approach: in fact, by definition the goal is to minimize the difference between the estimated and the measured data points, but there is no need to have an exact correspondence between the two. As a consequence, the fitted curve does not necessarily have to cross all the measured points, but only to approximate them: for this reason, it can be used as a *smoothing* technique, which is also very helpful to partially remove the experimental inaccuracies that introduce noise into the measurements themselves. This is the reason why even if the fitting is not perfect it is a powerful instrument that can be used to understand the general behaviour of the system in specific working conditions.

Bibliography

[1] A. Gladisch et al. «Evolution of Terrestrial Optical System and Core Network Architecture». en. In: *Proceedings of the IEEE* 94.5 (May 2006), pp. 869–891. ISSN: 0018-9219, 1558-2256. DOI: 10.1109/JPROC.2006.873430 (cit. on p. 1).

[2] Stefano Selleri. «Claude Chappe and the first telecommunication network (without electricity)». In: *URSI Radio Science Bulletin* 2017.360 (Mar. 2017), pp. 96–101. ISSN: 1024-4530. DOI: 10.23919/URSIRSB.2017.8113174 (cit. on p. 1).

[3] Roland Wenzlhuemer. «The Development of Telegraphy, 1870–1900: A European Perspective on a World History Challenge». en. In: *History Compass* 5.5 (Aug. 2007), pp. 1720–1742. ISSN: 1478-0542, 1478-0542. DOI: 10.1111/j.1478-0542.2007.00461.x (cit. on p. 1).

[4] F. P. Kapron, D. B. Keck, and R. D. Maurer. «RADIATION LOSSES IN GLASS OPTICAL WAVEGUIDES». en. In: *Applied Physics Letters* 17.10 (Nov. 1970), pp. 423–425. ISSN: 0003-6951, 1077-3118. DOI: 10.1063/1.1653255 (cit. on p. 1).

[5] *Optics in Our Time*. en. Cham: Springer International Publishing, 2016. ISBN: 978-3-319-31902-5. DOI: 10.1007/978-3-319-31903-2. URL: http://link.springer.com/10.1007/978-3-319-31903-2 (cit. on p. 2).

[6] Jean-Luc Auge, Vittorio Curri, and Esther Le Rouzic. «Open design for multi-vendor optical networks». en. In: *Optical Fiber Communication Conference (OFC) 2019*. San Diego, California: OSA, 2019, Th1I.2. ISBN: 978-1-943580-53-8. DOI: 10.1364/OFC.2019.Th1I.2. URL: https://opg.optica.org/abstract.cfm?URI=OFC-2019-Th1I.2 (cit. on p. 2).

[7] Wenfeng Xia, Yonggang Wen, Chuan Heng Foh, Dusit Niyato, and Haiyong Xie. «A Survey on Software-Defined Networking». en. In: *IEEE Communications Surveys & Tutorials* 17.1 (2015), pp. 27–51. ISSN: 1553-877X, 2373-745X. DOI: 10.1109/COMST.2014.2330903 (cit. on p. 2).

[8] Vittorio Curri. «GNPy model of the physical layer for open and disaggregated optical networking [Invited]». en. In: *Journal of Optical Communications and Networking* 14.6 (June 2022), p. C92. ISSN: 1943-0620, 1943-0639. DOI: 10.1364/JOCN.452868 (cit. on p. 2).

[9] Wikimedia Commons. *PSmall Form-factor Pluggable*. 2015. URL: https://commons.wikimedia.org/wiki/File:SFP_WDM_3.jpg (cit. on p. 3).

[10] Yoshiaki Tamura et al. «Lowest-Ever 0.1419-dB/km Loss Optical Fiber». en. In: *Optical Fiber Communication Conference Postdeadline Papers*. Los Angeles, California: OSA, 2017, Th5D.1. ISBN: 978-1-943580-24-8. DOI: 10.1364/OFC.2017.Th5D.1. URL: https://opg.optica.org/abstract.cfm?URI=OFC-2017-Th5D.1 (cit. on p. 5).

[11] Takemi Hasegawa, Yoshiaki Tamura, Hirotaka Sakuma, Yuki Kawaguchi, Yoshinori Yamamoto, and Yasushi Koyano. «The First 0.14-dB/km Ultra-low Loss Optical Fiber». en. In: () (cit. on p. 5).

[12] Saniya Anjum Yadgeer, S. Ray, and P.V. Joglekar. «Study of Chromatic Dispersion in Single-Mode Optical Fiber». en. In: *Journal of Physics: Conference Series* 2426.1 (Feb. 2023), p. 012026. ISSN: 1742-6588, 1742-6596. DOI: 10.1088/1742-6596/2426/1/012026 (cit. on p. 5).

[13] Tianhua Xu, Gunnar Jacobsen, Sergei Popov, Jie Li, Evgeny Vanin, Ke Wang, Ari T. Friberg, and Yimo Zhang. «Chromatic dispersion compensation in coherent transmission system using digital filters». en. In: *Optics Express* 18.15 (July 2010), p. 16243. ISSN: 1094-4087. DOI: 10.1364/OE.18.016243 (cit. on p. 6).

[14] R H Stolen and A Ashkin. «Optical Kerr effect in glass waveguide». en. In: (2014) (cit. on p. 6).

[15] Emmanuel Desurvire and Michael N. Zervas. «*Erbium-Doped Fiber Amplifiers: Principles and Applications*». en. In: *Physics Today* 48.2 (Feb. 1995), pp. 56–58. DOI: 10.1063/1.2807915. URL: https://pubs.aip.org/physicstoday/article/48/2/56/408388/Erbium-Doped-Fiber-Amplifiers-Principles-and (cit. on p. 6).

[16] Rodolfo Di Muro. «The Er3+-Fiber Gain Coefficient Derived from a Dynamic Gain Tilt Technique». en. In: *JOURNAL OF LIGHTWAVE TECHNOLOGY* 18.33 (2000) (cit. on p. 6).

[17] A.A.M. Saleh, R.M. Jopson, J.D. Evankow, and J. Aspell. «Modeling of gain in erbium-doped fiber amplifiers». In: *IEEE Photonics Technology Letters* 2.10 (Oct. 1990), pp. 714–717. ISSN: 1941-0174. DOI: 10.1109/68.60769. URL: https://ieeexplore.ieee.org/document/60769/ (visited on 12/24/2023) (cit. on p. 7).

[18] R. H. Stolen and E. P. Ippen. «Raman gain in glass optical waveguides». en. In: *Applied Physics Letters* 22.66 (Mar. 1973), pp. 276–278. ISSN: 0003-6951, 1077-3118. DOI: 10.1063/1.1654637 (cit. on p. 7).

[19] Essa Ibrahim Essa, Mshari A. Asker, and Fidan T. Sedeeq. «Evaluation of OADM Network: Simulation and an Overview Based on Metropolitan Applications». en. In: *2021 Fifth International Conference on I-SMAC (IoT in Social, Mobile, Analytics and Cloud) (I-SMAC)*. Palladam, India: IEEE, Nov. 2021, pp. 1410–1416. ISBN: 978-1-66542-642-8. DOI: 10.1109/I-SMAC52330.2021.9640753. URL: https://ieeexplore.ieee.org/document/9640753/ (cit. on p. 7).

[20] Yongcheng Li, Li Gao, Gangxiang Shen, and Limei Peng. «Impact of ROADM Colorless, Directionless, and Contentionless (CDC) Features on Optical Network Performance [Invited]». en. In: *Journal of Optical Communications and Networking* 4.11 (Nov. 2012), B58. ISSN: 1943-0620, 1943-0639. DOI: 10.1364/JOCN.4.000B58 (cit. on p. 8).

[21] Renato Ambrosone, Rocco D'Ingillo, Giacomo Borraccini, Stefano Straullu, Andrea D'Amico, Emanuele Virgillito, Alessio Giorgetti, and Vittorio Curri. «Autonomous Equalization of Independent Open ROADMs via NETCONF Protocol». en. In: *2023 23rd International Conference on Transparent Optical Networks (ICTON)*. Bucharest, Romania: IEEE, July 2023, pp. 1–4. DOI: 10.1109/ICTON59386.2023.10207261. URL: https://ieeexplore.ieee.org/document/10207261/ (cit. on p. 8).

[22] Vittorio Curri. «Software-Defined WDM Optical Transport in Disaggregated Open Optical Networks». en. In: *2020 22nd International Conference on Transparent Optical Networks (ICTON)*. Bari, Italy: IEEE, July 2020, pp. 1–4. ISBN: 978-1-72818-423-4. DOI: 10.1109/ICTON51198.2020.9203450. URL: https://ieeexplore.ieee.org/document/9203450/ (cit. on p. 8).

[23] C. Cox, E. Ackerman, R. Helkey, and G.E. Betts. «Techniques and Performance of Intensity-Modulation Direct-Detection Analog Optical Links». en. In: *IEEE Transactions on Microwave Theory and Techniques* 45.8 (Aug. 1997), pp. 1375–1383. ISSN: 0018-9480, 1557-9670. DOI: 10.1109/22.618439 (cit. on p. 8).

[24] Yixiao Zhu, Lilin Yi, Bo Yang, Xingang Huang, Jun Shan Wey, Zhuang Ma, and Weisheng Hu. «Comparative study of cost-effective coherent and direct detection schemes for 100 Gb/s/lambda PON». en. In: *Journal of Optical Communications and Networking* 12.9 (Sept. 2020), p. D36. ISSN: 1943-0620, 1943-0639. DOI: 10.1364/JOCN.390911 (cit. on p. 9).

[25] Gabriella Bosco. «Advanced Modulation Techniques for Flexible Optical Transceivers: The Rate/Reach Tradeoff». en. In: *Journal of Lightwave Technology* 37.1 (Jan. 2019), pp. 36–49. ISSN: 0733-8724, 1558-2213. DOI: 10.1109/JLT.2018.2886257 (cit. on p. 9).

[26] A. Tychopoulos, O. Koufopaulou, and I. Tomkos. «FEC in optical communications - A tutorial overview on the evolution of architectures and the future prospects of outband and inband FEC for optical communications». In: *IEEE Circuits and Devices Magazine* 22.6 (Nov. 2006), pp. 79–86. ISSN: 8755-3996. DOI: 10.1109/MCD.2006.307281 (cit. on p. 11).

[27] N.S. Alagha and P. Kabal. «Generalized raised-cosine filters». en. In: *IEEE Transactions on Communications* 47.7 (July 1999), pp. 989–997. ISSN: 00906778. DOI: 10.1109/26.774849 (cit. on p. 11).

[28] Rob Enns. *NETCONF configuration protocol*. Tech. rep. 2006 (cit. on p. 18).

[29] Martin Bjorklund. *YANG-a data modeling language for the network configuration protocol (NETCONF)*. Tech. rep. 2010 (cit. on p. 18).

[30] Jurgen Schonwalder, Martin Bjorklund, and Phil Shafer. «Network configuration management using NETCONF and YANG». en. In: *IEEE Communications Magazine* 48.9 (Sept. 2010), pp. 166–173. ISSN: 0163-6804. DOI: 10.1109/MCOM.2010.5560601 (cit. on p. 18).

[31] Cezary Zukowski, David B. Payne, and Marco Ruffini. «Optical splitters configuration for long-reach passive optical network deployment». en. In: *Proceedings of the 2013 18th European Conference on Network and Optical Communications & 2013 8th Conference on Optical Cabling and Infrastructure (NOC-OC&I)*. Graz, Austria: IEEE, July 2013, pp. 185–190. ISBN: 978-1-4673-5823-1. DOI: 10.1109/NOC-OCI.2013.6582888. URL: http://ieeexplore.ieee.org/document/6582888/ (cit. on p. 27).

[32] Svetlana Khonina, N. Kazanskiy, Ali Butt, and S. Karpeev. «Optical multiplexing techniques and their marriage for on-chip and optical fiber communication: a review». In: *Opto-Electronic Advances* 5 (July 2022), p. 210127. DOI: 10.29026/oea.2022.210127 (cit. on p. 28).

[33] Ming Yang, Shayan Shahramian, Henry Wong, Peter Krotnev, and Anthony Chan Carusone. «Pre-FEC and Post-FEC BER as Criteria for Optimizing Wireline Transceivers». en. In: *2021 IEEE International Symposium on Circuits and Systems (ISCAS)*. Daegu, Korea: IEEE, May 2021, pp. 1–5. ISBN: 978-1-72819-201-7. DOI: 10.1109/ISCAS51556.2021.9401125. URL: https://ieeexplore.ieee.org/document/9401125/ (cit. on p. 32).

[34] Eugen Lach and Wilfried Idler. «Modulation formats for 100G and beyond». en. In: *Optical Fiber Technology* 17.5 (Oct. 2011), pp. 377–386. ISSN: 10685200. DOI: 10.1016/j.yofte.2011.07.012 (cit. on p. 40).

[35] Wolfgang Freude et al. «Quality metrics for optical signals: Eye diagram, Q-factor, OSNR, EVM and BER». en. In: *2012 14th International Conference on Transparent Optical Networks (ICTON)*. Coventry, United Kingdom: IEEE, July 2012, pp. 1–4. ISBN: 978-1-4673-2229-4. DOI: 10.1109/ICTON.2012.6254380. URL: http://ieeexplore.ieee.org/document/6254380/ (cit. on p. 47).

[36] Zi-Qing Lu, Qin Han, Han Ye, Shuai Wang, Feng Xiao, and Fan Xiao. «High common mode rejection ratio InP 90° optical hybrid in ultra-broadband at 60 nm with deep-rigded waveguide based on × 4 MMI coupler*». en. In: *Chinese Physics B* 29.55 (May 2020), p. 054206. ISSN: 1674-1056. DOI: 10.1088/1674-1056/ab7b52 (cit. on p. 83).

[37] Darli Augusto De Arruda Mello and Fabio Aparecido Barbosa. *Digital Coherent Optical Systems: Architecture and Algorithms*. en. Optical Networks. Cham: Springer International Publishing, 2021. ISBN: 978-3-030-66540-1. DOI: 10.1007/978-3-030-66541-8. URL: http://link.springer.com/10.1007/978-3-030-66541-8 (cit. on p. 83).

[38] R. Paschotta. «Responsivity - an encyclopedia article». en. In: *RP Photonics Encyclopedia*. RP Photonics AG, 2005. DOI: 10.61835/xal. URL: https://www.rp-photonics.com/responsivity.html (cit. on p. 85).

[39] Kazuro Kikuchi. «Fundamentals of Coherent Optical Fiber Communications». en. In: *Journal of Lightwave Technology* 34.1 (Jan. 2016), pp. 157–179. ISSN: 0733-8724, 1558-2213. DOI: 10.1109/JLT.2015.2463719 (cit. on p. 85).

[40] Govind P. Agrawal. *Fiber-optic communication systems*. eng. Fifth edition. Hoboken, NJ: Wiley, 2021. ISBN: 978-1-119-73736-0 (cit. on p. 85).

[41] Seb J. Savory. «Digital Coherent Optical Receivers: Algorithms and Subsystems». en. In: *IEEE Journal of Selected Topics in Quantum Electronics* 16.5 (Sept. 2010), pp. 1164–1179. ISSN: 1077-260X, 1558-4542. DOI: 10.1109/JSTQE.2010.2044751 (cit. on p. 85).

[42] Xiangcheng Chen. «On Schottky Noise and Shot Noise». en. In: arXiv:1805.12207 (May 2018). arXiv:1805.12207 [physics]. URL: http://arxiv.org/abs/1805.12207 (cit. on p. 88).

[43] J. B. Johnson. «Thermal Agitation of Electricity in Conductors». en. In: *Physical Review* 32.1 (July 1928), pp. 97–109. ISSN: 0031-899X. DOI: 10.1103/PhysRev.32.97 (cit. on p. 88).